Journal of the
OPTICAL SOCIETY
of AMERICA

VOLUME 34, NUMBER 10 OCTOBER, 1944

The Physical and Photochemical Basis of Visual Resolving Power

Part I. The Distribution of Illumination in Retinal Images*

GEORGE M. BYRAM
Appalachian Forest Experiment Station, United States Forest Service, Asheville, North Carolina

INTRODUCTION

FOR the past 15 years, the Forest Service has made investigations of the relation between atmospheric haze and the visual range** of small forest fire smokes. It became apparent throughout the course of these investigations that although the visual range of a small body of smoke (or any other object of small angular diameter) was determined to a large extent by the scattering and absorption of light by the lower atmosphere, the nature of vision itself was equally important. It is not possible to derive equations for the visual range of a small object unless the relation between visual acuity and such factors as brightness, object-background contrast, and structure of the object are known. The answer to the question, "How far can an object of small angular diameter be seen through a hazy atmosphere?" will therefore depend on the solution of two problems:

(1) The determination of the effect of atmospheric haze on the contrast between a distant object and its background.
(2) The development of a general theory of visual acuity, and in particular the determination of the function relating visual acuity to the brightness contrast between a given test object and its background.

The first of these two problems has been considered in other publications,[1–5] and the two parts of the present paper deal only with the second problem. This analysis was originally developed to apply primarily to the visibility of smoke bodies but has been generalized to give a more comprehensive theory of visual acuity and photo-reception. The theoretical and experimental work is developed from a "blurred" image concept which is basically a diffraction theory of retinal image formation and when used in conjunction with a theory of photo-reception seems adequate for treating most problems of visual resolving power and the recognition of contour. The first part of this paper will be primarily concerned with the distribution of illumination in the retinal images of small objects, and with visual acuity phenomena at high brightness levels. The second part will deal with the more complex functions of the retina and with the photochemical aspects of visual acuity.

* Paper presented at the Winter Meeting of the Optical Society of America, held in New York City, March 2–4, 1944.

** The "visual range" of an object is the distance at which it is barely visible.

[1] E. O. Hulburt, J. Opt. Soc. Am. **25**, 125–130 (1935).
[2] E. O. Hulburt, J. Opt. Soc. Am. **31**, 467–476 (1941).
[3] G. M. Byram, J. Opt. Soc. Am. **25**, 388–392 (1935).
[4] H. D. Bruce, J. Agr. Research **62**, 161–178 (1941).
[5] W. E. Knowles Middleton, *Visibility in Meteorology* (The University of Toronto Press, Toronto, 1941).

BOSTON UNIVERSITY
COLLEGE OF LIBERAL ARTS
LIBRARY

THE DISTRIBUTION OF LIGHT IN RETINAL IMAGES

It has long been recognized that the borders or contours of retinal images were blurred and that "sharp" boundaries of the test object were not reproduced in the retinal image. For pupil apertures corresponding to daylight vision (2.0 mm to 2.5 mm), most of the blurring which occurs near the limit of resolution is caused by the diffraction of light passing through the circular pupil or iris diaphragm. Chromatic aberration (see Appendix III) also contributes to the blurring of images, but its effect near the limit of resolution for pupil apertures less than 2.5 mm is considerably less than that of diffraction. For a given pupil aperture, the blurring of images caused by chromatic aberration and diffraction is about the same for all individuals. The monochromatic aberrations (Appendix IV) vary considerably among different individuals, but for normal well-formed eyes, their effect on the blurring of foveal images at apertures below 2.5 mm is undoubtedly small compared with that of diffraction.

For small objects near the limit of resolution, blurring owing to diffraction is sufficiently great to modify the contrast in the retinal image. If H is the brightness of a small test object viewed on a background of brightness H_b, and if I and I_b are the corresponding illuminations on the retina, the equations of contrast are

$$\frac{\pm(H-H_b)}{H_b}=v \tag{1}$$

and

$$\frac{\pm(I-I_b)}{I_b}=u, \tag{2}$$

where v is the contrast between the object and its background and u the contrast in the corresponding retinal image. The contrast v is always considered positive regardless of whether $H>H_b$ or $H<H_b$; the same is true for u. The threshold value of u is usually written as $\Delta I/I$, but for brevity will be written here as u_t; the threshold value of v will be written as v_t.

When a test object is very small, v may be several times as great as u. However, when the test object is made larger $u\rightarrow v$, and for a large object at high brightness levels, the threshold condition may be written

$$v_t=u_t=\text{a constant}, \tag{3}$$

which may be regarded as a mathematical statement of Weber's law. However, in order to write $v=u$, or $v_t=u_t$, it is necessary to assume that only a negligible amount of light is scattered within the eye. The effect of retinal image blurring on the retinal image contrast led Hartridge[6] to believe that brightness discrimination might be the basic factor in visual acuity, and recent investigations[7–9] in the light of Hecht's theory of the photo-receptor process support this idea for some test objects. The main difficulty in relating visual acuity to intensity discrimination is in finding the distribution of illumination in the retinal image.

One of the earliest investigations on the distribution of illumination in optical images was the theoretical work of Lord Rayleigh.[10] Rayleigh derived equations giving the distributions of light intensity in the retinal image for a test object consisting of a long, black line on a background of uniform brightness. These equations were valid only for a rectangular aperture. Hartridge[6] used Rayleigh's equations for computing the retinal image curves for his observations on individual lines, but apparently did not realize that Rayleigh's equations were derived for a rectangular aperture. They would be somewhat in error if applied to a circular pupil. This is also true of the work of Shlaer,[7] and Hecht and Mintz,[8] who used Rayleigh's equations for computing the distribution curves for the retinal images of single black lines viewed against a luminous screen. The error in their curves depends mostly on the nature of the test object for which the distribution is computed. For individual black lines on a white background, such as were studied by Hecht and Mintz, the error in the computed value of u_t is only about 15 percent, which is not especially serious because the error in measuring differential thresholds is somewhat larger than this. In addition to

[6] H. Hartridge, J. Physiol. **57**, 52–67 (1923).
[7] Simon Shlaer, J. Gen. Physiol. **21**, 165–188 (1937).
[8] Selig Hecht and Esther U. Mintz, J. Gen. Physiol. **22**, 593–612 (1939).
[9] Simon Shlaer, E. L. Smith, and A. M. Chase, J. Gen. Physiol. **25**, 553–569 (1942).
[10] Lord Rayleigh, J. Roy. Microscop. Soc., pp. 447–482 (1903).

individual black lines, Hartridge[6] and Shlaer[7] determined the distribution of light in the retinal image for a test object consisting of alternate black and white bars.* Their computations apparently were based on Hartridge's earlier work[11] on chromatic aberration blurring which, for the grating test object, gives values of u_t more than twice as great as they should be.

Since knowledge of the distribution of light intensity in the retinal images of different types of test objects is so essential to an understanding of visual acuity phenomena, and since it is impossible to account for these phenomena on the basis of receptor chemistry unless this distribution is accurately determined, a general

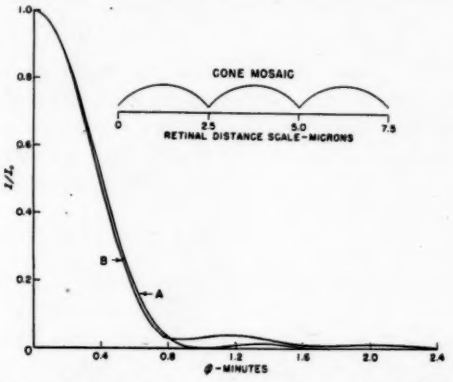

FIG. 1. Curve A is the theoretical distribution of illumination in the retinal image of a point source of light; curve B is the theoretical distribution across the image of a self-luminous line source of infinitesimal width. The iris aperture $2a$ is 2.43 mm for both curves.

method for finding the distribution will be derived. Neglecting for the present the chromatic and monochromatic aberrations in the optical system of the eye, the distribution of illumination I in the retinal image of a distant point source of light is given by the familiar intensity equation for a circular aperture,

$$I = I_0\left\{\frac{2}{z}J_1(z)\right\}^2, \tag{4}$$

where I_0 is the illumination at the center of the image and $J_1(z)$ is the Bessel function of the first kind of order 1 which is given by the series

$$J_1(z) = \frac{z}{2} - \frac{z^3}{2^3 2!} + \frac{z^5}{2^5 2! 3!} - \frac{z^7}{2^7 3! 4!} + \cdots.$$

The variable z is a dimensionless quantity which may be defined as the reduced angular distance of any given point P in the retinal image from the center of the image or diffraction pattern. It is related to the actual angular distance ϕ in radian measure* by the equation

$$z = \frac{2\pi a}{\lambda}\phi, \tag{5}$$

where a is the radius of the iris aperture (or the artificial pupil if one is used) and λ the wave-length of light. If ϕ is large it should be written as $\sin\phi$, but in visual acuity studies it is usually very small and even at low illuminations is seldom greater than 10 or 15 minutes. The angle ϕ is measured from the posterior node of the eye and to a close approximation $\phi = \rho/F$, where ρ is the linear distance of the point P from the center of the retinal image and F the focal length of the eye (the distance between the posterior node and the retina). To simplify numerical calculations it is convenient to assume that the diameter $2a$ of the normal iris is 2.43 millimeters. If ϕ is in minutes, then $z = 4\phi$ if the mean wave-length of visible light is assumed to be 0.555 micron and if F is 16 mm. The variables ϕ and z apply to the angular position of points in either the image plane or object plane.

It is important to note that if an artificial iris is not used, the aperture radius a must then apply to the actual iris which is a short distance beyond the cornea. However, the radius to use in Eq. (5) will not be the true radius of the iris, but will be the radius of a circle on the cornea which appears to coincide with the virtual image of the iris as seen from a point on the visual axis at a great distance from the cornea. If one measures the radius of another individual's iris by placing a scale at the surface of his cornea

* This test object is usually called a "grating" in the literature of vision but it should not be confused with a diffraction grating. However, if it consists of alternate opaque and transparent strips on a glass plate such as Shlaer used, it does have the properties of a diffraction grating for certain kinds of illumination. The grating used by the writer consisted of a series of equally spaced parallel black strips painted on a white diffuse reflecting surface.

[11] H. Hartridge, J. Physiol. 52, 175–246 (1918–19).

* Unless otherwise stated, all angles appearing in equations will be in radian measure, or in the reduced angular units of z. Numerical values of angles appearing in figures and in the text will be in minutes or degrees.

the above condition is approximately satisfied, and the apparent radius gives the correct value of a to use in Eq. (5). This point is discussed in more detail in Appendix II.

Equation (4) is plotted in Fig. 1 (curve A) with I/I_0 shown as a function of ϕ for a wave-length of 0.555 micron and 2.43-mm iris. This curve, which represents the intensity in the diffraction pattern, is actually half a diametric cross section of a diffraction surface. The central bright disk covers about 10 of the foveal cones. The spread of the diffraction pattern increases with wave-length, so this curve may be regarded as the approximate average distribution of intensity for white light.

An extended self-luminous source of light may be regarded as composed of an infinite number of point sources each giving an intensity distribution on the retina, the half cross section of which is identical to that shown by curve A in Fig. 1. For any given test object these patterns will overlap, and thus build up an image which is a fairly accurate replica of test objects of larger angular diameter, but which for small angular diameters may have little resemblance to the test object. The distribution of light in the "physical image" will differ from that in the "geometric image" which does not actually exist, or which may be regarded as the limiting form assumed by the physical or retinal image as the angular dimensions of the test object are increased without limit.

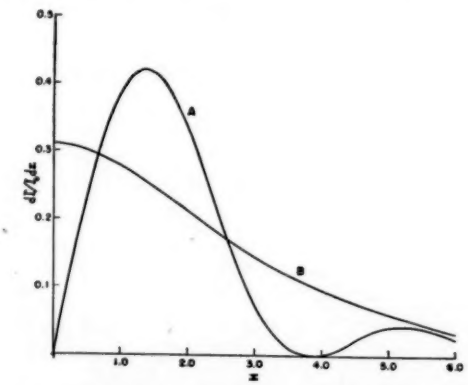

FIG. 2. The ordinates of curve A represent relative illumination at a point in the image of a screen contributed by a zone in the screen of reduced angular radius z. B is a similar curve computed from the chromatic aberration distribution [Eq. (11-b), Appendix III]. The ordinates of these curves may also be interpreted as the relative flux received by a zone of reduced angular radius z in the image of a point source of light.

Consider an observer who has his attention directed on a distant luminous screen of uniform brightness. For any given point P_0 in the screen there will be a corresponding point P_r in the image of the screen on his retina. It may be assumed that the light incident on P_r comes from a large number of circular zones in the screen which have P_0 as a center. The element of illumination dI at P_r contributed by any given zone in the screen of reduced angular radius z and width dz is

$$dI = KI_b \cdot \frac{4}{z^2} J_1^2(z) \cdot 2\pi z dz, \tag{6}$$

where K is a constant and I_b would be the illumination at P_r if the screen were of uniform brightness and infinite in extent. If a black disk is placed in front of the screen with P_0 at the center of the disk, the retinal illumination I at P_r is then given by the integral

$$I = 8\pi K I_b \int_{z_r}^{\infty} \frac{J_1^2(z)}{z} dz, \tag{7}$$

where z_r is the reduced angular radius of the disk. When Eq. (7) is integrated[12] the equation for the illumination at the center of the image of the disk is

$$I = 4\pi K I_b \{J_0^2(z) + J_1^2(z)\},$$

where $J_0(z_r)$ is the Bessel function of the first kind of order zero. If the disk is shrunk to a point, $z_r = 0$ and $I = I_b$, hence $K = 1/4\pi$. The illumination can therefore be written

$$I = I_b \{J_0^2(z_r) + J_1^2(z_r)\}, \tag{8}$$

and the fraction I/I_b can be found readily from tables of $J_0(z_r)$ and $J_1(z_r)$. The illumination at the center of a white disk on a black screen can be found by integrating Eq. (6) from 0 to z_r, thus giving

$$I = I_b \{1 - J_0^2(z_r) - J_1^2(z_r)\}, \tag{9}$$

which is complementary to Eq. (8).

[12] Andrew Gray, G. B. Mathews, and T. M. MacRobert, *A Treatise on Bessel Functions and their Application to Physics* (Macmillan and Company, London, 1931), pp. 178–221.

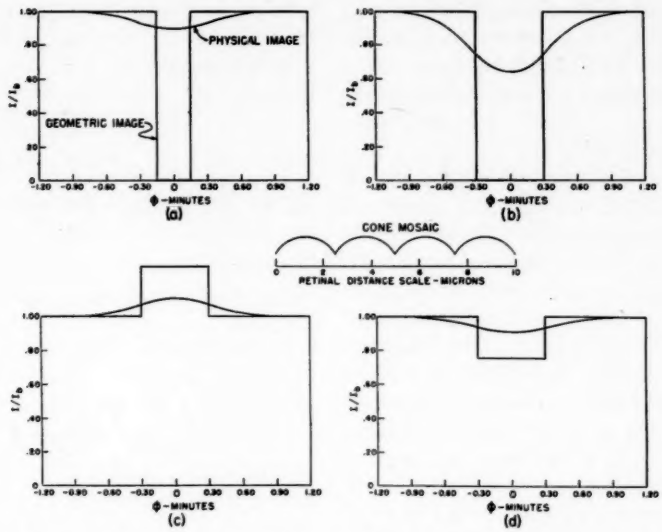

FIG. 3. Retinal image curves for 4 simple test objects: (a) threshold curve for a black disk on a white ground; (b) a supra-threshold curve for a black disk on a white ground; (c) a threshold curve for a white disk on a grey ground ($H>H_b$); and (d) a threshold curve for a grey disk on a white ground ($H<H_b$).

Equation (6) can be written as

$$\frac{dI}{I_b dz}=\frac{2}{z}J_1^2(z), \tag{10}$$

which gives the relative illumination at P_r contributed by any zone of reduced angular radius z. The quantity $dI/I_b dz$ is plotted as a function of z in Fig. 2, curve A. Certain zones in the screen contribute nothing to the illumination at P_r and the maximum contribution is made by the zone $z=1.35$ (or $\phi=0.34$ minute). Curve B is a similar curve computed on the assumption that chromatic aberration is the only cause of retinal image blurring (Appendix III). The ordinates of each of these curves may be interpreted also as the relative flux received by any given zone in the image of a point source of light. Since the total flux in the image is the area under either curve and since this must be independent of flux distribution, the area under both curves from $z=0$ to $z=\infty$ must be equal to unity.

If the test object is not in the form of a disk, the illumination at the center of the object cannot be determined by Eqs. (8) and (9). This is true also for a disk test object if P_r is not at the center of the image of the disk. In polar coordinates the general equation for determining I for any point in the retinal image for any given test object viewed against a self-luminous screen of finite extent is

$$I=\frac{I_b}{\pi}\int_A \theta\frac{J_1^2(z)}{z}dz, \tag{11}$$

where θ is the total angle subtended at P_0 by those parts of a zone of width dz not cut out by the test object. The integral is taken over the whole area of the screen or background. For most objects θ is a rather complicated function of z which is not necessarily continuous over the whole screen. The integration can best be performed by numerical or graphical methods, but the details of this procedure need not be given here. For a disk test object, a smooth curve drawn through plotted values of I represents the illumination in various parts of a diametric cross section of the retinal image. For non-symmetric objects, the nature of the cross section curves will depend on the direction in which they are taken. Figures 3(a) and 3(b) show the retinal image curves for a 2.43-mm pupil and a wave-length of 0.555 micron for black disks with angular radii

of 0.16 minute and 0.32 minute ($z_r=0.64$ and 1.28). Figures 3(c) and 3(d) show similar curves for a white disk on a grey background and a grey disk on a white background; the angular radius of both disks is 0.32 minute and the object background contrast v is 0.75.

The calculation of I from Eq. (11) requires considerable labor and this equation should be used only for those test objects for which the integral cannot be evaluated directly. Fortunately, it can be evaluated for three of the most useful objects used in visual acuity measurements, namely, a single black line on a luminous background, two parallel white lines on a black background, and a grating consisting of alternate black and white bars. The distribution function for these objects can be found by a modification of the equation which Struve[12, 13] derived for the distribution of intensity in the image of a straight border separating a white and black area. The rectangular coordinates η and ξ of an element of area $d\eta d\xi$ in the image (on the white side of the border) are parallel and perpendicular, respectively, to the border separating the black and white areas and are measured from some point P in the image. The intensity at the point P is proportional to the integral

$$\frac{2}{\pi}\int_{\xi_b}^{\infty}\int_{0}^{\infty}\frac{J_1^2(x)}{x^2}d\eta d\xi,$$

where

$$x=\frac{2\pi a}{\lambda}\frac{\zeta}{F}$$

and

$$\zeta^2=\eta^2+\xi^2.$$

Upon evaluating this integral, Struve obtained for the illumination at P,

$$I=I_bS(z), \tag{12}$$

where I_b is the illumination in the image at a great distance from the border on the white side and the function $S(z)$ is defined by the series

$$S(z)=\frac{1}{2}-\frac{2}{\pi^2}\left\{\frac{3}{1}\frac{2^2z}{1^2\cdot3^2}-\frac{5}{3}\frac{2^4z^3}{1^2\cdot3^2\cdot5^2}+\frac{7}{5}\frac{2^6z^5}{1^2\cdot3^2\cdot5^2\cdot7^2}-\cdots\right\}. \tag{13}$$

[12] Lord Rayleigh, "Wave theory of light," *Encyclopedia Britannica*, 9th ed., **24**, 421–459 (1878).

The reduced angular distance z of the point P from the border is related to the linear distance ξ_b by the equation

$$z=\frac{2\pi a}{\lambda}\frac{\xi_b}{F}=\frac{2\pi a}{\lambda}\phi. \tag{14}$$

On the black side of the border z is positive and on the white side negative. From Eq. (13) it follows that

$$S(z)+S(-z)=1, \tag{15}$$

which means that if a second white area equal in brightness to the first area were placed in contact

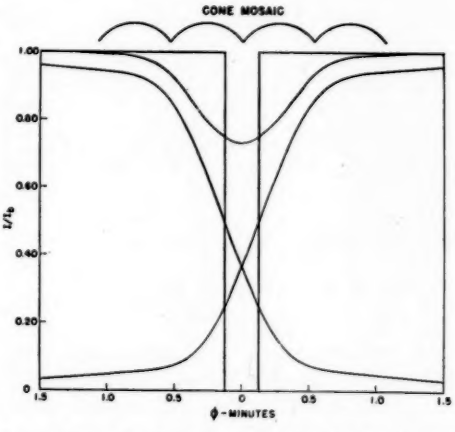

FIG. 4. The distribution of illumination in the retinal image of a straight black line on a white background may be regarded as the resultant of the illumination distributions for the images of the borders of two white areas not quite in contact.

with the first area, the illumination in the image would be uniform throughout. However, if the areas are not in contact but are separated by a reduced angular distance z_w, the resultant distribution of illumination in the retinal image would be equivalent to that for a black line, and from Fig. 4 it can be seen that I would be given by the equation

$$I=I_b\{S(z)+S(z_w-z)\}, \tag{16}$$

where I_b is the retinal illumination when the surfaces are in contact, that is, when the line is missing. Equations to be given later based on Eq. (16) are simplified if the origin is shifted to

the center of the line by making the substitution

$$t+z_0=z,$$

where z_0 is the half-width of the line and is equal to $z_w/2$. Equation (16) thus becomes

$$I=I_b\{S(z_0+t)+S(z_0-t)\}. \qquad (17)$$

The retinal image curve for a black line of any given width can be readily found from Eq. (16) or (17). The curve in Fig. 4 shows the distribution of illumination for a 2.43-mm pupil in the image of a line 0.25 minute wide, and illustrates how the curve may be regarded as the resultant of the two S curves.

If a white line of reduced angular width $2z_0$ were placed in the gap between the two white surfaces represented in Fig. 4, the resulting illumination in the retinal image would be constant and equal to I_b, provided the line were of the same brightness as the bordering areas. This means that the intensity distribution curve for a black line on a white background and the corresponding curve for a white line of equal width on a black background are complementary, and from Eq. (16) it follows that the distribution function for a white line of reduced angular width $2z_0$ is

$$I=I_b\{1-S(z_0+t)-S(z_0-t)\}$$
$$=\frac{2I_b}{\pi^2}\{\psi(z_0+t)+\psi(z_0-t)\}, \qquad (18)$$

where the function ψ represents the function defined by the series within the braces in Eq. (13). When $t=0$, $I=I_0$ where I_0 is the illumination at the center of the image of the white line, hence

$$I_0=\frac{4I_b}{\pi^2}\psi(z_0),$$

and Eq. (18) may be written in the alternate form

$$I=\frac{I_0}{2\psi(z_0)}\{\psi(z_0+t)+\psi(z_0-t)\}. \qquad (19)$$

Equation (19) can be verified by letting the angular width of the line become very small in comparison with the angular diameter of the basic diffraction disk. Denoting the reduced angular half-width of the line by δz_0, the general terms in the series for $\psi(\delta z_0+t)$ and $\psi(\delta z_0-t)$ are

$$\frac{(-1)^n 2^{2n+2}(\delta z_0+t)^{2n+1}}{1^2\cdot 3^2\cdot 5^2\cdot\cdots\cdot(2n-1)^2(2n+1)^3(2n+3)}$$

and

$$\frac{(-1)^n 2^{2n+2}(\delta z_0-t)^{2n+1}}{1^2\cdot 3^2\cdot 5^2\cdot\cdots\cdot(2n-1)^2(2n+1)^3(2n+3)}.$$

Expanding $(\delta z_0+t)^{2n+1}$ and $(\delta z_0-t)^{2n+1}$ by the binomial theorem and adding the two general terms gives (after dropping powers of δz_0 higher than the first)

$$\frac{(-1)^n 2^{2n+3}t^{2n}\delta z_0}{1^2\cdot 3^2\cdot 5^2\cdot\cdots\cdot(2n+1)^2(2n+3)}.$$

Forming a new series by letting n take the values $n=0, 1, 2, 3, \cdots n$, and dividing by

$$2\psi(\delta z_0)=2\left\{\frac{3}{1}\frac{2^2\delta z_0}{1^2\cdot 3^2}\right\}$$

gives the new distribution function

$$I=3I_0L(t),$$

where

$$L(t)=\frac{1}{1^2\cdot 3}-\frac{2^2t^2}{1^2\cdot 3^2\cdot 5}+\frac{2^4t^4}{1^2\cdot 3^2\cdot 5^2\cdot 7}$$
$$-\frac{2^6t^6}{1^2\cdot 3^2\cdot 5^2\cdot 7^2\cdot 9}+\cdots. \qquad (20)$$

This distribution function is identical with that given by Rayleigh[13] for a self-luminous line of infinitesimal width. The ratio I/I_0 for a thin white line is shown in Fig. 1, curve B. It differs from the distribution for a point source in that the intensity is nowhere zero, although it passes through definite maxima and minima.

The distribution function for a grating can be readily derived from Eq. (18). The intensity at any given point P in a grating consisting of n self-luminous lines, each of reduced angular half-width z_0, is the sum of the intensities contributed at this point by each line. If the width of the interspaces is equal to the width of the lines, the intensity contributed at the point P by the nth line to the left of the central or 0th line is

$$I=\frac{2I_b}{\pi^2}\{\psi(z_0+t+4nz_0)+\psi(z_0-t-4nz_0)\}, \qquad (21)$$

and the intensity contributed by the nth line to the right of the central line is

$$I=\frac{2I_b}{\pi^2}\{\psi(z_0+t-4nz_0)+\psi(z_0-t+4nz_0)\}. \quad (22)$$

Summing up the intensity for all lines gives a rather involved equation for I, but it reduces to simpler expressions at the centers of the lines and the centers of the interspaces where I has its maximum and minimum values. At the center of a line $t=0$ and the maximum intensity ratio may be written

$$\frac{\pi^2}{4}\frac{I_{\max}}{I_b}=\psi(z_0)+\psi(-3z_0)+\psi(5z_0)$$
$$+\cdots\psi\{-(4n-1)z_0\}+\psi\{(4n+1)z_0\}. \quad (23)$$

At the center of an interspace $t=2z_0$ and the minimum for I/I_b is

$$\frac{\pi^2}{4}\frac{I_{\min}}{I_b}=\psi(-z_0)+\psi(3z_0)+\psi(-5z_0)$$
$$+\cdots\tfrac{1}{2}\psi\{-(4n+1)z_0\}+\tfrac{1}{2}\psi\{(4n+3)\}. \quad (24)$$

These equations are sufficient for calculating the retinal contrast u in the image of a grating (see Appendix I). If the width of the lines and the width of the interspaces of a grating are not equal, the quantity $4nz_0$ in Eqs. (21) and (22) is replaced by the expression $2n(z_0'+z_0)$ where z_0' is the reduced angular half-width of the interspace. Calculation of intensities is not much more difficult than when z_0 and z_0' are equal. The reduced angular distance t is always measured from the center of the 0th line.

VISUAL ACUITY

If visual acuity is a phenomenon of retinal illumination discrimination, one might expect that for any given brightness level, the retinal threshold contrast u_t should be the same for all test objects. The retinal contrast for a black disk on a white background can be obtained by combining Eqs. (2) and (8) which results in

$$u=1-J_0^2(z_r)-J_1^2(z_r). \quad (25)$$

For a black line this equation becomes

$$u=1-2S(z_0)=\frac{4}{\pi^2}\psi(z_0). \quad (26)$$

However, if the threshold values of z_r and z_0 are determined experimentally, the corresponding retinal threshold contrast u_t will not be the same for both objects. For the disk it is about 0.10 and for the line about 0.02 when the angular diameter of the backgrounds is about 0.20 minute.

The intensity discrimination problem can be approached in another way. The intensity distribution functions derived thus far are valid only for black objects on white backgrounds or vice versa. However, these functions can be generalized to give the intensity distribution in the retinal images of grey objects on white backgrounds or white objects on grey backgrounds, which is always the situation when distant objects are viewed through the atmosphere. For a grey test object of brightness H seen against a white background of brightness H_b there will be corresponding illuminations I and I_b in the retinal image. By assuming that a grey object of brightness H viewed against a white ground of brightness H_b is equivalent to a black object on a background of brightness H_b-H upon which a luminous but perfectly transparent film of brightness H has been superimposed, it is possible to write the general distribution Eq. (11) in the form

$$I=I_b\left\{\frac{H}{H_b}+\frac{H_b-H}{H_b}\frac{1}{\pi}\int_A\theta\frac{J_1^2(z)}{z}dz\right\}, \quad (27)$$

which when combined with Eqs. (1) and (2) gives

$$u=v\left\{1-\frac{1}{\pi}\int_A\theta\frac{J_1^2(z)}{z}dz\right\}. \quad (28)$$

This equation expresses the retinal contrast u directly in terms of the object-background contrast v. Assume that the integral in Eq. (28) can be expressed as a power series in terms of z_a where z_a is some arbitrarily chosen angular dimension (in reduced angular units) of the test object. If this is true then the integral can also be expressed as a power series in terms of the angular unit α (either in minutes or in radians) corresponding to z_a. Assume the series to be of the form

$$1-A\alpha-B\alpha^2+C\alpha^3+D\alpha^4-\cdots$$

which when substituted in Eq. (28) gives

$$u=v(A\alpha+B\alpha^2-C\alpha^3-D\alpha^4+\cdots). \quad (29)$$

For the disk and line test object it is convenient to set α equal to their angular diameter, so for these objects, z_a will be equal to $2z_r$ and $2z_0$, respectively. Equation (29) is valid for white objects on a grey background, because a similar derivation for these objects gives the same equation. However, the equation in this form is valid only for individual objects on a uniform background and can be applied to a complex test object such as the grating only when v is unity.

The coefficients of α can be readily determined

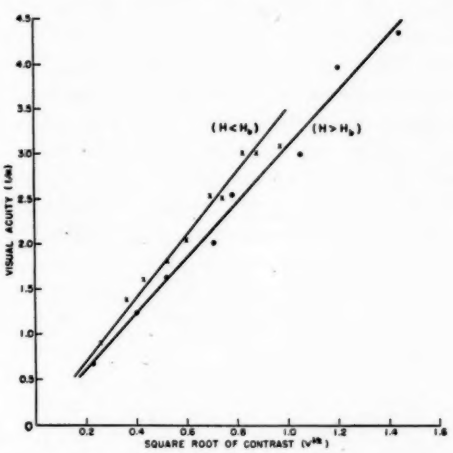

FIG. 5. Measured values of visual acuity for disks plotted as a function of the square root of the contrast. Data are shown for grey disks on a white background ($H<H_b$), and for white disks on a grey background ($H>H_b$). Each point is the average of 5 observations.

for those objects for which the integral in Eq. (28) can be evaluated. Equation (26) shows that the coefficients of the even powers of α are missing for the line test object and Eq. (29) thus becomes

$$u=v(A\alpha-C\alpha^3+E\alpha^5-G\alpha^7+\cdots). \quad (30)$$

When α is expressed in minutes the equation for u is

$$u=v(1.081\alpha-0.096\alpha^3+0.105\alpha^5-\cdots), \quad (31)$$

which can be used for values of α up to 0.7 minute.

Assuming that visual acuity is determined by illumination discrimination, the threshold value of u should be constant for any given brightness level even though v takes on different values. Denoting this value by u_t and since α is very small at threshold, powers of α higher than the first can be neglected and Eq. (30) becomes

$$u_t/A=v\alpha. \quad (32)$$

Visual acuity is conventionally defined as the reciprocal of the angle α where α is expressed in minutes. If α_0 is the value of α when v is unity (this occurs when $H=0$ or $H=2H_b$) Eq. (32) may be written in the visual acuity form*

$$1/\alpha=(1/\alpha_0)v. \quad (33)$$

An analogous equation can be derived for a disk test object. Expanding $J_0^2(z_r)+J_1^2(z_r)$ in Eq. (25) shows that for a disk the coefficients of the odd powers of α are missing and Eq. (29) becomes

$$u=v(B\alpha^2-D\alpha^4+F\alpha^6-H\alpha^8+\cdots). \quad (34)$$

If α is small at threshold, powers of α higher than the second can be neglected and the visual acuity equation is

$$1/\alpha=(1/\alpha_0)v^{\frac{1}{2}}. \quad (35)$$

If written in terms of the solid angle τ subtended by a test object, Eq. (35) holds for objects in the shape of squares, triangles, or any other shape such that near the limit of the visual range the object appears to be a formless spot. The equation in terms of τ is

$$1/\tau=(1/\tau_0)v. \quad (36)$$

Both Eqs. (35) and (36) may be regarded as generalized forms of the inverse square law.

Figure 5 shows measured values of visual acuity $1/\alpha$ plotted as a function of $v^{\frac{1}{2}}$; data are for grey disks on a white background and white disks on grey backgrounds. Figure 6 shows similar data for line test objects. These measurements are in good agreement with theory but

* By combining the air-light equation of Koschmieder (see references 4 and 5) with Eq. (33) it is possible to predict the visual range of a small smoke column with considerable accuracy.

show one peculiarity that was not predicted by Eqs. (33) and (35), namely, that $1/\alpha_0$ for $H>H_b$ is less than for $H<H_b$. For the disks the data also show that Eq. (35) holds for values of α considerably larger than could be expected when

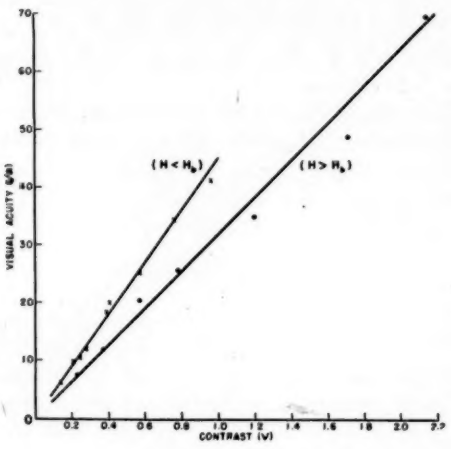

FIG. 6. Measured values of visual acuity for lines plotted as a function of the contrast. Data are shown for grey lines on a white background ($H<H_b$), and for white lines on a grey background ($H>H_b$). Each point is the average of 2 observations.

the higher powers of α are neglected in Eq. (34). This means that u_t is a function of α and decreases with increasing area of the retinal image in such a manner that at threshold the retina seems to require a constant flux differential rather than a constant illumination differential. It would thus appear that visual acuity, for the disk at least, is not determined entirely by illumination discrimination. Most investigators have assumed that the decrease in visual thresholds with increasing area demonstrates summation among the receptors. However, it will be shown in a later paper that the area-threshold effect is probably owing to fluctuations in the energy content of the visual stimulus.

Visual acuity is much greater for lines than for disks except for small values of v. All of the measurements shown in Figs. 5 and 6 were made outdoors with H_b kept constant at about 1200 millilamberts.

The angular diameter of the background against which a test object is seen has considerable effect on visual acuity. Figure 7 shows $1/\alpha_0$ for a black disk viewed on white backgrounds of various diameters. For the data in Figs. 5 and 6 the angular diameter of the backgrounds was about 22 minutes for the disks and about 18 minutes for the lines. It is well known that for photopic vision, visual acuity decreases rapidly with the angular distance of the image from the center of the fovea. Figure 8 shows visual acuity for a black disk on a white background plotted as a function of the angular distance of the image from the fovea.

The value of u_t (about 0.02) in Eq. (31) for individual lines at threshold is about the same as u_t, or $\Delta I/I$, for an extended bipartite field, although for both of these objects[8,14] u_t can be as low as 0.01 for large areas and backgrounds under the most favorable illumination. If the contrast v between a line and its background is gradually decreased, and if the angular diameter α of the line is at the same time increased in such a manner as to keep u equal to u_t, then α will ultimately become very large and the power series in Eq. (30) will approach unity. For a

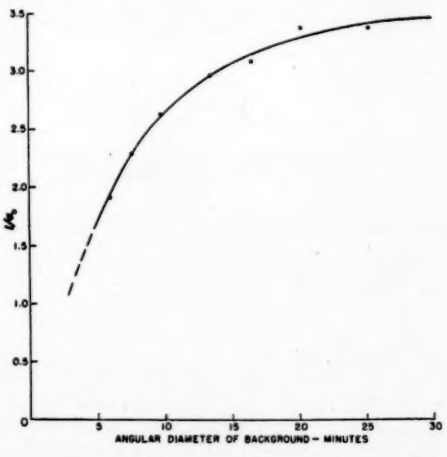

FIG. 7. The relation of visual acuity (measured for a black disk on a white background) and the angular diameter of the background.

very wide line Eq. (30) thus reduces to Weber's law in which $u_t=v_t=$ a constant.

The power series in Eq. (34) also approaches unity as $\alpha\rightarrow\infty$ and for large disk test objects

[14] Jacinto Steinhardt, J. Gen. Physiol. 20, 185–209 (1936).

this equation also reduces to Weber's law, although in this instance u_t will not remain constant when the angular diameter of the disk is increased without limit. For values of α between 0.3 and 1.0 minute, u_t is approximately 0.10, but for larger values of α, u_t gradually decreases and approaches 0.02 when α is very large.

There is also some evidence that visual acuity is not determined entirely by illumination discrimination for the grating test object. For the grating and for two parallel lines on a black background, u may be defined as

$$u=\frac{I_{\max}-I_{\min}}{I_{\max}}, \qquad (37)$$

where $I_{\max}$ and $I_{\min}$ are given in Eqs. (23) and (24). In determining u for the grating, n may be set equal to unity in Eqs. (23) and (24) because in visual acuity measurements z_0 is not small enough for lines other than those adjacent to the central line to have any appreciable effect on the contrast ratio. The retinal contrast in the image of a grating can be varied by altering the relative width of the bright and dark lines which is equivalent to changing the z_0'/z_0 ratio. Using a 2.0-mm artificial pupil, Shlaer[7] measured the visual acuity for three different gratings for which the ratio z_0'/z_0 was 1, 1/3, and 1/7. All gratings had the same number of lines per cm, and for the reciprocal of the angular distance between the centers of adjacent lines Shlaer obtained the visual acuity values 1.86, 1.84, and 1.75. The contrast v was unity for all gratings.

TABLE I. The retinal threshold contrast u_t for the visual acuity shown is given for three different gratings with different line-interspace, or z_0'/z_0, ratios. Computations of u_t were made from the data of Shlaer (reference 7).

z_0'/z_0	Visual acuity	u_t
1	1.86	0.133
1/3	1.84	.081
1/7	1.75	.062

Because of the small variation in visual acuity with the comparatively large variation in the relative width in the white and dark lines, Shlaer concluded that intensity discrimination was not the limiting factor in grating resolution and his calculations of retinal contrast based on Hartridge's chromatic aberration blurring theory seemed to support this conclusion. However, a somewhat different result is obtained if one computes the retinal threshold contrast for the

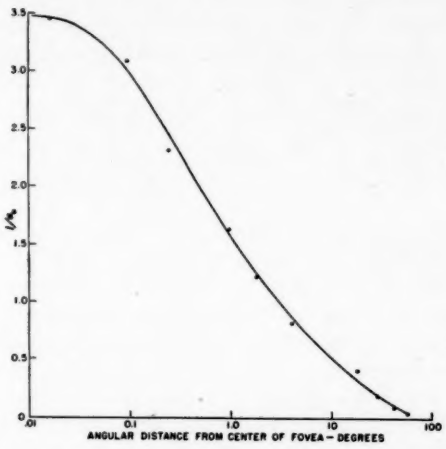

FIG. 8. The visual acuity for a black disk on a white background when the image falls on the outer retina; $1/\alpha_0$ is plotted as a function of the angular distance of the image from the center of the fovea.

three gratings from Eq. (37). Table I shows u_t for each of the three gratings as computed from Shlaer's data. Since a foveal cone is about 0.5 minute in angular diameter, the actual percentage difference in illumination on adjacent rows of cones would probably be about two-thirds as great as the values shown in the u_t column, or roughly 0.09, 0.06, and 0.04. These values are much smaller than those given by Hartridge's theory. It does appear that u_t decreases with the z_0'/z_0 ratio but since only a small change in the angular distance between the centers of adjacent grating lines can make a large change in u, the variation in u_t may not be significant. If corrections had been made for chromatic aberration, the values of u_t (for white light) would be slightly smaller than shown in Table I.

The retinal contrast in the image of a grating can be varied by changing the wave-length of light by which the grating is viewed. Shlaer, Smith, and Chase[9] obtained grating visual acuity data for different wave-lengths at high brightness levels which makes it possible to test the brightness discrimination criterion in a different way.

TABLE II. The product of visual acuity and wave-length, $(1/\alpha)\lambda$, is shown for different wave-lengths. Computations were made from the data of Shlaer, Smith, and Chase. The last column shows $\Delta I/I$ for a bipartite field for different wave-lengths; the data are those of Hecht, Peskin, and Patt (reference 15).

λ (microns)	$1/\alpha$	$(1/\alpha)\lambda$	$\Delta I/I$
0.670	1.80	1.21	0.129
.625	1.91	1.21	—
.605	1.99	1.20	.114
.575	2.08	1.20	.116
.555 ("white" light)	2.10	1.16	—
.535	2.14	1.14	.125
.490	2.11	1.03	—
.450	2.07	.93	.138

Using a grating with v and z_0'/z_0 equal to unity and making their observations through a 2.3-mm pupil, they found that (with the exception of blue and violet) visual acuity improves with decreasing wave-length. If one assumes that u_t is independent of wave-length and that visual acuity is determined by illumination discrimination, then u_t should be the same for all wave-lengths. From Eqs. (23), (24), and (37) it thus follows that $\psi(z_0)$, $\psi(-3z_0)$, and so on, should each be the same for all wave-lengths. This can be true only if z_0 is the same for all wave-lengths, but at threshold

$$z_0=\frac{2\pi a}{\lambda}\frac{\alpha}{2},$$

where α is the angular distance between the centers of adjacent lines. Since z_0 is assumed to be constant, the visual acuity $1/\alpha$ should be related to the wave-length λ by the equation

$$(1/\alpha)\lambda=a \text{ constant}. \tag{38}$$

Table II shows the product of visual acuity and wave-length in different parts of the spectrum.[9] Intensity discrimination seems to be a decisive factor in visual acuity for wave-lengths above 0.555 micron, because the product of visual acuity and wave-length is nearly constant. In the blue, green, and violet, u_t is apparently a function of wave-length so Eq. (38) is not valid in this part of the spectrum, although it seems probable that visual acuity is determined by intensity discrimination in the shorter wave-lengths in the same way as for the longer wave-lengths. If u_t increases toward the violet end of the spectrum, one would expect a similar increase in $\Delta I/I$ for a bipartite field. Such measurements have been made by Hecht, Peskin, and Patt[15] and are shown in the last column of Table II. Their results show a slight increase in $\Delta I/I$ for the shorter wave-lengths, but the increase may not be significant. The large values of $\Delta I/I$ which these observers obtained were owing to the short interval of time (1/25 of a second) that the bipartite field was observed.

For the actual solution of practical problems involving different kinds of test objects, it is sometimes more convenient to write the visual acuity equation in the form

$$1/\alpha=\phi(v/u_t), \tag{39}$$

and determine $\phi(v/u_t)$ experimentally rather than attempt to determine its analytical form. The function $\phi(v/u_t)$ is different for each test object, but it can be determined easily from observations of $1/\alpha$ for different values of v. This equation has one disadvantage in that $\phi(v/u_t)$ must in general be a function of retinal illumination, although this is of little consequence for daylight observations of distant objects since u_t is almost independent of retinal illumination when the illumination is high.

If one moves away from a line or disk test object of a given diameter viewed against a uniform background, he will notice that as the threshold is approached the object fades from view rather slowly and over a considerable distance he cannot be sure whether the object is visible or not. If a grating consisting of alternate black and white lines is viewed in the same manner, the lines will be plainly visible until the threshold is approached and then they will disappear rather suddenly. Two thin white lines viewed against a dark grey background behave in much the same way. The reason for this becomes apparent if one expresses the retinal contrast u for two bright lines (parallel and of infinitesimal width) on a black background as a power series in terms of α. This yields an equation similar to (34) in which the coefficients of the odd powers of α are missing. However, for this object the higher powers of α cannot be neglected

[15] Selig Hecht, J. C. Peskin, and M. Patt, J. Gen. Physiol. 22, 7–19 (1938).

near the threshold and even the α^4 and α^6 terms make appreciable contribution to the value of the series. This means that the interspace between two parallel bright lines on a dark background or the lines in a grating will disappear much more rapidly than an individual line or disk on a uniform background. This is shown in Fig. 9 in which the retinal contrast u is plotted as a function of α (on logarithmic scales) for a disk, line, and grating. Shlaer[7] attributes the sudden disappearance of the grating lines to the finite nature of the retinal mosaic. An experiment to be described in the second part of this paper indicates that this is also a factor but that its effect probably is much less than that owing to the large rate of change of u with respect to log α as the threshold is approached. One can verify this by observing a grating through a circular 0.5-mm aperture through which the abrupt disappearance of the lines is even more noticeable than for normal apertures although any one of the illumination gradients in the image extends over about 5 rows of cones.

Hartridge,[6] Shlaer,[7] and Hecht and Mintz[8] used Abbe's diffraction theory[10,16] of microscopic vision to account for the limiting values obtained in grating resolution for different sizes of aperture. According to this theory, a periodic grating structure illuminated by plane waves (the fronts of which are parallel to the grating) will not be visible unless the aperture transmits the 0th and the two first-order spectra formed by the grating, the plane of the aperture being parallel to the plane of the grating. If the grating is tilted at an angle between 0 and θ with respect to the aperture such that $\sin\theta=\lambda/d$ where d is the grating interval, then the transmission of the 0th and only one first-order spectrum is required for resolution. Abbe's theory applies primarily to the resolution of objects of periodic structure illuminated by plane waves of monochromatic light, so is not valid when the object is self-luminous or nearly so. Since most gratings in visual acuity observations are illuminated in such a way that they are in effect self-luminous, Rayleigh's general treatment[10] of grating resolution (which includes Abbe's theory as a special case) is more suitable.

[16] A. B. Porter, Phil. Mag. **11**, 154–166 (1905).

There is one marked difference between the curves in Fig. 9. For individual lines or disks on an extended background, u vanishes only when $\alpha=0$, but for two parallel lines or for a grating, u vanishes for finite values of α. This difference may be taken as the distinction between perception acuity and resolving power acuity. The distinction is somewhat artitrary because it is possible to construct test objects for which u can be made to vanish for any value of α (at least up to 3 or 4 minutes). Such objects will have the properties of both perception and resolving power acuity.

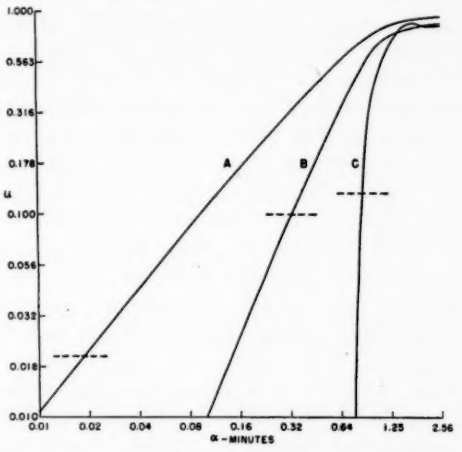

FIG. 9. The retinal contrast u for a 2.43-mm pupil is shown as a function of α on a double log scale for three different test objects: A, a black line on a white background; B, a black disk on a white background; and C, a grating in which the width of the bright lines is small compared with the width of the black interspace. For the black line and disk, α is their angular diameter, and for the grating lines α is one-half their angular separation. The threshold contrast u_t for each object is shown by the horizontal dotted line.

Although Eqs. (28) to (32) were derived from a diffraction theory of the blurring of retinal images, blurring owing to other causes could have led to similar equations. This is shown by the data in Fig. 10 which gives the visual acuity for grey disks on a white background for a near-sighted observer with and without his glasses, and indicates that for such an observer Eq. (28) should be written

$$u=v\left\{1-K\int_A\theta F(z)zdz\right\}, \qquad (40)$$

where $F(z)$ is an intensity distribution function with a greater spread than the distribution function of Eq. (4). The constant K is given by the equation (see Appendix III)

$$\frac{1}{K}=2\pi\int_0^\infty F(z)z\,dz.$$

The spread of the function $F(z)$ does not affect resolving power acuity and perception acuity in the same way. For perception acuity, u will vanish only when $\alpha=0$, regardless of the spread of $F(z)$. This means that an observer with slight ocular defects may still have good perception acuity provided his retina is sufficiently sensitive, that is, if he has a sufficiently low value of u_t. For resolving power acuity this is not true. Any increase in the spread of the distribution function will cause u to vanish at correspondingly higher values of α, and this loss cannot be compensated for by a sensitive retina. This was brought out clearly by the observer who furnished the data in Fig. 10. With glasses his visual acuity was above average for lines and disks, but slightly below average for a grating. From these experiments one might conclude that this observer had a highly sensitive retina, but that his resolving power acuity was reduced somewhat by residual aberrations which his glasses did not correct. This has an important bearing on tests for critical vision, because the most suitable test will depend on the visual task which an observer is to perform. Forest fire lookout men are expected to see very small objects (distant smokes) against a fairly uniform haze background, so for these men visual acuity is determined[17] for a small black spot on a white background rather than for letters on the usual Snellen type chart. The latter is more similar to the parallel line resolving power test. However, an observer with a high visual acuity rating for one test usually has a correspondingly high rating for the other.

The effect of retinal sensitivity on perception acuity may throw some light on the unusual visual powers which birds of prey are supposed to possess. If one assumes that the retina of a vulture or bird of prey is several times as sensitive as that of a man, it is conceivable that these birds could see small animals and insects at great distances because their perception acuity would be very high. However, it is doubtful whether their resolving power acuity is any better than, if as good as, that of a man because of the small dimensions of these birds' eyes. Physiologists estimate that the foveal cones in a hawk's eye are less than one-half the diameter of those in the human eye, but any advantage of small cone size probably is offset by the small dimension of the bird's eye and the ratio of cone diameter to diffraction disk diameter is about the same as for the human eye. Motion is undoubtedly an important factor in the vision of birds of prey, because from a height of 600 feet a small mouse should appear as an almost imperceptible blur not distinguishable from any other motionless object of similar size and brightness.

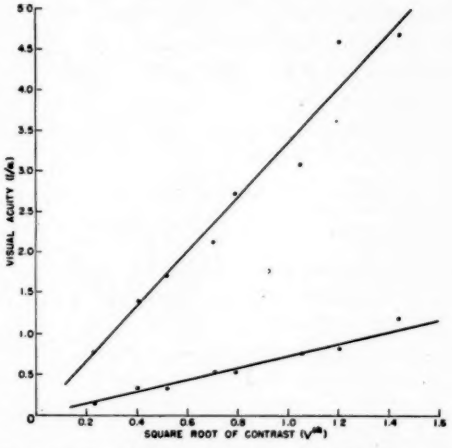

FIG. 10. Visual acuity for a near-sighted observer with and without his glasses determined for white disks on a grey background.

The validity of all of the equations for the distribution of light in retinal images based on diffraction blurring depends on three conditions: (1) diffraction is of the Fraunhofer class and the distribution of light in the image of each point source of light in the test object is given by Eq. (4); (2) the test object and its background must be self-luminous; (3) blurring owing to chromatic and monochromatic aberration is small compared with blurring owing to diffraction.

[17] G. M. Byram, Fire Control Notes **4**, 123–128 (1940).

In observing diffraction phenomena of the Fraunhofer class, the optical system is usually so arranged that plane waves fall upon the diffracting aperture and by means of a lens directly behind the aperture are focused on a screen. This arrangement is equivalent to a system without lenses in which both source and screen are at infinity. However, in the eye a large part of the refraction takes place at the cornea and the wave fronts reaching the iris diaphragm are concave rather than plane, and it is sometimes stated that an arrangement of this sort yields a diffraction pattern which differs from that obtained when an artificial iris is placed in front of the cornea. However, it can be shown (Appendix II) that the form of the pattern is identical in both instances.

The second assumption upon which the validity of the distribution equation depends is that if the test object is black, its background must be self-luminous, or if the background is black, the object (or objects) must be self-luminous. A self-luminous object is one in which all elements of its area radiate as independent sources and there is no permanent phase relation between the radiations coming from different elements of area. This condition is probably satisfied in almost all problems of ordinary vision, but not necessarily for certain observations with optical instruments, especially the microscope. Rayleigh[10] showed that the distribution of intensity in the images of gratings and individual black lines viewed against luminous backgrounds depended on the phase relations existing between different parts of the luminous background. For a transmission grating illuminated by plane waves at perpendicular incidence (no phase difference), he showed that the required angular separation of the bars for resolution was twice as great as when the grating was seen against a self-luminous background. For individual black lines he found that just the reverse was true, a line against the self-luminous background requiring twice the angular width for resolution that was required when there was no phase difference between different parts of the background.

For observers with normal, well-formed eyes it is probable that spherical aberration is negligible for pupil apertures below 2.5 mm (Appendix IV). For some individuals with exceptional eyes, spherical aberration may have no appreciable effect for apertures below 4.0 mm. Chromatic aberration usually cannot be neglected although, for the small retinal contrasts which occur at high brightness levels, its effect is small compared with that of diffraction. If in a visual acuity experiment large values of u are to be known with precision, the experiment should be performed with spectrally homogeneous (monochromatic) light. If heterogeneous (white) light is used, the computations for u should be based on a distribution function representing both diffraction and chromatic aberration.

The visual acuity equation (29) can be derived from Eq. (40) which does not depend on the first or third of the conditions just discussed. The function $F(z)$ in Eq. (40) may be a general distribution function which represents blurring owing to diffraction, chromatic aberration, and spherical aberration. If the integral in this equation can be expressed as a power series in terms of α, then the form of Eq. (29) remains unchanged. However, the test object must be self-luminous.

Fry and Cobb[18] have suggested an illumination distribution curve in the retinal images of narrow bright lines which is much wider than curve B in Fig. 1. They assume that the illumination across the retinal image of a line of infinitesimal width is proportional to Y where Y is given by the normal distribution equation

$$Y=\frac{1}{\sigma(2\pi)^{\frac{1}{2}}}\exp\left(-\phi^2/\sigma^2\right), \qquad (41)$$

where ϕ is the angular distance in minutes from the center of the image. From their experimental work the constant σ came out to be 0.73 minute. Although their observations were made through a 2.33-mm artificial pupil, it can be shown that if the distribution were given by Eq. (41) (with $\sigma=0.73$ min.) then thin parallel luminous lines could not be resolved unless their angular separation is at least 1.8 minute. When viewed against a faintly illuminated background such

[18] G. A. Fry and P. W. Cobb, Trans. Am. Acad. Ophthal. and Otolaryngol., pp. 423–428 (1935).

lines can be resolved when their angular separation is only 1 minute of arc, which is near the limit imposed by diffraction. However, if Eq. (41) were applied to a point source of light and if σ were given a smaller value, then this equation should approximate rather closely the intensity distribution function representing diffraction, chromatic aberration, and spherical aberration. For a black disk on a white background Eq. (40) would then reduce to the simple form

$$u=v[1-\exp(-\alpha^2/4\sigma^2)],$$

where the constant σ would determine the resolving power of the composite distribution function. Such a function would be applicable to large iris apertures which occur at low brightness levels.

DISCUSSION

The blurring of retinal images by diffraction and by aberrations in the optical system of the eye has long been recognized. No general method seems to have been developed for computing the distribution of illumination in retinal images except for Rayleigh's equations for individual lines and gratings, most of which are valid only for rectangular apertures. The main purpose of this paper has been to develop equations giving the distribution of illumination in foveal images, to apply them to certain tests of the illumination discrimination theory of visual acuity, and to derive from them visual acuity equations for high brightness levels.

If visual acuity is determined by illumination discrimination, then the retinal threshold contrast u_t should remain unchanged when the contrast v between the test object and its background is varied. Also, u_t should be the same for all objects.

For individual lines u_t does appear to be constant. For individual disks u_t varies in such a manner that the retina seems to respond to a constant flux differential rather than a constant retinal illumination differential. The case for the grating is somewhat in doubt, although computations from Shlaer's data indicate that for this test object u_t may not be constant.

It is convenient to make a distinction between perception acuity and resolving power acuity, although as far as the response of the receptors is concerned, there is no essential distinction. The apparent difference is due to the sudden change in the illumination distribution which occurs in the images of objects such as the grating when the angular distance between separate details in the image approaches a certain critical limit; this limit is determined by the size of the iris aperture and the wave-length of light. Such a change does not occur in the images of individual objects. This fact has an important bearing on the design of tests for critical vision. It may also explain the unusual visual powers which birds of prey are supposed to possess.

Quantitative knowledge of axial aberrations and the size of blur circles gives little information about the resolving power of the eye unless these factors are expressed in the form of intensity distribution functions. In turn, the resolving power of a distribution function is ambiguous unless certain quantities such as contrast and structure of the test object are arbitrarily specified. It seems probable that the eye accommodates in such a manner that the retina intersects that part of the light beam across which the intensity distribution function has a maximum resolving power for the particular test object under observation.

A determination of the distribution of illumination in retinal images gives much information about the nature of visual acuity, but leaves several important questions unanswered. It is difficult to see why u_t should not be the same for all test objects, and why the contours or borders of test objects should not appear blurred as the distribution of illumination in retinal images would indicate. To account for the high resolving power of the fovea it is necessary to assume that each cone has a highly insulated pathway to the central nervous system, yet visual acuity is affected by size of background and is greater for long lines than for short lines which would indicate the existence of interaction or summation processes. However, interaction and summation are not compatible with the assumption of insulated pathways.

The above phenomena apparently cannot be explained by classical physical theory alone, and

a comprehensive theory of visual acuity can be developed only from an analysis utilizing the concepts of photochemistry and the quantum theory. The photochemical aspects of visual acuity and related phenomena will be discussed in the second part of this paper.

APPENDIX

I. Calculation of Intensities in the Grating Test Object

Some caution must be used in calculating grating intensities from Eqs. (23) and (24) because the general terms $\psi\{(4n+1)z_0\}$ and $\psi\{(4n+3)z_0\}$ approach $\pi^2/4$ rather than zero as $n\to\infty$. Equation (23) must therefore contain an odd number of terms and Eq. (24) an even number with one more term than Eq. (23).

When $(4n+1)z_0$ is large, the ascending power series for $\psi\{(4n+1)z_0\}$ converges very slowly and is inconvenient for calculating purposes. Struve[13] gives an asymptotic series for

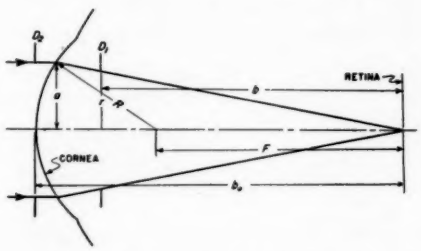

FIG. 11. Diagram of the reduced eye.

$S(z)$ which with only a slight modification can be used for calculating $\psi(z)$. This series for $\psi(z)$ may be written approximately

$$\psi(z)=\frac{\pi^2}{4}-\left(\frac{1}{z}+\frac{1}{12z^2}\right)+\frac{\pi^{\frac{1}{2}}}{4}\frac{\cos(2z+\pi/4)}{z^{5/2}},$$

which is suitable for calculations when z is large.

II. The Nature of an Optical Image

A large part of the refraction in the eye takes place at the cornea and the wave fronts reaching the iris diaphragm are concave (toward the retina) rather than plane. Gullstrand[19] implies that this condition produces a different distribution of light on the retina than if the diaphragm were in front of the cornea where it would receive plane waves. If this is true, then the diffraction in the eye is not of the Fraunhofer class. Gray, Mathews, and MacRobert[12] treat this problem in considerable detail, and from their basic theory it can be shown that in any optical system diffraction will be of the Fraunhofer class provided that the screen and image plane coincide, regardless of the position of the aperture and source.

If a point source of light lies on an axis passing through the center of a circular aperture and perpendicular to the plane of the aperture, the intensity at a point P on a screen, the plane of which is also perpendicular to the axis, can be expressed in terms of Lommel's U and V functions.[12] The intensity is directly proportional to M^2 which in terms of the U functions is given by the equation

$$M^2=\pi^2a^2(2/y)^2(U_1^2+U_2^2), \tag{1-a}$$

where

$$U_1=(y/z)J_1(z)-(y/z)^3J_3(z)+(y/z)^5J_5(z)-\cdots,$$

and

$$U_2=(y/z)^2J_2(z)-(y/z)^4J_4(z)+(y/z)^6J_6(z)-\cdots.$$

The variables y and z are given by the equations

$$y=\frac{4\pi}{\lambda}\frac{c+b}{2cb}a^2, \tag{2-a}$$

and

$$z=\frac{2\pi}{\lambda}\frac{\rho}{b}a, \tag{3-a}$$

where a is the radius of the aperture, ρ the distance of a given point on the screen from the axis, c is the distance from the edge of the aperture to the source, and b the distance from the screen to the pole of a wave front at the aperture; hence, c and b are approximately the distances from the aperture to the source and from the aperture to the screen. The distance c is positive to the left of the aperture and b is positive to the right of the aperture. The U functions are suitable when $y/z<1$, but if $y/z>1$ then M should be expressed in terms of the V functions[12] which are expanded in ascending powers of z/y.

When $y=0$, Eq. (1-a) reduces to

$$M^2=\pi a^2(2/z)^2J_1^2(z)$$

and the diffraction is of the Fraunhofer class. It thus remains to determine under what conditions $y=0$. Obviously this occurs when $b=\infty$ and $c=\infty$, or when $\pm c=\mp b$. This latter condition can be fulfilled by introducing a lens of the appropriate focal length somewhere between the source and screen. If between the aperture and the screen there is placed a lens such that the image of the screen coincides with the plane of the source, then b is transformed to $-c$. Similarly, if between the aperture and the source there is placed a lens such that the image of the plane of the source coincides with the screen then c is transformed to $-b$. If there are several lenses in the optical system and if there are lenses between both the aperture and screen and aperture and source, then b and c will become virtual distances b' and c' with respect to the aperture, and if the system is "in focus," b' will be transformed to $-c'$ or vice versa. From the standpoint of physical optics, one might state that there is no definite focal plane, but that the best image is obtained when y vanishes. When this occurs the plane of the physical image coincides with the plane of the geometric image and the diffraction is of the Fraunhofer

[19] H. Von Helmholtz, *Physiological Optics*, edited by J. P. C. Southall (Optical Society of America, 1924), Volume I.

class. However, the spread of the diffraction pattern (as measured by the diameter of the first dark ring) will depend on the position of the aperture in the optical system.

The situation is modified slightly if the source and screen are in media which have different indices of refraction; this occurs in the case of the eye. If the index of refraction of air is assumed to be unity, and if the index of refraction of the fluids in the reduced eye (Fig. 11) is n, then in Eqs. (2-a) and (3-a) λ must be replaced by λ/n if the aperture is inside the cornea because the wave-length of light decreases when it enters the denser medium. This causes no change in the ratio y/z but increases the magnitudes of y and z. Equation (3-a) becomes

$$z=\frac{2\pi}{\lambda/n}\frac{\rho}{b}r,$$

$$=\frac{2\pi}{\lambda}\frac{\rho}{b/n}r. \tag{4-a}$$

In Fig. 11 consider any aperture D_1 of radius r which just "fits" the cone of light converging on the retina. Let b_0 be the distance from the cornea to the retina and let a be the value of r when the aperture is just inside the cornea or when b is approximately equal to b_0. If r/b is small then

$$r/b=a/b_0.$$

In the reduced eye all refraction takes place at the cornea, and both nodes are at the center of curvature of the cornea. The distance between this point and the image plane approaches the principal focal length F of the eye as $c\rightarrow\infty$. Hence if R is the radius of curvature of the cornea,

$$F=b_0-R=b_0/n,$$

and

$$\frac{r}{b/n}=\frac{a}{b_0/n}=\frac{a}{F}.$$

Equation (4-a) can now be written

$$z=\frac{2\pi}{\lambda}\frac{\rho}{F}a, \tag{5-a}$$

and the index of refraction does not appear in the equation for z. This point is sometimes confusing, and is not always stated correctly in textbooks on physical optics.

If the aperture D_2 of radius a is placed just outside the cornea, b_0 must be replaced by b_0/n because of the change in the divergence angle in the transition between media of different indices of refraction; Eq. (5-a) thus remains unchanged.

For all practical purposes the conditions in the actual eye are identical with those in the reduced eye, except that the two nodes do not quite coincide and F is therefore measured from the posterior node.

When the eye is sharply focused on a point source of light, the diffraction pattern on the retina will be of the Fraunhofer class, because c is transformed to $-b$, and y will therefore be zero. If an observer is nearsighted or farsighted, then c will be transformed to $-b\pm\Delta F$ where ΔF is the distance of the image plane from the retina, and y becomes

$$y=\pm\frac{2\pi}{\lambda}\frac{\Delta F}{F^2}a^2.$$

The distribution on the retina would thus be given in terms of the U and V functions,[12] but will not be of the Fraunhofer class.

III. Chromatic Aberration

Helmholtz[19] derived an equation giving the distribution of light in the retinal image of a point source of light when the blurring was caused by chromatic aberration. Since the form of the relative spectral luminosity function was not known at that time, he was not able to allow for the sensitivity of the eye to different wave-lengths and he points out that if the lower sensitivity near the limits of the visible spectrum were taken into consideration, the distribution would be somewhat narrower than that which he obtained. The following derivation of the distribution function is somewhat different from the method used by Helmholtz, but the effect of visual sensitivity to different wave-lengths is taken into account. The illuminant is considered to have an equal energy spectrum.

The derivation is simplified if it is made for the "reduced eye" in which all refraction takes place at the cornea.

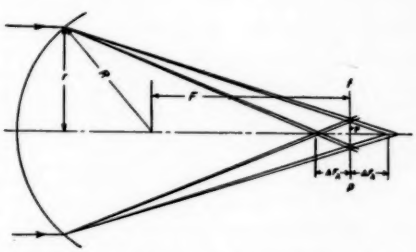

FIG. 12. Diagram showing chromatic aberration in the reduced eye.

Unlike spherical aberration, chromatic aberration produces no definite circle of confusion unless one arbitrarily selects two wave-lengths as representing the limits of the visible spectrum, but this is unnecessary. The focal plane fp (Fig. 12) is assumed to be the plane in which light of the wave-length ($\lambda_m=0.555$ micron) for maximum visual sensitivity is brought to a focus.

Light of any other wave-length λ will be brought to a focus in another plane which is separated from the plane fp by a distance ΔF_λ. The aberration ΔF_λ for any given wave-length is the same for all apertures. The derivation is further simplified if one assumes that the dispersion of the eye fluids (mostly water) is constant throughout the visible region of the spectrum. This assumption gives a good approximation of the water dispersion curve for wave-lengths between 0.490 micron and 0.630 micron, but is considerably in error for wave-lengths shorter than 0.490 micron where the dispersion increases rapidly. However, this is of little consequence, because for an equal energy spectrum about 85 percent of the visual stimulus is furnished by wave-lengths between 0.490 and 0.630 micron. The assumptions of constant dispersion and an equal energy spectrum make it possible to replace the relative spectral luminosity func-

tion by an even function $f(\Delta\lambda)$ such that

$$f(\Delta\lambda)=\tfrac{1}{2}\{L(0.555+\Delta\lambda)+L(0.555-\Delta\lambda)\}, \quad (1\text{-b})$$

where $\pm\Delta\lambda$ has been written in place of $\pm(\lambda-0.555)$, and where $L(0.555\pm\Delta\lambda)$ is the relative spectral luminosity function, values of which are given in I.C.I. tables of the standard observer. From Fig. 12 it can be seen that any given point in a zone $2\pi\rho d\rho$ in the focal plane receives light of wave-lengths $0.555+\Delta\lambda$ and $0.555-\Delta\lambda$ from two points 180° apart in the aperture zone $2\pi r dr$. For fixation on a distant point source of light the element of energy flux dE received in the focal plane by a zone of radius ρ and width $d\rho$ from a zone in the cornea of radius r and width dr will be

$$dE=c\cdot 2\pi r dr\cdot 2\pi\rho d\rho\cdot(1/\rho),$$

where c is a constant depending on the distance and intensity of the point source. The factor $1/\rho$ must be introduced since for any given value of r, dr, and $d\rho$, the value of dE must be the same for all values of ρ; this follows from the assumptions of constant dispersion and an equal energy spectrum. The corresponding element of luminous flux dL on zone $2\pi\rho d\rho$ is

$$dL=c\cdot f(\Delta\lambda)\cdot 2\pi r dr\cdot 2\pi\rho d\rho\cdot(1/\rho),$$

and the element of illumination dI on the zone of radius ρ is

$$dI=dL/2\pi\rho d\rho=2\pi c f(\Delta\lambda)(r/\rho)dr. \quad (2\text{-b})$$

The dispersion is assumed to be constant so

$$\Delta\lambda=-k\Delta n, \quad (3\text{-b})$$

where n is mean index of refraction of the fluids within the eye. If F is the focal length of the reduced eye and if R is the radius of curvature of the cornea, then F and R are related by the equation

$$F=R/(n-1). \quad (4\text{-b})$$

Differentiating F with respect to n gives for the aberration ΔF_λ

$$\Delta F_\lambda=-R\frac{\Delta n}{(n-1)^2}. \quad (5\text{-b})$$

From Fig. 12 it follows that when r is small

$$\rho/\Delta F_\lambda=r/(R+F),$$

which when combined with Eq. (4-b) gives for ΔF_λ

$$\Delta F_\lambda=\frac{\rho nR}{r(n-1)}. \quad (6\text{-b})$$

Combining Eqs. (3-b), (5-b), and (6-b) gives for $\Delta\lambda$

$$\Delta\lambda=kn(n-1)\rho/r,$$

hence the intensity I at any distance ρ from the center of the image is

$$I=c\int_0^a f\left\{\frac{kn(n-1)\rho}{r}\right\}\frac{2\pi r}{\rho}dr. \quad (7\text{-b})$$

The relative intensity given by this equation is infinite when $\rho=0$, and to compare its effect on image blurring with that of the distribution given by Eq. (4), it is necessary to establish a more general theorem on the resolving power of a distribution function. Assume that the integral in Eq. (7-b) can be expressed by the function $F_1(z)$ where the reduced angular distance z is given by the equation

$$z=\frac{2\pi a}{\lambda}\frac{\rho}{F}=\frac{2\pi a}{\lambda}\frac{\rho(n-1)}{R}.$$

Assume that the point source is replaced by an extended source or screen composed of a large number of infinitesimal sources. If a circular black disk of reduced angular radius z is placed at the center of the screen, the illumination at the center of the disk is

$$I=K_1 I_b\int_z^\infty F_1(z)(2\pi z)dz. \quad (8\text{-b})$$

If the disk is shrunk to a point $I=I_b$, hence the constant K_1 is given by the equation

$$1/K_1=2\pi\int_0^\infty F_1(z)z dz.$$

There are several possible ways for comparing the resolving power of different distribution functions, some of which lead to ambiguous results. Apparently the best method is to compare the reduced angular radius z_r' of a circular black disk, which gives a certain image contrast u for one distribution function $F_1(z)$, with the reduced angular radius z_r of another black disk which gives the same image contrast for another distribution function $F_2(z)$. The ratio z_r/z_r' is the relative resolving power of the two distributions for a black disk on a luminous background.

Combining Eq. (8-b) and Eq. (2) gives for the image contrast u

$$u=1-2\pi K_1\int_{z_r'}^\infty zF_1(z)dz=2\pi K_1\int_0^{z_r'}zF_1(z)dz. \quad (9\text{-b})$$

A similar equation holds for a distribution function $F_2(z)$ and a black disk of reduced angular radius z_r; hence if u is the same in both images it follows that

$$K_1\int_0^{z_r'}zF_1(z)dz=K_2\int_0^{z_r}zF_2(z)dz, \quad (10\text{-b})$$

which gives the desired relation between z_r' and z_r. Usually the integrals must be evaluated by graphical or numerical methods.

For the chromatic aberration distribution $zF_1(z)$ is from Eq. (7-b)

$$zF_1(z)=\frac{4\pi^2 a(n-1)}{\lambda R}\int_0^a f\left(\frac{kR\lambda nz}{2\pi ar}\right)rdr. \quad (11\text{-b})$$

Integrating this equation graphically for different values of z gives the function $zF_1(z)$ shown in Fig. 2, curve B, for which $a=1.21$ mm, $R=5.45$ mm, $n=1.34$, and $k=25$ microns. If $F_2(z)$ represents the diffraction distribution of Eq. (4), then Eq. (10-b) takes the simplified form

$$K_1\int_0^{z_r'}zF_1(z)dz=1-J_0^2(z_r)-J_1^2(z_r). \quad (12\text{-b})$$

For any given value of z_r, there will be a corresponding value of z_r' for which the area under curve B, Fig. 2, from 0 to z_r' will be equal to the right member of Eq. (12-b), that is, equal to the area under curve A, Fig. 2, from 0 to z_r. The

ratio z_r/z_r' will therefore depend on the value of z_r and hence on the contrast u. For an aperture $2a=2.43$ mm, the ratio z_r/z_r' is about 8.0 when $u=0.02$, and about 2.0 when $u=0.10$. In both instances the resolving power of the chromatic aberration distribution function is greater than that of the diffraction distribution function and diffraction is the principal cause of the image blurring. However, when u is greater than 0.45 the ratio z_r/z_r' is less than unity, and chromatic aberration contributes more to the blurring of the image than diffraction does, even though the diameter of the aperture remains unchanged. Values of the retinal contrast u computed from Eq. (25) for monochromatic light will therefore be larger than the actual contrast for white light. The error will be small for small values of u but may be considerable when u is large.

The meaning of the z_r/z_r' ratio can be made more clear by interpreting the curves in Fig. 2, or the integrals of Eq. (10-b), in a different way. In the distribution of light in the image of a point source, the flux received by a zone of radius z and width dz is directly proportional to the ordinates of these curves. The areas under the curves from 0 to ∞ must be equal since each represents the total flux in the image. If equal areas under the A and B curves from 0 to z_1 and 0 to z_2 are chosen so that each area is the same fraction u of the total area under either curve, then z_1 and z_2 will be equal to z_r and z_r', respectively. For example, if $u=0.10$, then for curve B 10 percent of the total flux in the image of the point source is concentrated in a circle with only $\frac{1}{3}$ the diameter of the corresponding circle for curve A which contains the same fraction of the total flux.

The theorem expressed in Eq. (10-b) can be generalized to give the relative resolving power of different intensity distributions for objects other than a black disk on a white background. The results show that resolving power or resolution is an ambiguous concept unless certain parameters such as image contrast and structure of test object are arbitrarily specified.

There might be some question as to validity of the assumption of an equal energy spectrum in the derivation of Eq. (7-b). This assumption merely simplifies the derivation, and it can be shown that if the distribution of energy flux E is given by the equation

$$E=\phi(\lambda),$$

then Eq. (7-b) remains unchanged provided that

$$\phi(\lambda)+\phi(2\lambda_m-\lambda)=\text{a constant.} \qquad (13\text{-b})$$

Since $\phi(\lambda)$ is an arbitrary function restricted only by Eq. (13-b), it can be made to approximate the standard I.C.I. illuminants,[20] as well as many other illuminants, rather closely. If there are no restrictions on $\phi(\lambda)$, then Eq. (7-b) assumes a more complex form.

The chromatic aberration for different wave-lengths for the reduced eye is about the same as that for the actual eye. Ames and Proctor[21] give the measured chromatic aberration ΔF_λ for three different observers, the average of which is shown in Table III. The theoretical value of ΔF_λ for the reduced eye, computed from Eq. (5-b) and tables giving the dispersion of water, is shown in the last column. The accommodation is assumed to be such that $\Delta F_\lambda=0$ when $\lambda=0.550$ micron.

TABLE III. The measured chromatic aberration for the actual eye is about the same as that for the theoretical aberration for the reduced eye. The experimental values of ΔF_λ are the average measurement for three observers as given by Ames and Proctor. Theoretical values of ΔF_λ are computed from Eq. (5-b).

λ (microns)	ΔF_λ (in millimeters) Measured	Theoretical
0.700	0.210	0.190
.650	.156	.133
.600	.066	.076
.550	.000	.000
.500	.085	.114
.465	.190	.209

IV. The Monochromatic Aberrations

The monochromatic aberrations of the eye have been the object of extensive investigations, but they are not even yet fully understood. Along the optic axis or along the visual axis (these two axes do not quite coincide) the aberration is sometimes called "spherical" aberration, although the aberration cannot be regarded as equivalent to the spherical aberration in an optical system consisting of centered spherical refracting surfaces which bound isotropic refracting media. Even in normal eyes the refracting surfaces of the cornea and the crystalline lens are not necessarily spherical and the index of refraction of the lens is greater at the center than at the edge.

Because of the complexity of the ocular refracting system, theoretical investigations of spherical aberrations along the visual axis probably are not very reliable and the best estimate of the effects of spherical aberration is to be found from direct measurements of this quantity. Ames and Proctor[21] give the axial aberrations for two observers for different corneal zones and their results are shown in Fig. 13. The curve for observer Ames gives the mean aberrations of corresponding zones on the temporal and nasal side of the visual axis (horizontal meridian). The curve for observer Chapman shows aberrations in a vertical meridian above the visual axis. The aberration in the writer's eye was measured by a slightly different method than that used by Ames and Chapman, and each measurement includes the aberrations of both the temporal and nasal zones (horizontal meridian). All three curves are for the right eye and for relaxed accommodation. The dotted curve shows the spherical aberration for the reduced eye of Appendix III as computed from the equation

$$\Delta F=\frac{r^2}{2Rn(n-1)},$$

where F is the focal length of the eye, r the radius of the corneal zone, R the radius of curvature of the cornea, and

[20] A. C. Hardy, *Handbook of Colorimetry* (The Technology Press, Massachusetts Institute of Technology, 1936).

[21] A. Ames and C. A. Proctor, J. Opt. Soc. Am. **5**, 22–84 (1921).

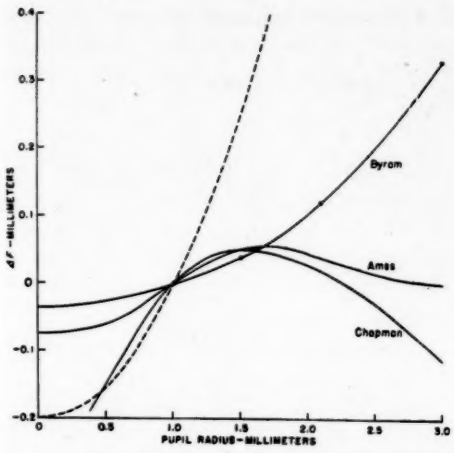

FIG. 13. Spherical aberration curves for three different observers. The curves of observers Ames and Chapman are plotted from the data given by Ames and Proctor (reference 21). The aberration ΔF is assumed to be zero for a zone with a 1-mm radius. The dotted curve shows the theoretical spherical aberration for the reduced eye ($R = 5.45$ mm and $n = 1.34$).

n the index of refraction of the fluids within the eye. For comparison, all curves have been moved up or down so that the aberration ΔF would be zero at the 1.0-mm zone.

Although observations were made for only three observers, these curves indicate that a large amount of the spherical aberration in the eye is corrected (actually overcorrected for the outer zones of Chapman's eye). The magnitudes of the aberrations have but little meaning unless they can be interpreted in terms of the distribution of intensity in the image of a point source. By a rather laborious derivation this distribution function can be determined, and the results show that its resolving power is much greater than that of diffraction distribution if the pupil aperture $2a$ is less than 2.5 mm. For persons with exceptional vision, the effects of spherical aberration along the visual axis may be negligible compared with diffraction for apertures up to 4.0 mm. This is indicated by the visual acuity measurements of Cobb.[22]

The effects of both spherical aberration and diffraction in an imperfect optical system can be treated as a general diffraction phenomenon, since the wave fronts leaving the last refracting surface in the system are slightly distorted from a spherical form. This means that there will be phase differences between the disturbances arriving at the focus from different parts of the wave front, the result of which will be a decrease in the intensity at the focus or center of the diffraction pattern. There must therefore be a corresponding increase in the intensity in the outer zones of the diffraction pattern because the total flux in the pattern must be the same regardless of the shape of the wave fronts. This point of view (apparently due to Rayleigh) has the advantage of simplifying the physical concepts involved in image formation, but unfortunately its mathematical treatment is quite difficult and with the exception of a few preliminary calculations by Rayleigh no one seems to have made much use of it.

There are several opinions as to how the eye accommodates to achieve maximum visual acuity. Ames and Proctor[21] believe that accommodation is such that the retina intersects the narrowest portion (circle of least confusion) of the light beam coming from any given point in the test object. Gullstrand[19] suggests that the plane of intersection is determined by the trend of the caustic curves. It is doubtful whether either of these ideas is sufficient to explain how the eye accommodates. If planes are passed through arbitrary points on the visual axis, the distribution of illumination on these planes (for a point source of light) will in general be given by different distribution functions. It would seem logical that the eye would accommodate so that the retina would coincide with the plane in which the distribution function gives a maximum contrast for the object under observation. Since the relative resolving power of different distribution functions depends both on contrast and structure of the test object, it would appear that accommodation for maximum visual acuity would not necessarily be the same for all objects. However, the differences would be very slight.

[22] P. W. Cobb, Am. J. Physiol. **36**, 335–346 (1915).

Note on Specular Densities and Forward Scattering

FRANZ URBACH
Institute of Optics, University of Rochester, Rochester, New York
(Received July 7, 1944)

THE measurement of specular photographic density should be an absorption measurement in which no light scattered by the photographic layer interferes with the measurement of the transmitted light. In fact, a certain contribution of light scattered in the direction of the transmitted beam is never completely avoidable.

F. H. G. Pitt[1] has shown how this contribution can be determined, using the fact that the transmitted and the scattered beam depend differently on the geometrical conditions of the measurement. This makes possible the determination on the one hand of the "true" specular density of a given sample, and, on the other hand, of the scattering of the sample in the direction of the transmitted beam. The latter is usually difficult to determine just because of the interference of the directly transmitted light. This "forward scattering" of the sample can be characterized by an empirical magnitude, the "scattering constant" S. If the sample be regarded as a secondary light source, S represents its brilliancy in the direction of the transmitted beam, per unit illumination of the sample by the primary light source. It has been shown by Pitt that S is in fact independent of the geometrical configuration. It is, however, naturally strongly dependent on the density of the sample. Pitt gives some empirical data concerning this dependence without further discussion although at least their qualitative interpretation will certainly have occurred to him.

It will be shown here that a crude quantitative treatment leads to a more complete understanding of Pitt's empirical data and indicates that one of his results is an example for a rather general rule.

An absorbing and scattering sample of area a is placed between a point-like source and any light measuring instrument. Let the light source be at a distance d from the receiver and d_1 from the sample. The specularly transmitted light will be, with a given light source, proportional to $10^{-D}/d^2$ where D represents the specular density of the sample. The light scattered by the sample onto the receiver will be proportional to $(1/d_1)^2 \times aS/(d-d_1)^2$. The apparent transmission of the sample measured in this arrangement will be:

$$T_{\text{app}} = 10^{-D} + d^2 aS/d_1^2(d-d_1)^2.$$

This formula has been derived and tested by Pitt, and the "scatter-constant" S has been found to be actually independent of the position of the sample.

Concerning the dependence of S on the density, Pitt summarizes the result of his measurements as follows: "It can be seen that S increases rapidly to a density of approximately 0.4 and then decreases asymptotically towards 0. . . . The ratio of the illumination due to the scattered light to the specular illumination, when $d_1 = d/2$ increases almost linearly with density." Table I gives Pitt's numerical results.

TABLE I.

Diffuse density	Scattering constant S	True specular density	Ratio of illumination owing to scattered light to specular illumination
0.14	1.15	0.18	0.008
0.33	1.77	0.42	0.022
0.61	1.19	0.81	0.036
0.83	0.86	1.01	0.041
1.50	0.25	1.75	0.069
1.62	0.22	1.98	0.101
2.00	0.10	2.49	0.140

The behavior of S as a function of D is obviously owing to the fact that at low densities the scattering increases with the amount of the silver deposit, while at higher densities the absorption of the scattered light in the layer overcompensates this increase. The mathematical formulation can be based on the following assumptions. For an infinitesimally thin layer, taken as a secondary light source, the brilliancy of the layer is proportional to its density dD and to the flux density in the layer. The latter assumption will hold if the directional distribution of the flux is

[1] F. H. G. Pitt, Phot. J. **78**, 486 (1938).

sufficiently constant. The first assumption certainly holds if the particle size distribution is constant, independent of the density, since the density is then simply a measure for the number of scattering centers. But also with varying grain sizes the assumption will be good within reasonable limits because for not too small grains both the density and the scattering power should increase with increasing grain size.

Consider now an infinitesimally thin layer within the sample parallel to the surface of the sample and at such a depth that the density between the layer and the surface which faces the light source is D'. If the incident flux density is unity at the surface of the layer it is $10^{-D'}$ in the infinitesimal layer considered. If we disregard the illumination produced within the layer by its own scattering, which is certainly justified for low densities, we may put as a fair approximation

$$dS = \text{const.} \times dD' \times 10^{-D'} \times 10^{-(D-D')}, \quad (1)$$

where the last factor represents the absorption of the scattered light in the layer on its way towards the measuring instrument. D' is variable while D is constant; the integration from $D'=0$ to $D'=D$ yields

$$S = cD \times 10^{-D}. \quad (2)$$

c should be a constant characterizing the material

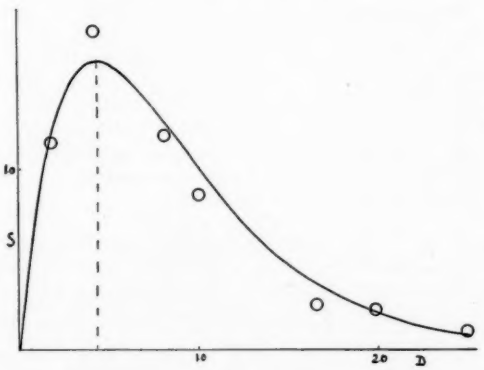

FIG. 1.

and independent of D. In fact the function (2) has the general shape described by Pitt, and the quantitative agreement (see Fig. 1) can be regarded as fair if we take into account the uncertainty of S shown by the irregular behavior of the empirical points in Pitt's Fig. 4. Note that the relatively complicated curve is represented with a single adjustable parameter (the value $c=10$ has been used in Fig. 1).

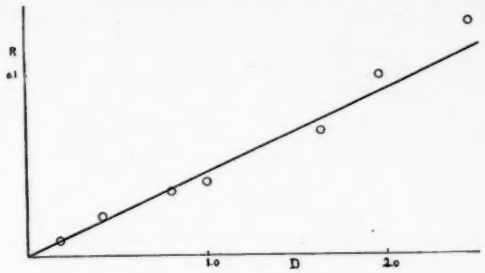

FIG. 2.

If we calculate now the ratio R of the scattered light to the specular illumination, that is, the ratio between the two terms in formula (1), using our expression (2) for S we obtain

$$R = ca\frac{d^2}{d_1^2(d-d_1)^2} \times D.$$

In agreement with Mr. Pitt's statement quoted above, this ratio is a linear function of D. Beyond this agreement our derivation suggests that the slope of the straight line is not an independent empirical magnitude but is determined on the one hand by the geometrical data of the arrangement and on the other hand by the empirical constant c of formula (2). A check of this relation with the data given by Pitt ($d=150$ cm, $d_1=75$ cm, $a=6.6$ cm^2) and with the constant from Fig. 1 we obtain

$$R=0.046.$$

Figure 2 shows again satisfactory agreement of our deductions with Pitt's data.

The most striking feature of our interpretation of Pitt's experiment is, however, obtained by analyzing the position of the maximum in Fig. 1. By differentiation of (1) we find for the density at which the maximum occurs:

$$D = {}^{10}\log e = 0.43.$$

In Pitt's paper the position of the maximum occurs as a purely empirical result and the specific value given by Pitt as quite incidental.

According to our consideration, however, this value is by no means incidental. It is independent not only of the experimental arrangement but also of the material as long as it fulfills our basic assumptions. It represents the intrinsic relationship of the definitions of scattering and absorption. It should hold, thus, quite generally also in other fields of physics (like x-ray or neutron scattering) that *the forward scattering of an absorbing and slightly scattering layer reaches a maximum if the fraction of the incident beam, which is transmitted specularly, is just equal to 1/e.*

Book Review

Experimental Spectroscopy.

RALPH A. SAWYER. Pp. 323+viii, Figs. 107. Prentice-Hall, Inc., New York, 1944. Price $5.00.

Any disappointment which a prospective owner of Commander Sawyer's long-awaited book may feel on seeing its small size will be dissipated on inspecting its contents. Presumably wartime necessity has forced the publishers, by using thin paper and narrow margins, to make a big book look like a small one, but this half-inch thick treatise on what a good experimental spectroscopist ought to know should remain on shelves long after many of its bulkier contemporaries have vanished. It is distinguished by clarity of explanation, meticulous treatment of detail, and that authoritative touch which comes only from long familiarity with the subject matter involved.

Sawyer has filled a long-standing gap in spectrographic literature by giving thorough treatment to the design, adjustment, and use of all the modern types of spectrographic equipment which are in ordinary laboratory use, though he does not touch on interferometric spectroscopy. Of thirteen chapters, five are devoted to spectroscopic apparatus, with almost equal emphasis on prism and grating instrumentation. Light sources, photographic procedures, wave-length determinations, and intensity determinations each form the subject of a chapter, as do the infra-red and vacuum ultraviolet regions.

Any reservations to temper the enthusiasm of the reviewer must arise in the present case from sins of omission rather than commission. Sawyer's position as an outstanding authority on the spectrochemical analysis of materials, and the important contributions which he has made in this field, make one regret that he did not find it possible to devote more than a single chapter of moderate length to this subject. Further, absorption spectrophotometry has been almost entirely omitted, perhaps because other books already available have given great emphasis to this side of spectrographic analysis. We may hope, however, that these limitations will be removed in future editions of the book, which should be a standard text for many years.

Sawyer has solved a very difficult problem in writing a treatise which should be appealing to the laboratory analyst whose background of spectroscopic theory is limited, and at the same time to the research worker who wants to have available between two covers the basic material of the experimental side of his profession.

GEORGE R. HARRISON
Massachusetts Institute of Technology

Design Method for a Schmidt Camera with a Finite Source

FRANK BENFORD
Research Laboratory, General Electric Company, Schenectady, New York
(Received August 12, 1944)

THE Schmidt camera is normally designed for astronomical work or for distant objects. Since in these cases the received radiation is substantially parallel there is a minimum number of variables in a solution by ray tracing. Lucy[1] has shown that even if the curved face of the correcting plate is outward the first angle of refraction is small and this angle appears only as a cosine in the equations. This cosine may be set equal to unity without introducing appreciable error, and hence it vanishes as a variable from the equations. The remaining variables arising at the second refracting face and at the mirror may be reduced to a single variable and the path length thus expressed as a function of a single angle.

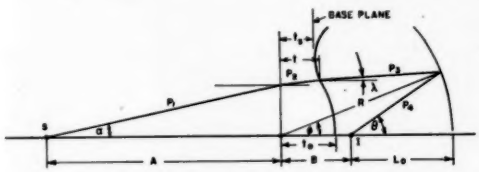

FIG. 1. This conventional ray diagram of a Schmidt camera shows one ray turned from a source at S to an image at I. The correcting plate has a minimum thickness t_0 that is determined from considerations of mechanical strength and rigidity.

In the present design for a plastic plate the source is at a relatively short distance and the angles of incidence and first refraction are large and cannot be approximated. These additional variables add greatly to the difficulties in attaining an equation with a single variable. In the method here outlined these difficulties are avoided by dividing the design into two regions and combining these regions by a graphical method that yields 5-place accuracy without undue effort. This paper is confined to describing the graphical part of the method.

In Fig. 1 a ray from the source S follows the path $P_1P_2P_3P_4$ to the image point I. All such paths must have a common optical length P such that

$$P=P_1+\mu P_2+P_3+P_4, \qquad (1)$$

where μ is the refractive index of the plate. At the zone of the plate having a minimum thickness t_0 a plane is passed perpendicular to the optic axis and this plane is the base plane for the graphical part of the work.

Selecting some angle ϕ, Fig. 1, so that the ray will pass near the minimum point of the plate the path P_3+P_4 is computed to a base plane at $t_0=0.020$, and then to a second plane to the right, say at $t=0.021$. These two paths subtracted in turn from P will give the lengths of the incomplete paths P_1+P_2 that will satisfy Eq. (1). They are plotted as line ϕ in Fig. 2.

If the camera exactly fulfilled the sine law we would have, from Fig. 1,

$$\sin\theta/\sin\alpha=\text{constant} \qquad (2)$$

and this would immediately give data for the

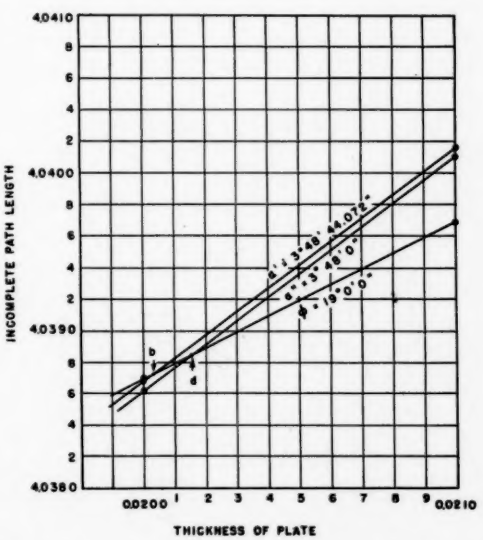

FIG. 2. The variation of path length with thickness of plate is here used to find two trial thicknesses at b and d that satisfy the path length condition, but b and d are not real solutions since the rays P_2 and P_3 do not join at these points.

[1] Frank Allen Lucy, J. Opt. Soc. Am. **30**, 251 (1940).

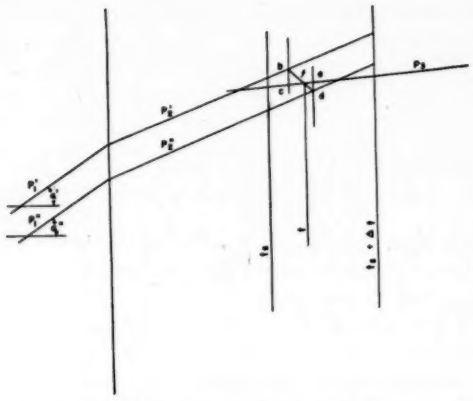

FIG. 3. This diagram shows the two imaginary solutions at b and d and the real solution at f where the line bfd intersects the ray P_3.

completion of the solution. This operation carried out gives the line plotted as α' in Fig. 2, and the intersection of lines ϕ and α indicates a thickness of 0.02003, at the point b, as satisfying Eq. (1).

If the heights of lines ϕ and α are computed for the plane at 0.02003 it will be found that they do not agree. This means that the solution is imaginary since the rays do not join, and hence this is not *the* solution. Taking another trial value of α, as α'' in Fig. 2, a second point d is found for a plane at 0.020156, and from these two points it is now possible to find a third point that will give a real solution of Eq. (1).

In Fig. 3 the various rays and planes are shown schematically. It is evident that there will be a point f on a straight line through b and d that will be on the ray P_3 and hence be a real solution to the path length equation. It will be realized that the entire region now under investigation is less than 0.001 (when the focal length of the camera is unity) on a side, and the variation of path length with α may, therefore, be taken as linear over the distance bd. The graphical solution may be made by plotting the heights of b, d, and f against plate thickness, as in Fig. 4. Here the line bd intersects ϕ (or ray P_3) at thickness 0.020053, and this is one point on the desired optical surface.

Similar solutions were made for a number of points and from these a plot was made of the section of the plate in a meridian plane. The relative thickness was multiplied by 10, so that four figures could be read and the fifth estimated. An alternative procedure is to find an equation by curve fitting as was done by Lucy, from which the contour can be computed at points selected for the use of the die maker.

The solution here outlined might, of course, be done by writing equations for the various rays and planes and solving for intersections. This process would have added very materially to the work of computing but the greater accuracy would have been largely wasted since a sixth significant figure is beyond the skill of the die maker.

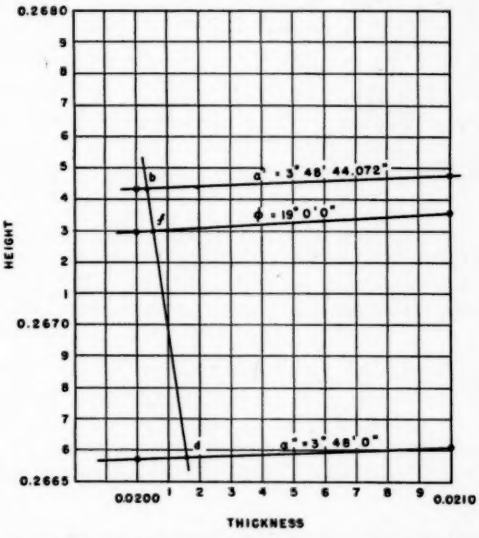

FIG. 4. The heights from the optic axis of b and d lead to a graphical determination of height f which satisfies the path length condition and the height condition at the same time. The correct plot thickness for ray $\phi = 19°$ is given by the point f.

A Novel Graphical System for Representing Tone Reproduction Data

PAUL W. DORST
Department of Lithographic Research, University of Cincinnati, Cincinnati, Ohio
(Received July 31, 1944)

CONVENTIONAL tone-reproduction graphs are excellent for laboratory use, but they fail to tell a complete story to many practical workers to whom they could be of great benefit. With the express purpose of presenting data so that they may be more readily interpreted, the following graphical system was devised for illustrating tone relationships in photographic and graphic arts processes. Over a period of several years, individuals having widely different degrees of acquaintance with photographic science and techniques have found this system more expressive than the one in current use. At the same time it has been found suitable for solving tone-reproduction problems rapidly, with perhaps slightly less precision than the conventional method used by Jones.[1]

This system departs in four ways from past practice: (1) All tone values are expressed in terms of density or equivalent density; (2) all tone values are represented on vertical axes; (3) highlight and shadow tones are always shown in the same relative positions, whether they refer to negative or positive images; (4) data for a series of successive operations are shown on horizontally-spaced vertical axes, corresponding points being connected with straight lines. The details of this system are best illustrated by the following example applying to simple photographic operations.

ILLUSTRATION OF THE SYSTEM

Camera Image Characteristics

Flare or non-image forming light prevents the optical image formed by the lens in a camera from being a tone-for-tone counterpart of the object or scene being photographed. In a complete tone analysis, therefore, it is necessary to consider the formation of the camera image as a distinct operation in itself. The effect of the flare light on the relationship between object tones and image tones is shown in Fig. 1.

Object tones are expressed as equivalent relative object density, hereafter called *object density* D_0. $D_0=\log (B_0 \max/B_0)$, where $B_0 \max$ is the maximum brightness occurring in the object and B_0 is the brightness of the object area under consideration. The maximum brightness in the object thus corresponds to an object density of zero. Image tones are likewise expressed as equivalent relative image density, hereafter termed *image density* D_i. $D_i=\log (I_i \max/I_i)$, where $I_i \max$ is the maximum illumination existing in the image, and I_i is the illumination of the image area being evaluated.

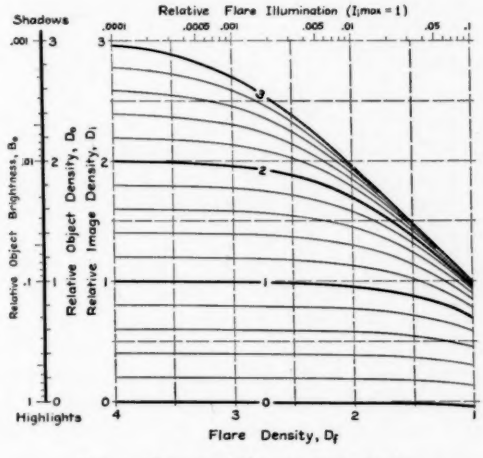

FIG. 1. Characteristics of camera image.

The flare light also is expressed as an equivalent relative image density, hereafter called *flare density* D_f. $D_f=\log (I_i \max/I_f)$, where I_f is the flare illumination in the image plane. By thus evaluating flare, it becomes possible to illustrate all object-image tone relationships on a single set of universal curves applying to any object-density range. If flare is evaluated in terms of flare factor, or the ratio of *object brightness scale* to *image illumination scale*, as used by Jones and Condit,[2] it is necessary to know the object

[1] L. A. Jones, J. Frank. Inst. **202**, 469, 589 (1926); **203**, 111 (1927); **204**, 41 (1927).

[2] L. A. Jones and H. R. Condit, J. Opt. Soc. Am. **31**, 651–678 (1941).

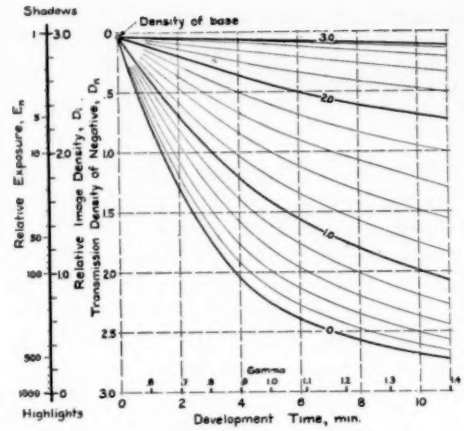

FIG. 2. Characteristics of negative material.

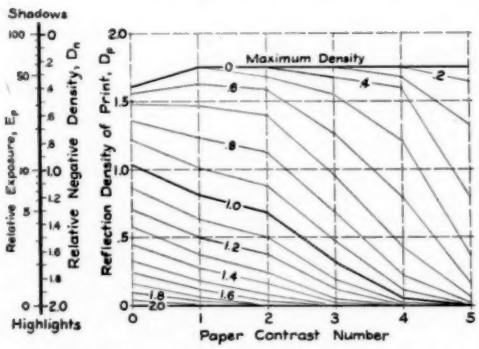

FIG. 3. Characteristics of positive printing papers.

brightness scale before the value of image density corresponding to any intermediate value of object density can be computed.

In Fig. 1 flare density is shown on the horizontal axis of the rectangular graph, and image density on the vertical axis. Each curve represents a different value of object density, with increments of 0.2 in object density. The scale of object density on the isolated vertical axis at the left of the rectangular graph has division lines showing the values for which curves are given. This scale is especially convenient in graphing data for a series of consecutive operations according to the present system, as explained later. The adjacent scale of relative object brightness may be used for converting brightness to density, and in adjusting exposures by trial and error.

The following analysis of the construction in Fig. 1 applies also to the graphs for the other operations (Figs. 2 and 3). An isolated vertical scale shows a convenient series of *input* densities with constant increment, and corresponding values of some other factor which may be of use. A rectangular graph, in which the horizontal axis is assigned to an operation variable and the vertical axis to *output* densities, contains a family of curves corresponding to various values of *input* density, with equal increments. The vertical spacing of these curves therefore indicates density differences or tone separations.

Negative Material Characteristics

The family of curves in Fig. 2 shows the characteristics of a typical commercial negative material,[3] customarily illustrated by a family of H and D or "characteristic" curves. These are actually time-density curves, which have had rather limited use in photographic technology. Gamma is indicated by the uniform vertical spread of the individual curves in the middle region, corresponding to the straight-line portion of an H and D curve; and the vertical spread between adjacent curves at any place on the graph represents an average gradient ($\Delta D/\Delta \log E$) of the H and D curve for the selected increments of image density

In a manner analogous to Fig. 1, a scale of image density, or input density, is included, along with a scale of relative exposure values equivalent to the image density values. This scale is useful in adjusting actual exposures. The scale of negative densities, unlike that in Fig. 1, increases downward, so that values representing highlight and shadow tones occupy the same relative positions on the two graphs. This consistent placement of highlight and shadow values facilitates mental association with the actual tones, and also simplifies the graphical combination of data for successive operations.

Positive Material Characteristics

Following the same general scheme, the characteristics of a typical series of commercial

[3] Eastman Super Ortho Press Film, developer D-19 at 65 F. See *Kodak Reference Handbook* (Eastman Kodak Company, Rochester, 1941), p. 282.

contact papers[4] are illustrated in Fig. 3. Relative negative densities, the *input* densities for the positive printing operation, are again shown on an isolated vertical scale, along with a scale of equivalent exposures. In this case, the increment in negative density is taken as 0.1, because the more contrasty papers (Nos. 4 and 5) give too great a separation in print density for an increment of 0.2. Straight lines, instead of smooth curves, are drawn between corresponding points in the rectangular graph, because points lying between the vertical lines have no practical significance. In constructing Fig. 3 from conventional curves,[4] the value of zero relative negative density was arbitrarily chosen for convenience.

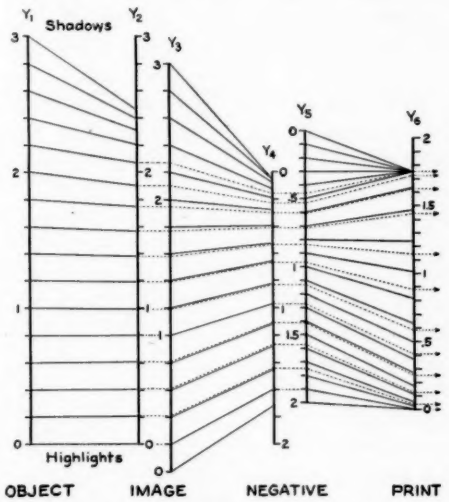

FIG. 4. Combined characteristics.

Combination Graphs

Graphs of the type illustrated in Figs. 1–3 lend themselves nicely to a rather unconventional, but expressive, method of combining data for a series of successive operations. In a given case, the input densities for an operation are found on the isolated vertical scale at the left of the graph for that operation, while the corresponding output densities lie on a vertical line which may be drawn on the rectangular graph at the proper value of the variable represented on the horizontal axis. These respective sets of input and output densities are transferred to two vertical axes, horizontally spaced apart by a convenient distance. Corresponding values are then connected with straight lines, which may be called *relation lines*. This graphical construction is illustrated in Fig. 4, in which axis Y_1 contains values of object density and axis Y_2 contains corresponding values of image density for a flare density of 2.6. Values on Y_1 and Y_2 were transferred from Fig. 1. The relation lines between Y_1 and Y_2 indicate close correspondence between object and image tomes in the highlight region, and increasing compression of image tones in the shadow region.

In the same way, axes Y_3 and Y_4 and the intervening relation lines in Fig. 4 show the relations between image densities and negative densities for the negative material whose characteristics are given in Fig. 2, the development time being 3 minutes. Axes Y_5 and Y_6 and the intervening relation lines illustrate the tone relations between the negative and print when the print is made on the No. 1 paper whose characteristics are shown in Fig. 3.

The vertical-axis plots for the individual operations are assembled by juxtaposing the output axis for one operation with the input axis for the succeeding operation. The individual plots may be laid out on separate cards or sheets of paper for convenience in alignment, although there is generally little difficulty in laying out the entire diagram in succession on a single sheet of paper. Since output densities are relative, and since they enter the following operation as a series of exposures, the respective values of input and output density may or may not lie opposite each other. Thus in Fig. 4, the scales on Y_2 and Y_3 do not match horizontally. The vertical placement of the two pairs of juxtaposed scales corresponds to adjustment of exposure to bring about the optimum distribution of output densities, and may be accomplished roughly by inspection. Scales of exposure time can be laid out on an extension of one of the juxtaposed axes, to be read against an index on an extension of the other, so that exposure times may be read off directly.

The intermediate axes having been aligned as in Fig. 4, object tone values may be traced through the successive operations by projecting

[4] Velox Grade F Glossy. See *Kodak Reference Handbook* (Eastman Kodak Company, Rochester, 1941), p. 554.

horizontally from Y_2 to Y_3, drawing additional relation lines where necessary, as shown by the dotted lines, and continuing in this manner to Y_6 for the finished print densities. The additional relation lines are located by interpolation, which can be done with fair accuracy by inspection, proper cognizance being taken of the original relation lines on either side of the interval being interpolated. The arrowed dotted lines extending to the right of axis Y_6 indicate the reflection densities of the positive print corresponding to object densities of 0.0, 0.2, 0.4 . . . 2.2, for the conditions illustrated. An over-all process graph can be constructed by showing only axes Y_1 and Y_6, with straight relation lines between.

DISCUSSION

Actual data are more easily explained by means of this system than is the system itself. It possesses both advantages and disadvantages. Graphs of the H and D type, in which input data are represented on the horizontal axis and output data on the vertical axis, are more suitable for certain purposes, and cannot be supplanted entirely by this system. It should be feasible to employ both types of graphs, however, each for different purposes, as is sometimes done in electronics. In fact, the rectangular graphs shown herewith are somewhat analogous to the "plate-family characteristics" currently employed in connection with electronic tubes.[5]

Evaluation of object and image tones in terms of equivalent density, to correspond with the evaluation of negative and positive tones, rather than in terms of brightness and illumination, lessens the mental effort required to compare tones throughout a reproduction process. The consistent representation of tone values on vertical axes, with highlight and shadow tones always in the same relative positions, markedly facilitates visualization. Although both the method of representing data for individual operations and the method of combining data for successive operations are unconventional, experience has shown that the entire system is readily grasped. One advantage of the method shown in Fig. 4 is that any number of operations may be accommodated on a single graph without confusion.

A disadvantage of this graphical system is that corresponding values of input and output tones are given with precision only for certain increments. Intermediate values must be interpolated. Another inconvenience is that these operation curves are most easily constructed by picking points from smooth curves of the H and D type, which therefore must be constructed first from experimental data.

Details of this system may, of course, be varied as desired. Highlight values may be placed at the top instead of the bottom, to agree with the artist's conception of "high" and "low" tones, although density values for positive images will then increase downward instead of upward. For most purposes it is practical to prefix the negative sign to values of density for negative images.

Photographic speed assignments can be incorporated in rectangular graphs of the type shown in Fig. 2 by choosing the end curve of a family to represent the exposure value for which the speed is calculated, and marking this curve with the exposure value or speed, or both. The speed assignment based on a limiting value of gradient,[6] which has been adopted as the American Standard Method for Determining Photographic Speed and Speed Number,[7] is a logical starting point for a family of curves, and it appears that an analogous principle should be applied to families of curves for photographic printing papers.[8] In either case it would be wise to include curves for minimum and maximum output density values, say in dotted lines, as well as for the useful values of output density.

[5] See *RCA Receiving Tube Manual*, Technical Series RC-14, 1940 (RCA Manufacturing Company, Inc., Harrison, New Jersey, 1940), p. 10.

[6] L. A. Jones, J. Frank. Inst. **227**, 297, 497 (1939).

[7] J. Opt. Soc. Am. **33**, 479–486 (1943).

[8] L. A. Jones and C. N. Nelson, J. Opt. Soc. Am. **32**, 558–619 (1942).

The Relative Merits of Red and White Light of Low Intensity for Adapting the Eyes to Darkness

WILLIAM M. ROWLAND AND LOUISE L. SLOAN
AAF School of Aviation Medicine, Randolph Field, Texas
(Received June 26, 1944)

IN an article recently published by Lowry,[1] it claimed that the reduction in time necessary to dark adapt the eyes after exposure to red light of low intensity is not significantly different from that required after exposure to white light of the same (photopic) intensity. While this conclusion is possibly correct for the particular conditions investigated by Lowry, under other experimental conditions a definite difference can be demonstrated in the effects produced by adaptation to red and to white light of the same photopic intensity.

Before discussing Lowry's experiments in detail we shall present the results of experiments made by the authors at the Wilmer Institute, Johns Hopkins Medical School, and at the School of Aviation Medicine. Figure 1 shows the rate of dark adaptation after exposure of the eye to 58 millilamberts (a) of red light and (b) of white light. The numerical data are given in Table I. The brightness of the red and white pre-exposure fields was determined by the same subject who served as observer for the adaptation experiments. The photometric measurements were made by equality-of-brightness photometry using a small photometric field. Consequently, it may be assumed that for this particular observer the *photopic* brightness of the red and the white pre-exposure fields were equal. The adaptation curves were determined with a 1° white stimulus located in the nasal field 15° from the fixation point. (The perimetric light sense tester described by Sloan[2] was used in making the determinations of the light threshold.) The adaptation curves therefore show the rate of recovery of sensitivity of the retinal rods. It is obvious from Fig. 1 that dark adaptation proceeds much more rapidly after pre-exposure to red than to white light at a brightness level of 58 millilamberts.

Further experiments were then made to determine what brightness of the white pre-exposure field would have the same effect on rod adaptation as 58 millilamberts. Figures 2 and 3 show the adaptation curves after pre-exposure to fields illuminated to 2 millilamberts and 1 millilambert. The numerical data are given in Table I. The

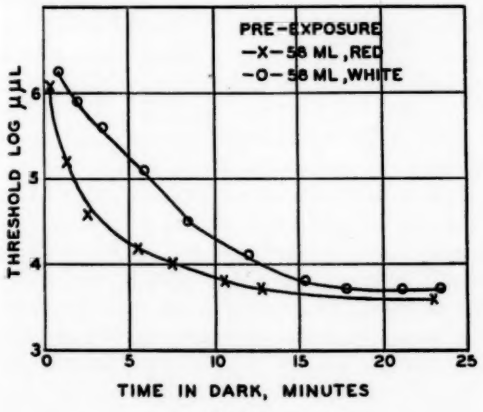

FIG. 1.

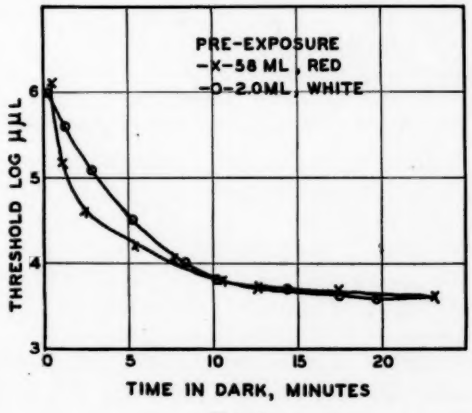

FIG. 2.

former curve lies slightly above, the latter slightly below, the curve obtained after exposure to 58 millilamberts of red light. We may conclude, therefore, that a white surface somewhere

[1] Earl M. Lowry, J. Opt. Soc. Am. **33**, 619 (1943).

[2] Louise L. Sloan, Arch. Oph. **22**, 233 (1939).

TABLE I. Rate of dark adaptation after pre-exposure to various intensities of red and white light.

Pre-exposure to 58 ml red		Pre-exposure to 58 ml white		Pre-exposure to 2.0 ml white		Pre-exposure to 1.1 ml white	
Time in dark, minutes	Threshold log μμl	Time in dark, minutes	Threshold log μμl	Time in dark, minutes	Threshold log μμl	Time in dark, minutes	Threshold log μμl
0.3	6.1	0.8	6.25	0.3	6.0	0.6	5.4
1.2	5.2	1.9	5.90	1.2	5.6	1.8	4.7
2.3	4.6	3.4	5.6	2.8	5.1	4.0	4.2
5.3	4.2	5.8	5.1	5.1	4.6	6.6	3.9
7.6	4.05	8.4	4.5	8.4	4.0	10.7	3.7
10.5	3.8	11.4	4.1	10.2	3.8	12.8	3.6
12.6	3.7	15.2	3.8	14.4	3.7		
17.4	3.7	17.7	3.7	17.5	3.6		
22.8	3.6	20.8	3.7	19.7	3.6		
		23.6	3.7				

TABLE II. Rate of dark adaptation after pre-exposure to various intensities of red and white light.

Pre-exposure to 3 ml red		Pre-exposure to 3 ml white		Pre-exposure to 12 ml red	
Time in dark, minutes	Threshold log μμl	Time in dark, minutes	Threshold log μμl	Time in dark, minutes	Threshold log μμl
0.5	4.43	0.7	5.10	0.5	4.78
1.9	3.95	1.5	4.48	1.8	4.45
4.6	3.73	3.9	3.90	2.9	4.13
5.9	3.68	5.5	3.90	5.3	3.95
7.9	3.60	7.8	3.73	7.3	3.80
9.8	3.58	9.3	3.73	10.5	3.75
10.6	3.68	10.4	3.60	12.7	3.60
		11.7	3.75	15.3	3.73
0.6	4.35	0.5	5.13		
1.8	4.0	1.9	4.73		
3.4	3.73	4.0	4.25		
5.3	3.55	6.9	3.98		
6.7	3.73	8.4	3.90		
9.1	3.50	10.6	3.80		
12.0	3.73	12.1	3.60		
		13.3	3.63		

between 1 and 2 millilamberts in brightness has the same effect on rod adaptation as a red surface of 58 millilamberts. This indicates that if the brightness of the red and the white surfaces could be measured by the rods instead of by the cones, 58 millilamberts of red would match in brightness 1 to 2 millilamberts of white light.

A further check on the scotopic brightness of the red light was obtained in another way. The transmission of the gelatine used to obtain the red light when measured in the usual way (photopic vision) was 4.55 percent. Measurements of the light threshold at 15° from the fixation point in the nasal field were made with and without this red gelatine in front of the eye. The threshold was 2.92 log units higher with the red gelatine, indicating that the scotopic transmission is no more than 0.12 percent whereas the photopic transmission is 4.55 percent. If, therefore, the transmission of the red filter as measured in scotopic vision is about 1/38 of its transmission as measured in photopic vision, then 58 millilamberts of red light is, in rod vision, equivalent to 58/38 or about 1.5 millilamberts of white light. This figure is in close agreement with that obtained experimentally.

It should be pointed out that exposure to such high intensities of light, when goggles are worn, would occur only when the general illumination was quite high. This may be the case when subjects taking a night vision test must be dark adapted prior to taking the test, and during this preliminary period of dark adaptation must remain outdoors or in a room exposed to high intensities of daylight. On the flying line, floodlights or searchlights may expose the eyes of the pilot to high intensities of illumination at a time when maximum dark adaptation is desirable. It is, however, unlikely that the illumination of "ready rooms" will provide brightnesses on the working plane much above 30 millilamberts unless supplementary individual lights are used in addition to the general illumination. The red dark adapter goggles in use at the present time have a transmission of approximately 10 percent. Viewed through red goggles, therefore, the apparent brightness on the working plane may be only about 3 millilamberts. At these lower levels, it is possible that the superiority of red over white light of the same photopic intensity is not as great as was found at higher levels.

In a second series of experiments, the red filter used was taken from a standard dark adapter goggle. Its total transmission (photopic), measured as before, was found to be 12.6 percent. The red filter used in the first series of experiments not only had a lower total transmission (4.6 percent) but also was a deeper red in color, because the "cut-off" point in the spectrophotometric transmission curve was nearer the long wave-length end of the spectrum.

In order to simulate the brightness levels which might be found in "ready rooms," a comparison was made of the affect on dark adaptation of pre-exposure to three millilamberts of red and to three millilamberts of white light. Two

independent dark adaptation curves were determined after exposure to the red light, and two after exposure to the white light. The experimental procedure was as follows: The observer was first dark adapted for 30 minutes, then adapted for 5 minutes to the red pre-exposure field. The curve of dark adaptation was then determined at a point 15° from fixation in the nasal field. Following this, he was adapted to the white pre-exposure field for five minutes, and a second curve of dark adaptation determined. Pre-exposure to the white field for five minutes was then repeated and the curve of dark adaptation measured once more. Pre-exposure to the red was then repeated and followed by determination of the curve of dark adaptation.

The results are shown in Fig. 4. The numerical data are given in Table II. As before, dark adaptation is seen to proceed more rapidly after exposure to red, although the difference is not as marked as in the experiments made at a higher intensity with a redder filter. Figure 5 shows the rate of dark adaptation after previous exposure to 12 millilamberts of red and for comparison the average curve of dark adaptation after exposure to 3 millilamberts of white. The numerical data are given in Table II. It is apparent that with the standard red dark adapter goggles 12

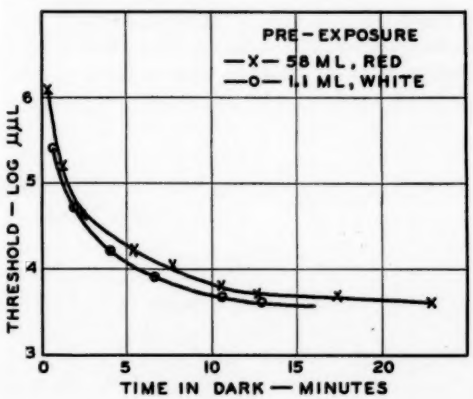

FIG. 3.

millilamberts of red and 3 millilamberts of white produce approximately the same degree of adaptation of the rods.

It should be remembered that red illumination for reading, writing, card playing, inspection of colored maps, etc., is, in certain respects, less satisfactory than ordinary artificial light. The color of objects is distorted in red light. Red figures on a white background such as are employed in standard playing cards are nearly

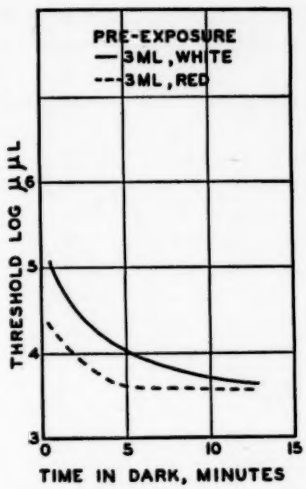

FIG. 4.

invisible. Because the eye is more hypermetropic for red than for white light, and possibly for other reasons, red light would cause more eye strain. Whether the advantage of red light in providing more complete dark adaptation of the retinal rods is sufficient to offset the disadvantages will depend upon the requirements of the particular situation. If we take the data in Figs. 4 and 5 as representative, we may conclude that the individual who has been adapted to 3 millilamberts of red light will require only 5 minutes in the dark for the rods to reach their maximum sensitivity, whereas if white light of the same intensity were used, it would require about 10 minutes. The threshold after 1 minute of dark adaptation would be about 0.7 log unit lower in the first case than in the second. In order to provide the same degree of dark adaptation as is provided by exposure to 3 millilamberts of white light, about 12 millilamberts of red light could be used. It is probable that reading with four times as much red light would produce less eye strain than with the lower amount of white light.

It must be recognized that the need for complete dark adaptation of the rods applies only to certain situations, for example, that in which another plane must be seen as a dark object against the sky or other background whose brightness is below the cone threshold. Under such conditions, the object can be seen only by making use of a more sensitive paracentral region of the retina.

The procedure used in Lowry's experiments was such that the degree of dark adaptation of the central retina, rather than of a paracentral region, was determined. After pre-exposure to a red or to a white field whose brightness was 3.4 millilamberts, measurements were made of the time required to perceive a test field of very low brightness (log micromicrolamberts equal to 4.54). The test field subtended a visual angle of 12°, and a small spot of red light at its center was used to maintain fixation. In our experiments, it will be recalled, threshold measurements were made with a 1° test spot, 15° from the fixation point in the nasal field. This difference in procedure is probably responsible for the difference in the results. Threshold measurements made with centrally fixated test fields, even though these extend beyond the fovea, will depend in part upon the response of the foveal cones. Since the red and the white pre-exposure fields were chosen so as to have an equal effect upon the cones, the differential effect of red and white would be much less than in a paracentral region of the retina where the threshold of the dark adapted eye depends entirely upon rod response.

Lowry's studies are of value in that they call attention to the conditions under which adaptation to dim red light offers little practical advantage in comparison with the use of the same

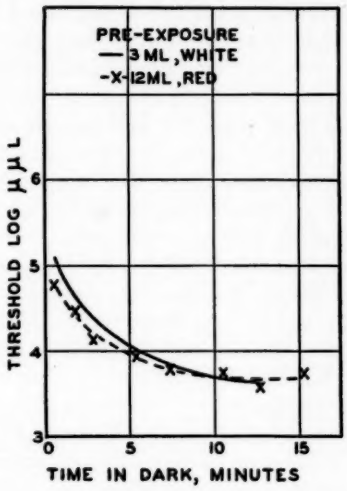

FIG. 5.

levels of white light. Whenever tasks requiring rod vision are involved, however, the use of red light is advisable. Lowry, in his discussion of the problem, has overlooked the fact that red and white lights of equal brightness in photopic vision are far from equal in scoptic vision.

JOURNAL OF THE OPTICAL SOCIETY OF AMERICA VOLUME 34, NUMBER 10 OCTOBER, 1944

Visual Data Applied to Lighting Design

PARRY MOON, *Massachusetts Institute of Technology, Cambridge, Massachusetts*

AND

DOMINA EBERLE SPENCER, *Tufts College, Medford, Massachusetts*

(Received May 8, 1944)

1. INTRODUCTION

IMPORTANT quantitative research on vision has been in progress for at least 80 years, and particularly valuable data have been obtained within the last decade. It is an unfortunate fact, however, that not only have the various investigations been conducted under different conditions and with different observers, but the results have been expressed in different units. Comparison of data has therefore been difficult, and little has been done to obtain standard curves that can be applied to illuminating engineering practice.

The purpose of this paper is to correlate some of the existing visual data and to find what practical conclusions can be drawn from these data. Consideration is first given to two kinds of results:

(1) Data on minimum-perceptible contrast between large contiguous surfaces with uniform surround.
(2) Data on minimum visual angle for small objects, high contrast, and uniform surrounds.

From this study, empirical equations are developed to represent average visual thresholds as functions of helios. These equations lead directly to conclusions regarding the gain in vision to be obtained by raising the room illumination. Results are given in the form of tables and graphs.

2. CONTRAST

The first quantity to be considered is *minimum perceptible contrast*. Measurements are made to determine the just-noticeable helios difference between a test object and its background. Experimental conditions are ordinarily simplified as much as possible, so that the background is uniform and fills nearly the whole field of view while the object is a circular disk of comparatively large size. Usually the object subtends a visual angle of at least 0.02 radian (1°).

The visual threshold can be defined under these conditions as $(H_B-H_0)_{\min}$, where H_B is the helios of the background and H_0 is the helios of the test spot. The helios threshold has been used extensively by Stiles and Crawford[1] and has been called by them, "brightness difference threshold" and "liminal brightness increment." But most writers prefer a related concept. Evidently, the quantity (H_B-H_0) is obtainable directly from the physical measurements, but it is not intimately associated with the visual sensation. For this reason, many investigators use *contrast*, which is not so simply related to the physical measurements but which has a better psychological interpretation.

Contrast may be defined in general as

$$c=(H_B-H_0)/H_B. \tag{1}$$

This quantity is a property of two contiguous surfaces. If one surface is larger than the other, the larger is considered as the "background" and the contrast is calculated by Eq. (1). Theoretically, c may vary from $-\infty$ to $+1$, and in practice the range of values is limited only by the available range of helios or of reflection factor.

Contrast in general is a physical property of a pair of surfaces, not a property of the eye. One may consider the *minimum perceptible contrast*, however, based on visual tests. By analogy with Eq. (1),

$$c_{\min}=(H_B-H_0)_{\min}/H_B. \tag{1a}$$

The quantity $c_{\min}$ is often called the "Weber-Fechner fraction."[2] In the special case of uniform incident flux density D on an extensive background of reflection factor ρ_B and an object of reflection factor ρ_0, Eq. (1) becomes

$$c=(\rho_B-\rho_0)/\rho_B, \tag{1b}$$

[1] W. S. Stiles and B. H. Crawford, Proc. Roy. Soc. **B113**, 496 (1933).
[2] P. Moon, *Scientific Basis of Illuminating Engineering* (New York, 1936), p. 421.

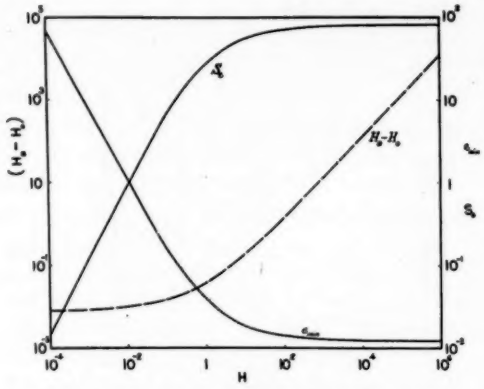

FIG. 1. Three ways of representing contrast data: (*a*) helios threshold, (H_B-H_0); (*b*) minimum perceptible contrast, $c_{\min}$; (*c*) contrast sensitivity, S_c.

which is independent of the absolute value of D. This constancy of c corresponds roughly to the fact that the *appearance* of the ensemble is essentially unchanged over a fairly wide range of D.

In the past, no distinction has been made between (H_B-H_0) and (H_0-H_B). It seems more precise, however, to define c as in Eq. (1), so that contrast is positive for an object that is darker than its background and negative for an object that is lighter than its background. The most definite test conditions are obtained with a uniform helios H_B for the entire visual field and with a test spot of helios H_0 exposed only momentarily. Then the eye adapts itself to the background, the adaptation helios[3] is $H_A=H_B$, and conditions are thoroughly standardized. With most other modern test conditions, Eqs. (1) and (1a) are unambiguous, though if the test field consists of two equal rectangles with a dark surround (Lummer-Brodhun photometer head) there is no way to decide which is H_B and which is H_0. Even in this case, however, the numerical values of $c_{\min}$ will be determined ordinarily within a few percent because H_B and H_0 will be almost the same.

Holladay[4] and a few other investigators have employed the reciprocal of $c_{\min}$, which is called *contrast sensitivity*. Thus the results of research have been expressed in three ways in the literature: as helios threshold, as contrast, and as contrast sensitivity. Typical curves for the three are shown in Fig. 1. Further confusion has been caused by the multiplicity of brightness units. In the present paper, all results will be given in terms of the contrast $c_{\min}$ and with the helios H expressed in blondels.

Among the latest data on minimum perceptible contrast are those of Hecht, Peskin, and Patt.[5] Results were obtained over a very wide range of helios with monocular vision and an artificial pupil. The test object subtended an angle of 12° and the illuminated surround subtended an angle of 40°. The data are very consistent, though the lowest values of $c_{\min}$ exceed 0.04, which is unusually high for such tests. These large values may be caused by the fact that the test object was exposed for only 0.04 sec.

The experimental results for two observers are plotted in Fig. 2. The circles represent the data of observers J.C.P. and M.P. with light obtained from incandescent lamps. Results with red light are shown by the squares. The points of Fig. 2 represent the results for natural pupil instead of artificial pupil. The original data were

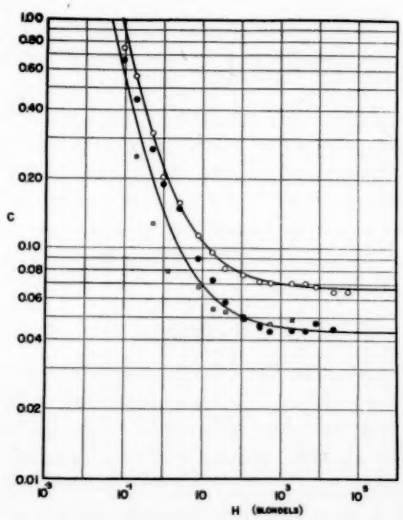

FIG. 2. Minimum perceptible contrast as a function of helios, experimental data of Hecht, Peskin, and Patt (see reference 5) corrected for natural pupil. ○ Observer J.C.P., incandescent lamps; ● observer M.P., incandescent lamps; □ observer M.P., red light; — Eq. (2), $n=2$.

[3] P. Moon and D. E. Spencer, J. Opt. Soc. Am. **33**, 444 (1943).

[4] L. L. Holladay, J. Opt. Soc. Am. **12**, 310 (1926).

[5] Hecht, Peskin, and Patt, J. Gen. Physiol. **22**, 9 (1938).

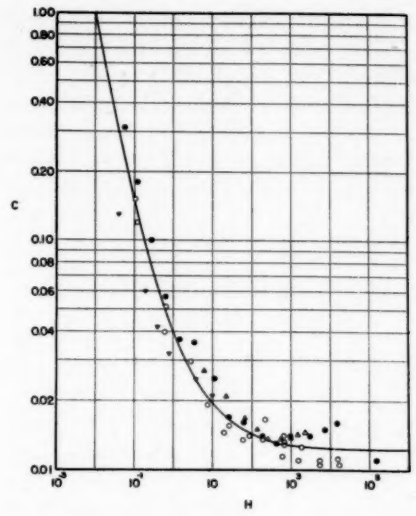

FIG. 3. Minimum perceptible contrast as a function of helios. Natural pupil. ○ Stiles and Crawford (reference 11), observer B.H.C.; △ Lowry (reference 12); ▽ Blanchard (reference 13); ● Steinhardt (reference 14), 3° 44′ field, corrected to natural pupil; — Eq. (2), $n=2$.

shifted to the left by the method of a previous paper.[6] Since no data on pupil size are available for these particular observers, the average[6] correction curve was used. In Fig. 2 only cone vision is considered, the results at very low values of helios (rod vision) being omitted.

Hecht[7] found that all data on minimum perceptible contrast, for human beings as well as for various animals, can be expressed by an equation of the form

$$c_{\min}=\frac{c_\infty}{H}(A_1+H^{1/n})^n, \qquad (2)$$

where $c_{\min}$ = minimum perceptible contrast at helios H,
c_∞ = minimum perceptible contrast for $H\rightarrow\infty$,
A_1, n = constants.

Other equations are possible, but Eq. (2) appears to be the simplest one that will fit the data. Hecht found[5] that the original data for artificial pupil were fitted by Eq. (2) with $n=2$. We find that when the data are corrected for natural pupil, the value of n is still 2. The curves of Fig. 2 were plotted for the Hecht equation

$$c_{\min}=\frac{c_\infty}{H}(A_1+H^{\frac{1}{2}})^2. \qquad (2a)$$

The same value of A_1 is found for both observers, but c_∞ is different, as shown in Table I.

Researches on minimum perceptible contrast have been conducted by a number of scientists. Excellent data were obtained in the nineteenth century by Aubert[8] and by König and Brodhun.[9] Their results, however, seem to add nothing to the recent investigations in which the helios is more precisely specified. Accordingly, these early data have been omitted in this paper, as well as a number of results[10] that did not agree with the average. Figure 3 shows data of Stiles and Crawford,[11] Lowry,[12] Blanchard,[13] and Steinhardt.[14] All the results were obtained with natural pupil except those of Steinhardt, which were corrected[6] before plotting.

The points of Fig. 3 show more scatter than those of Fig. 2. In fact, they do not allow a decision to be made between $n=2$ and $n=3$ in

TABLE I. Contrast, values of constants in the Hecht equation.

Fig.	Observer	A_1	c_∞
1	J.C.P.	0.808	0.0670
1	M.P.	0.808	0.0435
2	Average	0.808	0.0123

TABLE II. Comparison of visual acuity and visual angle.

Visual acuity (min.$^{-1}$)	α	α (microradian)
0.10	10 min.	2910
1.0	1 min.	291
2.0	0.5 min.	145
120	0.5 sec.	2.4

[6] P. Moon and D. E. Spencer, J. Opt. Soc. Am. **34**, 319 (1944).
[7] S. Hecht, J. Gen. Physiol. **18**, 767 (1935).
[8] H. Aubert, *Physiologie der Netzhaut* (Breslau, 1865).
[9] A. König and E. Brodhun, Sitz. Akad. Wiss. Berlin, p. 917 (1887).
[10] A. H. Holway, J. Opt. Soc. Am. **27**, 120 (1937); C. H. Graham and E. H. Kemp, J. Gen. Physiol. **21**, 635 (1938); B. H. Crawford, Proc. Roy. Soc. **B129**, 94 (1940).
[11] W. S. Stiles and B. H. Crawford, Proc. Roy. Soc. **B116**, 55 (1934).
[12] E. M. Lowery, J. Opt. Soc. Am. **21**, 132 (1931).
[13] J. Blanchard, Phys. Rev. **11**, 81 (1918).
[14] J. Steinhardt, J. Gen. Physiol. **20**, 185 (1936).

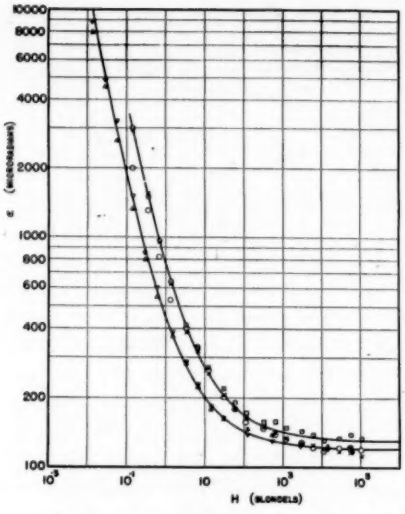

FIG. 4. Visual angle as a function of helios. Artificial pupil. △ Shlaer, Smith, and Chase (reference 15), observer A.M.C., red light; ▽ Shlaer, Smith, and Chase (reference 15), observer E.L.S., red light; × Shlaer (reference 15), observer A.M.C., inc. light, central fixation; □ Shlaer (reference 15) observer E.L.S., inc. light, central fixation; ○ Shlaer (reference 15), observer A.M.C., inc. light, no special fixation; — Eq. (5), $n=2$.

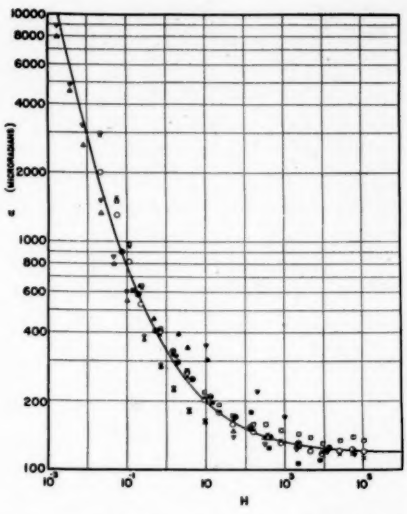

FIG. 5. Visual angle as a function of helios. Natural pupil. *Data for natural pupil:* ● Lythgoe (reference 16), average for 4 observers; ■ MacAllister, 3 observers; ▲ Conner and Ganoung, 7 observers; ▼ Cobb and Moss, 9 observers. *Corrected for pupil size:* △ Shlaer, Smith, and Chase (reference 15), A.M.C., red light; ▽ Shlaer, Smith, and Chase (reference 15), E.L.S., red light; × Shlaer (reference 15), A.M.C., inc., central fixation; □ Shlaer (reference 15), E.L.S., inc., central fixation; ○ Shlaer (reference 15), A.M.C., inc., no special fixation; — $n=3$.

the Hecht equation. In view of the definitely better fit with $n=2$ in Fig. 2, however, we have chosen the same value for Fig. 3. The constants for the plotted curve are listed in Table I. Note that the constant A_1 is the same for all three curves (Figs. 2 and 3).

Some of the scatter of the points at high helios may be caused by non-uniform surrounds. Other factors that may influence the results are size of test object and time of exposure. Differences between observers are also important. It is believed, however, that the curve of Fig. 3 represents good conditions as accurately as any single curve can represent them. Thus we recommend that, in the absence of more specific data, the minimum perceptible contrast be represented by the equation,

$$c_{\min}=\frac{0.0123}{H}(0.808+H^{\frac{1}{2}})^2. \qquad (3)$$

This equation applies only when conditions are as follows: natural pupil, cone vision, uniform surround, large comparison surfaces (10°–20°), sufficient exposure time (>0.1 sec.). A change in the size of comparison surfaces or the exposure time appears to have no effect on the constant 0.808 but does change the value of c_∞. The effect of a non-uniform surround will be considered in another paper.

3. VISUAL ANGLE

Among the most important visual tests are measurements of visual acuity. These tests, as in the case of contrast, may be divided into two groups: those made with an artificial pupil and those with natural pupils. It is found that the analytical representation of the Stiles-Crawford effect[6] allows the two groups to be compared and shows that they are in excellent agreement.

Before considering the data, one must first decide on the best method of representing them. It has been customary to use visual acuity and to specify it in reciprocal minutes, but there are several disadvantages to this method. Ordinarily one wishes to obtain the size of object that can be seen at a given distance or the distance at

which a given object will be visible. In either case, the visual acuity is converted into visual angle and this angle must be converted to radians. It seems much better to specify visual angle rather than visual acuity and to express this angle directly in radians. Since visual angles are very small, the angle α in radians is essentially equal to the tangent, so

$$\alpha \cong \tan\alpha = w/l, \quad w = \text{width of object}, \quad l = \text{distance from eye to object}. \tag{4}$$

The only disadvantage to this specification is that the numbers associated with α are very small and are therefore not as easy to remember as the familiar ones for visual acuity. But this difficulty is eliminated by expressing α in microradians. The range will then be from approximately 1 to 10,000 microradians as shown in Table II. The visual angle of 2910 microradians is near the upper limit for cone vision, values of 100 to 200 correspond to good visual acuities with broken-circle test objects, while the extraordinary value of 2.4 was obtained by Hecht for a single-line test object at high helios.

Among the most recent data on visual acuity are those of Shlaer, Smith, and Chase.[15] A black broken-circle test object was viewed against a uniform background that extended to a diameter of 30°. Monocular vision was employed with a 2-mm artificial pupil. The triangles of Fig. 4 show the experimental results for red light obtained from incandescent lamps with a Wratten No. 70 filter. The same observers worked also with unmodified light from incandescent lamps, care being taken to ensure central fixation. These results are shown by the crosses and squares of Fig. 4. Data are also given for one observer with no special fixation.

TABLE III. Visual angle, constants in the Hecht equation.

Reference	Light	A_2	α_∞ (radian)
Artificial pupil, Eq. (5), $n=2$			
Shlaer, Smith, and Chase	Red	0.941	119.8×10^{-6}
Shlaer	Inc.	1.432	130.8×10^{-6}
Natural pupil, Eq. (5), $n=3$			
Lythgoe, av. of 4 obs.	Inc.	0.412	118.3×10^{-6}
Shlaer	Inc.	0.412	118.3×10^{-6}
Hecht and Mintz, $n=3$	Inc.	1.100	1.442×10^{-6}
Hecht and Mintz, $n=2$	Inc.	1.433	1.950×10^{-6}

TABLE IV. Lythgoe's experimental results compared with calculated values of visual angle, Eq. (5).

H	α observed	α calculated	Percent difference
0.0785 blondel	899×10^{-6}	893×10^{-6}	0.7
0.1938	584	591	1.2
0.548	407	401	1.5
1.982	296	277	6.4
4.60	249	228	8.4
13.02	208	191	8.2
55.9	170	161	5.7
135.8	153	149	2.7
418	139	139	0
2240	130	130	0
13720	124	124	0

The Hecht equation applies to Fig. 4, or

$$\alpha = \frac{\alpha_\infty}{H}(A_2 + H^{1/n})^n, \tag{5}$$

where α = minimum perceptible visual angle (radians) for background helios H,

α_∞ = visual angle for $H \to \infty$,
A_2, n = constants.

Hecht found that for most data obtained with artificial pupil, $n=2$. The curves of Fig. 4 are plotted by use of Eq. (5) with $n=2$ and with the other constants as listed in Table III. It will be noted that excellent agreement is found between the experimental and calculated values.

Now consider the data obtained with natural pupil. The most consistent results are probably those of Lythgoe.[16] They are indicated by the black circles of Fig. 5. It is found, however, that Eq. (5) with $n=2$ will not fit these data, though if $n=3$ a good agreement is obtained. The curve of Fig. 5 is plotted for $n=3$, $A_2=0.412$, and $\alpha_\infty = 118.3\times10^{-6}$ (radian). Other data obtained with natural pupil are those of Conner and Ganoung,[17] Cobb and Moss,[18] and some un-

[15] Shlaer, Smith, and Chase, J. Gen. Physiol. **25**, 553 (1942); S. Shlaer, J. Gen. Physiol. **21**, 165 (1937).

[16] R. J. Lythgoe, Medical Research Council, Report of Committee upon Physiology of Vision (London, 1932).

[17] J. P. Conner and R. E. Ganoung, J. Opt. Soc. Am. **25**, 287 (1935).

[18] P. W. Cobb and F. K. Moss, J. Frank. Inst. 205, **831** (1928).

published results obtained at M.I.T. by C. C. MacAllister.

Lythgoe used a broken-circle test object which was exhibited at various angles. The observer was required to tell in which of 8 positions the test object was placed. Statistical analysis was made of the percentage of correct answers, and the size of objects was taken as that which resulted in 56.25 percent correct answers. The object was black and was seen against a white background illuminated by means of incandescent lamps. Conner and Ganoung used the same method as did MacAllister. Cobb and Moss employed a double-bar test object. The MacAllister results are in approximate agreement with those of Lythgoe and show even lower visual angles in some cases. The values of Cobb and Moss and of Conner and Ganoung indicate the same general trend but differ in magnitude from the Lythgoe data, perhaps because of differences in observers.

The data of Fig. 4 for artificial pupil were then corrected by use of the Stiles factor[6] and are included in Fig. 5. The transformed points are seen to be in good agreement with Lythgoe's data, the difference between the curve and the transformed points being less than the scatter of the natural-pupil data. In fact, the Shlaer results for no special fixation, transformed to natural pupil (white circles), are in as good accord with the curve as are Lythgoe's results. The other data of Shlaer, for incandescent sources, are slightly high or low, depending on the observer, while the data for red light are consistently low. Table IV shows a comparison of Lythgoe's experimental results with the values calculated by Eq. (5).

The test objects considered in the foregoing discussion have all been broken circles or similar shapes that approximate letters of the alphabet. The research of Hecht and Mintz[19] deals with an entirely different type of test object in the form of a long wire seen against a luminous background. Unlike previous tests made in Hecht's laboratory and mentioned in this paper, these measurements were made with binocular vision and natural pupil. The wire was viewed against a uniform disk subtending a visual angle of approximately 15° and the outer part of the field was dark. Three sets of data were obtained with observer S. H. The first series was of a preliminary nature and is not considered here. The other two are shown by circles in Fig. 6.

Hecht represented these data[19] by Eq. (5) with $n=2$. Such a curve is shown in Fig. 6 and the constants are given in Table III. It is also possible to represent the data with $n=3$ as shown by the dotted curve. The absence of data at very high helios makes it difficult to decide between the two. The use of $n=3$ would give better conformity with the natural-pupil data of Fig. 5, but only further experimental research can prove which representation is the better.

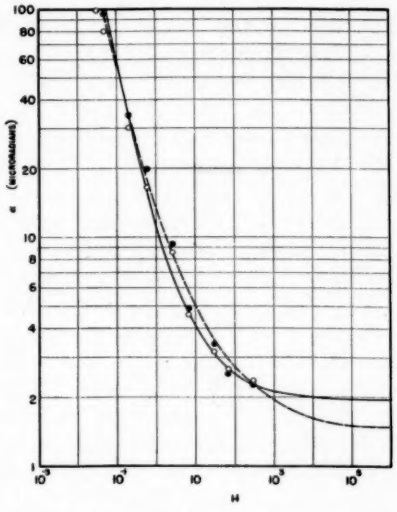

FIG. 6. Results of Hecht and Mintz. Single-bar test object. Natural pupil. ○ Series II, observer S.H.; ● Series III, observer S.H.; — $n=2$; - - $n=3$.

To summarize, one may say that the average of numerous data for cone vision with broken-circle test objects and large uniform surrounds is expressible by the equation

$$\alpha=\frac{118.3\times10^{-6}}{H}[0.412+H^{\frac{1}{3}}]^3, \qquad (6)$$

where α is the minimum perceptible visual angle (radians) and H is the helios of the background and surround (blondels). For single-bar test objects of considerable length, the best repre-

[19] S. Hecht and E. U. Mintz, J. Gen. Physiol. **22**, 593 (1939).

sentation is perhaps

$$\alpha=\frac{1.950\times10^{-6}}{H}[1.433+H^{\frac{1}{2}}]^2. \qquad (7)$$

Note that the magnitude is hardly more than 0.01 as great as the visual angle in Eq. (6). Both equations apply to observers with excellent eyes and under most favorable conditions. The average person will not be able to obtain such low values of α for a given helios. Glare sources or any other non-uniformity in the helios of the surround will likewise raise the minimum visual angle.

4. PRACTICAL APPLICATIONS

In the previous sections, equations have been obtained to represent visual data. These equations can be applied to many problems in optics and illuminating engineering and they are more convenient than the use of the data in their original form. For example, in the inspection of a manufactured product it may be necessary to distinguish small differences in reflection factor. Equation (3) applies:

$$c_{\min}=\frac{0.0123}{H}(0.808+H^{\frac{1}{2}})^2. \qquad (3)$$

With a known helios, the equation can be used to determine the minimum perceptible difference in reflection factor. Or if the minimum contrast is specified, the required incident flux density D is

$$D=\frac{0.653}{\rho(9.0c_{\min}^{\frac{1}{2}}-1)^2}, \qquad (3a)$$

where ρ is the reflection factor of the background.

Another application is to visual photometry. At the highest values of helios, Eq. (3) shows that a contrast of about 1 percent is distinguishable. If one wishes to use a visual photometer at $H=0.01$, however, the equation shows that the minimum perceptible contrast is 1.0. This means that under these conditions the eye itself limits the accuracy of visual photometry to approximately ±50 percent.

Of greater practical value is the equation for minimum angle. Equation (6) gives the relation between H and α:

$$\alpha=\frac{118.3\times10^{-6}}{H}[0.412+H^{\frac{1}{2}}]^3. \qquad (6)$$

This equation may be used to determine the minimum size object that can be seen at a given distance, the maximum distance at which a given object can be seen, or the helios required for a given α. Thus Eq. (6) is applicable to the determination of the size of letters to be used in a highway sign or an advertising sign which must be legible at a given distance. Or the incident flux density required for a given α may be obtained from

$$D=\frac{0.0700}{\rho(20.4\alpha^{\frac{1}{2}}-1)^3}. \qquad (6a)$$

A similar expression is found for a single-bar test object such as a wire or a flag pole silhouetted against the sky. In this case, Eq. (7) is employed instead of Eq. (6).

It should be remembered that the foregoing equations are based on optimum conditions—good observers and uniform visual fields. With average observers and non-uniform fields, the values of $c_{\min}$ and α must be increased.

5. S CURVES

In the test procedure employed in many researches, the observer varies the size or the contrast continuously until he reaches the threshold of visibility. The results of such tests depend to some extent on the limit that the individual sets up unconsciously, and this limit may vary from day to day. To obtain a more precise criterion, Lythgoe[16] presented definite test objects and required the observer to specify how the test object was oriented. The number of correct answers, expressed as a fraction of the number of observations, was called y.

A broken-circle test object was exhibited in any one of eight positions. An answer was required for each presentation, even when the observer was guessing, and thus the lowest value of y to be expected is 0.125. When y is plotted against the logarithm of the visual angle, an S-shaped curve is obtained. The value of α is determined most accurately where the slope of

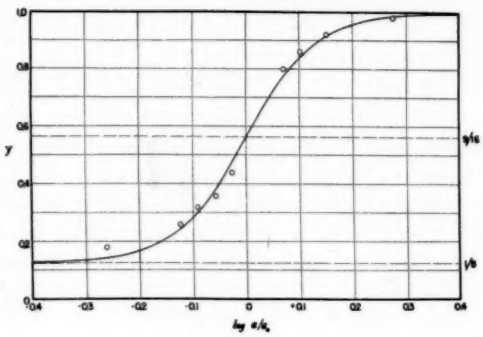

FIG. 7. S curve. Observer "C," light from incandescant lamps, black broken-circle test object against white background, $H_A=H_B=14$ blondels. Each point represents 50 observations.

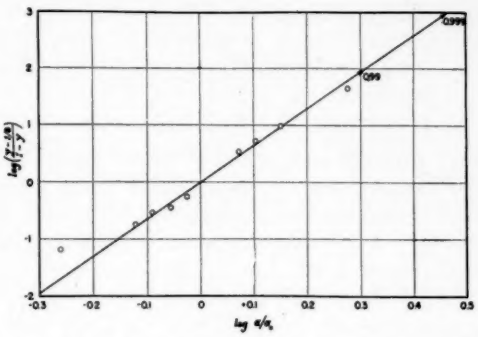

FIG. 8. Curve and data of Fig. 7 plotted on a different scale. $k=6.5$. ○ Experimental points; — Eq. (8); + Calculated points for $y=0.990$ and $y=0.999$.

the curve is a maximum, which is found to be at $y=\frac{9}{16}=0.5625$. Accordingly, the value of α corresponding to $y=\frac{9}{16}$ is always taken, and at each helios it is this value that is used in Fig. 5.

The question now arises, how will the curve of Fig. 5 be altered if the criterion is changed to any other value of y. For a given helios, how large must the object be so that it will be seen 90 percent of the time or 99 percent? This information can be found by an examination of the experimental S curves. Figure 7 shows such a curve obtained by a single observer at the Massachusetts Institute of Technology. The standard broken-circle test objects ($\rho=0.04$) were presented on a white background ($\rho=0.87$) with a large, uniform surround as in the Lythgoe tests[16] and the Conner-Ganoung tests.[17] The test object was spun rapidly by means of an electric motor and was suddenly stopped in one of 8 positions by a magnetic clutch. Tests showed that the clutch acted in a random manner and in a large number of trials, the test object was exhibited approximately the same number of times in each position. Each point of Fig. 7 represents 50 observations.

Lythgoe found that the S curve could be represented by the equation,

$$\frac{\alpha}{\alpha_0}=\left(\frac{y-\frac{1}{8}}{1-y}\right)^{1/k}, \qquad (8)$$

where y = fraction of total answers that are correct,

α = visual angle (radian) corresponding to y,

α_0 = visual angle corresponding to $y=\frac{9}{16}$,

k = constant.

This equation is found to be in good agreement with the M.I.T. tests, as shown by the curve of Fig. 7 which was plotted by use of Eq. (8) with $k=6.5$.

Since Eq. (8) can be written

$$\log\left(\frac{y-\frac{1}{8}}{1-y}\right)=k\log(\alpha/\alpha_0), \qquad (8a)$$

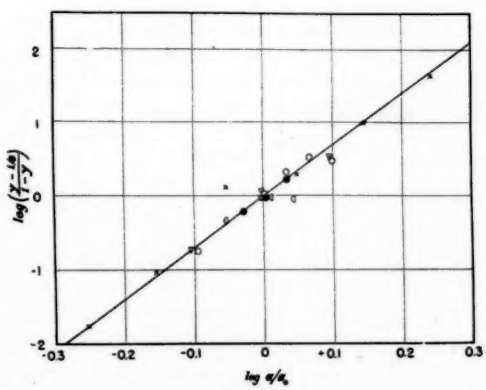

FIG. 9. S curve for $H_A=H_B=0.14$ blondel. $k=6.9$. ○ Observer B, × C, △ G, ▽ L, ● M, ◐ S, ◗ T, □ U.

a plot of the experimental data for

$$\log\left(\frac{y-\frac{1}{8}}{1-y}\right) \quad vs. \quad \log(\alpha/\alpha_0)$$

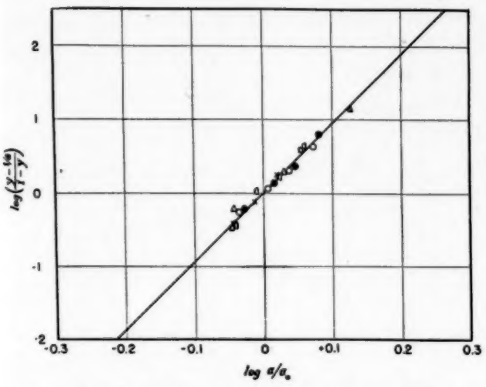

FIG. 10. S curve for $H_A = H_B = 590$ blondels. $k = 9.3$.

should give a straight line, and the slope of this line should be equal to k. Figure 8 shows the same data and same curve as Fig. 7. The slope of the curve is 6.5. Two other representative S curves are shown in Figs. 9 and 10, one for a low value of helios and the other for a high value. The slopes are found to be 6.9 for $H = 0.14$ and 9.3 for $H = 590$ blondels, showing a tendency toward sharper judgments at high helios. This tendency is indicated also by Fig. 11. Here values of k are plotted against helios. The new results are in approximate agreement with those of Lythgoe and extend his values to higher H. There is considerable scatter in the points of Fig. 11 since, with a few exceptions, the tests

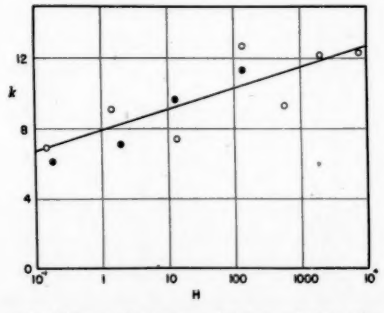

FIG. 11. Slopes of S curves. Values of k in Eq. (8). ● Lythgoe; ○ M.I.T.

were designed to establish the point at $y = \frac{9}{16}$, not to determine the shape of the S curve. Consequently, readings were taken as near this point as possible, which makes difficult the precise determination of slope.

Since the increase in k is small over the helios range used in lighting practice, it seems permissible to select an average value such as $k = 10$. Figure 12 shows a plot of Eq. (8), with $k = 10$, the horizontal scale being logarithmic in $(1-y)$. It will be noted that an increase from $y = \frac{9}{16}$ to $y = 0.90$ multiplies the visual angles by only 1.23. Even an increase to $y = 0.999$ multiplies the visual angles by less than 2. Graphically this means that the visual-angle curve (Fig. 5) is translated upward by log $\alpha = 0.3$ or less. In other words, the size-range between half-seeing and complete seeing is rather narrow. *If a certain object is so small that it is visible only half the*

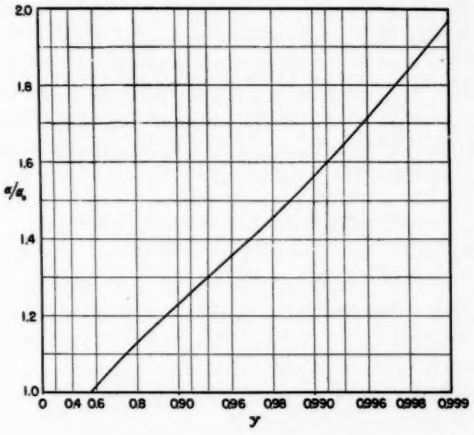

FIG. 12. Calculated change of visual angle as the criterion is varied. The quantity y is the number of correct answers, expressed as a fraction of the number of observations; α_0 is the visual angle corresponding to $y = 0.5625$.

time, doubling the size will make it visible all the time.

The size of object that is seen for any given fraction y of the number of observations can be expressed by means of Eqs. (5) and (8):

$$\alpha = \frac{\alpha_\infty}{H}\left(\frac{y-\frac{1}{8}}{1-y}\right)^{1/k}(A_2 + H^{1/n})^n. \qquad (9)$$

If the approved constants for C test objects are used, Eq. (9) becomes

$$\alpha = \frac{118.3\times10^{-6}}{H}\left(\frac{y-\frac{1}{8}}{1-y}\right)^{0.10}(0.412 + H^{\frac{1}{3}})^3, \quad (9a)$$

where α is in radians and H is in blondels. This equation can be solved for H:

$$H=\frac{0.0700}{\left[\left(\frac{\alpha}{118.3\times10^{-6}}\left(\frac{1-y}{1-\frac{1}{8}}\right)^{0.10}\right)^{\frac{1}{3}}-1\right]^{3}}. \quad (9b)$$

Equation (6) and Fig. 5 give threshold values of visual angle. Obviously they cannot be used directly to establish satisfactory values of luminous flux density for a given visual task. A safety factor must be introduced, to make possible the performance of the task over long periods of time with minimum fatigue. It was with a hope of establishing scientifically such a safety factor that the work outlined in this section was undertaken. The result, however, turns out to be negative, for the safety factors calculated in this way are found to be too small to meet the requirements of everyday experience. In Section 6 another method is investigated that gives more practical results.

6. FLUX DENSITY REQUIRED FOR ADEQUATE VISION

A subject of frequent and acrimonious debates among illuminating engineers is what value of luminous flux density is required for satisfactory vision. When König's data were taken as reference, which was generally the case until recently, the statement was often made that no appreciable improvement in vision was obtained by raising the helios above 30 blondels (approximately 3 lumens/ft.^{2} from a perfectly diffusing background). Uhthoff's work[20] indicated 35 blondels as the approximate helios beyond which there is no appreciable gain in vision, Cohn[21] (1895) gave 17, Snellen[22] (1896) gave 30 to 50, and Clark[23] (1924) gave 43. Others advocated much higher values. Even the modern tests have not led to any unanimity of opinion. As Lythgoe* points out, if visual acuity is plotted against brightness on a linear scale, the position of the apparent knee of the curve depends on the scale. And if a logarithmic scale is employed for the ordinates, the curve appears to be practically flat when it is actually changing at an appreciable rate.

Yet, despite these experimental values of 20 to 50 lumens/m^2, it is common knowledge that we see better in daylight outdoors ($D=10^3$ to 10^5 lumens/m^2) than we do in artificially lighted rooms. The belief has arisen that a justification of these facts of common experience requires a radically different kind of test which somehow evaluates "visual comfort" or "visual fatigue." Much research has been devoted to such tests, and measurements have been made on heart rate, muscular tension, and blink rate[24] as a function of helios. A re-examination of the *threshold data*, however, indicates that they alone

TABLE V. Helios required for a given delos.

T	Helios (blondels) From contrast data	From angle data
0.99	26,100	1,860,000
0.98	6,330	229,000
0.95	972	13,750
0.90	223	1,540
0.80	46.8	152
0.70	7.0	34.7
0.50	3.79	3.99
0.20	0.426	0.196
0.10	0.139	——

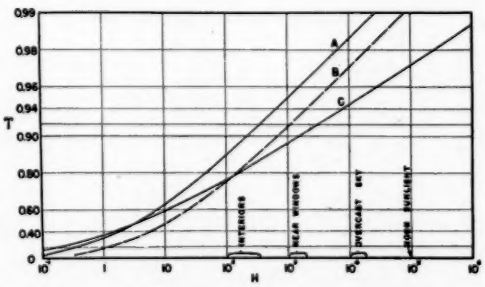

FIG. 13. Delos as a function of helios. *A*, for contrast, T_c; *B*, for angle, single-bar test objects; *C*, for angle, *C* test objects, T_α.

[20] W. Uhthoff, Arch. Ophthal. **32**, 171 (1886).
[21] Cohn, Arch. Augenhlk. **31**, 197 (1895).
[22] H. Snellen, Ophthal. Rev. **15**, 164 (1896).
[23] J. H. Clark, *Lighting in Relation to Public Health* (Baltimore), p. 185.
* Reference 16, p. 28.

[24] M. Luckiesh and F. K. Moss, *The Science of Seeing* (New York, 1937).

TABLE VI. Incident flux density required for a given visual acuity.

Υ_α (Relative visual acuity)	Flux density (lumen/m²) $\rho=1.00$	0.80	0.50	0.20	0.10	0.04
0.98	2.29×10^5	2.86×10^5	4.58×10^5	1.15×10^6	2.29×10^6	5.72×10^6
0.95	1.37×10^4	1.72×10^4	2.74×10^4	6.87×10^4	1.37×10^5	3.44×10^5
0.90	1540	1926	3080	7700	1.54×10^4	3.84×10^4
0.80	152	190	304	760	1520	3800
0.70	34.7	43.3	69.4	173	347	867
0.50	3.99	4.99	7.98	20.0	39.9	99.8
0.20	0.196	0.245	0.392	0.980	1.96	4.90

may suffice to show how vision improves as helios increases.

According to Eq. (2a),

$$H=\left[\frac{A_1}{(c/c_\infty)^{\frac{1}{2}}-1}\right]^2. \tag{10}$$

The corresponding equation dealing with visual angle is obtained from Eq. (6),

$$H=\left[\frac{A_2}{(\alpha/\alpha_\infty)^{\frac{1}{2}}-1}\right]^3. \tag{11}$$

From these expressions one can plot the helios required to give any specified ratio c_∞/c or α_∞/α. The quantities c_∞ and α_∞ represent best possible vision; that is, vision with uniform fields of extremely high helios. The ratios c_∞/c and α_∞/α are always less than unity and become lower as vision becomes poorer. The latter ratio has a definite physical significance. If w is the width of an object that can just be discerned at distance l, then

$$\alpha\leqq\tan\alpha=w/l \tag{12}$$

and

$$\alpha_\infty/\alpha=l/l_\infty, \tag{12a}$$

where l_∞ is the greatest distance at which the same object can be seen under best conditions. Thus α_∞/α represents the "visibility distance" at a given helios H, expressed as a fraction of the "visibility distance" at very high helios.

These ratios occur so frequently and have such definite significance that it is convenient to represent them by a special name. They might be called "relative visibility," "visual efficiency," or "relative vision," but since all such names are likely to cause confusion, a new name is preferable. The ratios α_∞/α and c_∞/c will be called *delos* ($\delta\tilde{\eta}\lambda os$ = visible) and will be denoted by the Greek letter upsilon (Υ). The experimental data indicate that the two ratios are not greatly different. If it is necessary to distinguish between them, however, a subscript may be used on the symbol and the quantity may be called "delos with respect to angle, Υ_α" or "delos with respect to contrast, Υ_c."

Table V gives some values computed by Eqs. (10) and (11). The table lists the values of helios that are required for a given delos. For vision equal to 98 or 99 percent of optimum ($\Upsilon=0.98$ or 0.99), very high values of helios are necessary. But if less stringent visual requirements are satisfactory, the helios can be greatly reduced. Since a white surface in direct sunlight has a helios of approximately 100,000 blondels, it is evident that a few of the calculated values of Table V are higher than are obtainable even outdoors. Note, however, that up to sunlight values the equations are not extrapolated but are based on the experimental data shown in Figs. 3 to 5. The upper horizontal line in the third column of the table divides the values into practical and impractical. The lower horizontal lines indicate a division between adequate and inadequate values for interior lighting.

The calculated values of delos are plotted in Fig. 13. Both scales are logarithmic. There is no reason to expect that the curves for Υ_α should be identical with the one for Υ_c. Three curves are shown, one based on visual angle with C objects, Eq. (6); one for visual angle with single-bar test objects, Eq. (7); and the third for contrast, Eq. (3). All curves show the same general trend. They indicate that vision is almost perfect ($\Upsilon=0.95$ to 0.99) for outdoor conditions with an

overcast sky. For reading near a window in the daytime, vision is still between 0.90 and 0.95, which agrees with the qualitative results of everyday experience. But with a helios of 10 blondels obtained with artificial lighting, Fig. 13 shows that the delos has fallen to approximately 0.60. Vision in ordinary lighting practice is reduced even further by non-uniformity. Figure 13 is based on the assumption of a completely uniform surround, as noted previously.

The practical conclusions with regard to lighting are shown to better advantage in Table VI. Since ordinary visual tasks in rooms are more directly related to visual acuity than to contrast discrimination, the Υ_α results of Table V have been used. To obtain these values of helios, however, the incident flux density on the work must be increased inversely as the reflection factor of the surface. For example, if the work consists of white paper with a reflection factor of 0.80, the third column is used; while if the task consists of sewing on dark cloth, the last column is used.

Since direct sunlight gives at most only 10^5 lumens/m^2, it is evident that the values in the upper part of the table have no meaning in practice. The broken horizontal line in Table VI indicates the upper limit for available outdoor illumination. Evidently, 90 to 95 percent vision can be obtained even on the darkest materials in direct sunlight. The lower broken line indicates the maximum illumination obtained in present interior lighting, where values of D above 500 lumens/m^2 are seldom obtained. The table indicates that for outdoor lighting (region between the two broken lines) vision ranges between 70 and 95 percent while for artificial lighting vision will generally be less than 80 percent.

It should be pointed out again that these results are based on visual tests obtained with entire absence of glare and with observers having excellent eyes. It is found, however, that the constants A in Eqs. (10) and (11) are almost the same for different observers. Defective vision appears to change only c_∞ and α_∞. Since this section is based only on relative values, the curves and tables should continue to apply without change even for observers having somewhat defective vision.

7. SUMMARY

An examination was made of data on minimum perceptible contrast with large contiguous surfaces. The data are represented by the equation

$$c_{\min}=\frac{0.0123}{H}(0.808+H^{\frac{1}{3}})^2, \qquad (3)$$

which applies when cone vision is employed with a natural pupil and a large uniform surround. H is the helios (blondels) of the uniform surround.

A similar investigation was made of the data on minimum visual angle α. The equation is

$$\alpha=\frac{118.3\times10^{-6}}{H}[0.412\times H^{\frac{1}{3}}]^3 \qquad (6)$$

where α is in radians. Equation (6) applies to the broken-circle test object and is an approximation for other letters and similar objects. For single-bar test objects of considerable length,

$$\alpha=\frac{1.950\times10^{-6}}{H}[1.433+H^{\frac{1}{3}}]^2. \qquad (7)$$

The foregoing equations are based on the criterion of $y=0.5625$. In other words, the observer is distinguishing the object only about half the time. It is interesting to see how these results are altered if the criterion is changed. Lythgoe found that the effect could be expressed by the equation

$$\frac{\alpha}{\alpha_0}=\left(\frac{y-\frac{1}{8}}{1-y}\right)^{1/k}, \qquad (8)$$

where α_0 is the visual angle corresponding to $y=0.5625$. Our data show that k is approximately 10, so the visual angle corresponding to any helios H and any y is

$$\alpha=\frac{118.3\times10^{-6}}{H}\left(\frac{y-\frac{1}{8}}{1-y}\right)^{0.10}(0.412+H^{\frac{1}{3}})^3. \qquad (9a)$$

Equation (9a) applies specifically to the standard broken-circle test object and approximately to any letter or similar object. A similar expression can be found for single-bar test objects by use of Eqs. (7) and (8). It is found that a change in

criterion has comparatively little effect. A change from the usual value of $y=\frac{9}{16}$ to $y=0.999$ changes the size of the object by less than 2.

The purpose has been to correlate existing visual data and present it in a form that can be used in engineering practice. Hitherto, such applications have been limited by the fact that the data have been scattered through many scientific publications and no analytic representation has ordinarily been available. One application of the equations of the present paper is to the question of how much light is needed in the lighting of rooms. All modern data show that *there is no optimum value of helios:* the higher the helios, the better the vision. But the question still remains, how much reduction in vision is caused by the fact that artificial lighting systems cannot reach daylight flux densities. In considering this question, we introduce the ratio,

$$\Upsilon=\alpha_x/\alpha$$

which is called *delos*. Evidently the delos is always less than unity and represents a sort of "relative visibility." According to Eq. (11), the helios required for a given delos is

$$H=\left[\frac{0.412}{(1/\Upsilon)^{\frac{1}{3}}-1}\right]^3. \tag{11a}$$

Table V gives some computed values, and Fig. 13 presents the results in graphical form. The values are in agreement with everyday experience. They determine the helios to be employed to obtain any desired delos.

In conclusion we express our thanks to Mr. C. C. MacAllister for his work on visual acuity and on S curves, to the National Youth Administration, and to the observers, Messrs. P. B. Black, L. S. Castleman, M. S. Cettei, A. B. Gold, G. J. Laurent, V. Lippitt, R. S. Mabee, R. A. Schiffmann, and J. M. Topalian.

The Eastman Color-Temperature Meter Used as an Anomaloscope*

LOUISE L. SLOAN
AAF School of Aviation Medicine, Randolph Field, Texas

THE Eastman color-temperature meter[1] is a device for measuring the color-temperature of light sources. One-half of a circular, bipartite field is illuminated by light passing through a filter with maximum transmittance of 580 mμ, the other half by light passing through a two-band filter with maximum transmittances at about 520 mμ and 680 mμ, respectively. The proportion of light transmitted in each of the two bands will vary with the color-temperature of the source. These proportions can also be varied by changing the effective color-temperature of the source with an amber wedge. This wedge is circular, and any desired thickness may be interposed in the light beam by rotation of the controlling knob.

The instrument may be used as an anomaloscope[2] by employing a constant light source and determining the proportions of red and green in the mixture field required by different individuals to obtain a color match in the two halves of the field. For this purpose it is more convenient to substitute a scale graduated in degrees of arc for the one graduated to read color-temperatures. Deuteranomalous subjects will require a greater proportion of green than the normal observer, protanomalous subjects a greater proportion of red. In preliminary experiments with normal and color deficient subjects, it was found that with any one light source, the range was not sufficient to permit normal, deuteranomalous, and protanomalous observers all to match the two fields in color. When, for example, a 60-watt lamp is used, some of the deuteranomalous group are not able to obtain sufficient green in the red-green mixture. If, however, a green filter, for example, is placed over the eyepiece so as to change the proportions of red and green required for a match, the deuteranomalous and the normal group can match the two fields, but some of the protanomalous group cannot because they require more red in the mixture.

Figure 1 shows the results of tests in which a 60-watt lamp was used as the source of light, and a green gelatine filter (Wratten No. 11) was used when necessary to extend the range. The match settings for normal subjects were determined both with and without the auxiliary filter, those of protanomalous subjects without the filter, and those of deuteranomalous subjects with it.

In later studies a simpler procedure was adopted in which the dial controlling the red-green ratio was set in turn at a series of selected points, and the subject was required at each setting to name the colors of the two halves of the field. From the answers given, a "point of reversal" or point at which the mixture field changes from green to red can be determined for each subject. The series of 11 dial settings used in the color-naming test is indicated in Table I. These are assigned arbitrary numbers from +5 to −5. This table shows typical responses for normal, protanomalous, and deuteranomalous

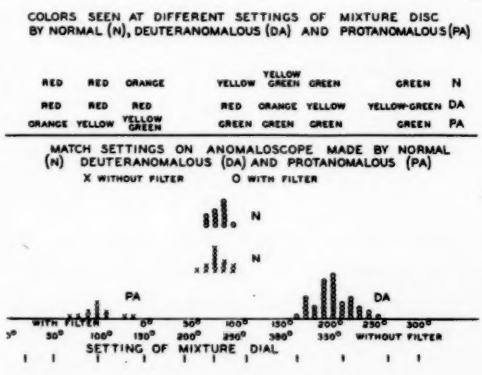

FIG. 1. Distribution of match settings for normal and color deficient subjects.

subjects and for those with a marked defect, probably indicative of complete or almost complete loss of perception for red and green. The latter group differ from the anomalous and the normal subjects in that, as the proportions of

* Paper presented at the Winter Meeting of the Optical Society of America, held in New York City, March 2–4, 1944.

[1] E. M. Lowry and K. S. Weaver, J. Soc. Mot. Pict. Eng., pp. 298–306 (March, 1939).

[2] This use of the color-temperature meter was suggested to the author by Dr. F. L. Dimmick.

TABLE I. Typical records for normal and color deficient subjects.

Settings on arbitrary color scale	Degrees on scale	Normal		Deuteranomalous		Protanomalous		Marked defect			
						Color of field					
		Upper	Lower	Upper	Lower	Upper	Lower	Upper	Lower	Upper	Lower
+5	300	y	g	y	g	or	g	or	y	r	y
+4	270	y	g	y	g	or	g	or	y	r	y
+3	210	y	g	y	reddish* tinge	or	g	or	y	r	y
+2	160	y	g	y	light red	or	g	or	or	y	y
+1	110	y	g	y	r	or	g	or	or	g	g
0	80	y	y*	y	r	or	g	or	or	y	y
−1	50	y	or	y	r	or	g	or	or	y	y
−2	150	y	or	y	r	y	g	or	or	r	r
−3	100	y	r	y	r	y	y*	or	or	r	r
−4	50	y	r	y	r	y	r	or	or	g	g
−5	10	y	r	y	r	g	pink	or	or	g	g

With auxiliary filter / Without filter

* Point of reversal. y—yellow. g—green. r—red. or—orange.

red and green are varied from a maximum of green to a maximum of red, no consistent series of color names is given.

A total of 308 subjects has been tested with this simplified procedure. One hundred of these were classed as normal on the basis of tests with either an abridged 17-plate version of the American Optical Company Pseudo-Isochromatic Charts or with the Rabkin Polychromatic Charts or with both. The remaining 208 subjects failed the chart tests. Figure 2 shows the location of the points of reversal for the normal and anomalous subjects. Those of the normal group range from +1.0 to −0.5. (If the mixture field appears greenish at 0, reddish at −1.0, the point of reversal is recorded as −0.5.) In the color deficient group, 58 percent were classed as deuteranomalous, 20 percent as protanomalous. Eighteen percent showed evidence of a marked defect with no definite point of reversal. Eight subjects, or approximately four percent of the entire color deficient group, gave perfectly normal responses on this test. Two of these men were tested on two other forms of anomaloscope by more detailed procedures and again gave entirely normal responses. On these instruments, the Hecht and the Rand anomaloscopes, the range as well as the midpoint of the match setting was determined and in neither case was there any evidence of abnormality.

The eight subjects who failed the pseudo-isochromatic chart tests but gave normal responses on the anomaloscope made relatively few errors in reading the charts. Their scores on the color threshold test[3] were better than those made by 76 percent of color deficient individuals. Six of these men took part in practical field tests requiring the identification of red, green, and yellow pyrotechnic signals. In these tests all with normal color vision and about 10 percent of color deficient subjects were able to identify the signals without error. The six who passed the anomaloscope test were included in the small group who made no errors in identifying the pyrotechnic signals. All findings suggest that those who pass the anomaloscope test, but fail

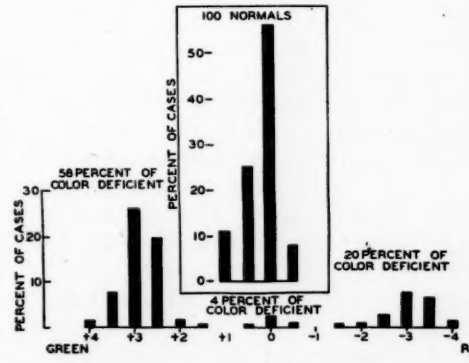

FIG. 2. Distribution of points of reversal for normal and color deficient subjects.

tests employing pseudo-isochromatic charts, have a relatively mild defect.

Of the various simple tests for color blindness

[3] This test will be described in an article to be published in the *American Journal of Ophthalmology*.

which have been described in the literature, none has been found to detect a greater percentage of red-green color deficiency than the pseudo-isochromatic type. For this reason, and because large groups can be examined in a very short time, this type of test is of especial value as a screening test which will detect color deficient subjects with all degrees of defect. However, in the selection of flying personnel, for example, such tests are open to the objection that color deficient individuals can be, and have frequently been, coached to pass them.

As a screening test, the chief objection to the anomaloscope is the fact that about 4 percent of color deficient individuals are not detected. This objection is unimportant, however, when this small group who apparently have only a slight defect can be shown to have adequate color perception for the particular tasks to be required of them. If the color-naming procedure is used, the anomaloscope test requires even less time than a test with the abridged version of the American Optical Company charts. Since this particular anomaloscope uses gelatine filters, it might be possible to reproduce the colors corresponding to the eleven settings of the dial for lantern slide projection, and thus test large groups simultaneously with considerable saving of time. Such a test could easily be devised so that intentional deception on the part of the examinee as to the status of his color vision would be almost impossible.

A Useful Tool for Shaping Spectrographic Graphite Electrodes

E. JOHN EASTMOND
Western Regional Research Laboratory, Albany, California*

(Received August 7, 1944)

DIRECT current arc methods of spectrographic analysis commonly employ graphite electrodes with a central cup sample cavity. The size of this cavity is dependent on the form of the sample under investigation and the amount found necessary to give spectra suitable for the analysis required. Satisfactory results have been reported for cavities varying from wide shallow cups[1] to drilled holes of a centimeter[2] or more in depth. Several tools have been described[3] for simplifying and standardizing the cutting procedures.

For certain dry powder and dry ash samples encountered at this laboratory, an electrode with a central post and annular ring cavity (Fig. 1) has proved to give a steadier and more reproducible arc[4] than was possible with a central cavity. A somewhat similar shape, but more difficult to cut, has been used elsewhere in the analysis of stainless steel filings.[5] As previously described, the arc strikes chiefly to the central post and "wandering" around the cup rim is largely avoided. No serious background results provided exposures are not continued after the sample has been completely burned.

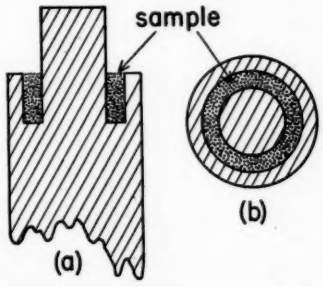

FIG. 1. Graphite electrode with annular ring sample cavity. (*a*) Longitudinal section. (*b*) Top view.

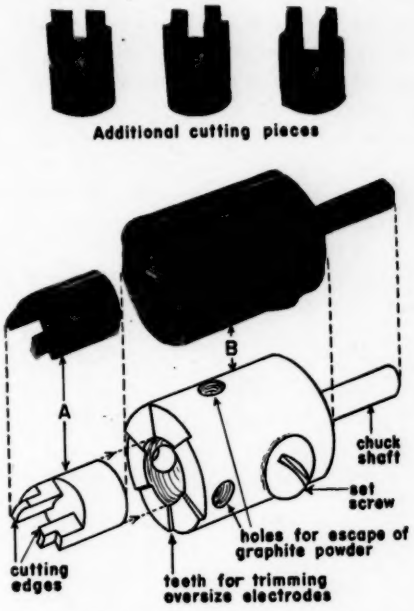

FIG. 2. Electrode cutting tool, unassembled.

While this electrode can be prepared with a small motor-driven electrode cutter and ordinary twist drills, such a procedure involves three separate steps and consequently necessitates considerable handling and expenditure of time. It is also difficult to reproduce drill settings from one batch of electrodes to another. The simple tool described here makes possible, in a single cutting operation, the shaping of a cavity of exactly reproducible size and shape.

The tool (shown unassembled in Fig. 2) consists of two essential pieces machined from tool

* Bureau of Agricultural and Industrial Chemistry, Agricultural Research Administration, U. S. Department of Agriculture.

[1] B. F. Scribner and C. H. Corliss, J. Opt. Soc. Am. **33**, 515 (1943).

[2] R. T. O'Connor, Ind. Eng. Chem. Anal. Ed. **13**, 597 (1941).

[3] A. T. Myers and B. C. Brunstetter, Ind. Eng. Chem. Anal. Ed. **11**, 218 (1939); K. R. Majors and T. H. Hopper, Ind. Eng. Chem. Anal. Ed. **13**, 647 (1941); H. I. Oshry, J. W. Ballard, and H. H. Schrenk, J. Opt. Soc. Am. **32**, 672 (1942); E. S. Hodge, Ind. Eng. Chem. Anal. Ed. **14**, 260 (1942); R. R. Hampton and H. N. Campbell, J. Opt. Soc. Am. **34**, 12 (1944).

[4] C. R. Jeppesen, E. J. Eastmond, and H. G. Logan, J. Opt. Soc. Am. **34**, 313 (1944).

[5] M. F. Hasler, C. E. Harvey, and H. W. Dietert, Ind. Eng. Chem. Anal. Ed. **15**, 102 (1943).

steel. Part *B* serves as a guide and is provided with cutting teeth on the front face so that any oversized electrode is trimmed to the proper size to insure uniform wall thickness. The $\frac{1}{8}$-in. chuck shaft on the back has been chosen to fit the available small motor-driven chuck. Part *A* is the cutting piece and is set into *B* with a set screw. It is machined and ground to shape and tempered to maintain the cutting edges.

Since reproducibility was sought, no attempt was made to make an adjustable cutting piece, but additional sizes and shapes are secured by different cutting pieces, each replaceable as a unit. The size is varied by varying either the width *e* or the depth *g* (Fig. 3) of the cutting edge, thus changing either the annular width or depth of the ring cavity in the electrode. The most suitable size for the material being tested in determined by experiment. The dimensions given in the diagram of Fig. 3 were found to be satisfactory for determination of lead in the ash of pectinous materials.[4]

An operator can prepare from 10 to 15 electrodes per minute with the small motor-driven electrode cutter used in this laboratory. Suitable alterations in design would make possible the adaptation to other types of motor-driven chucks or small lathes.

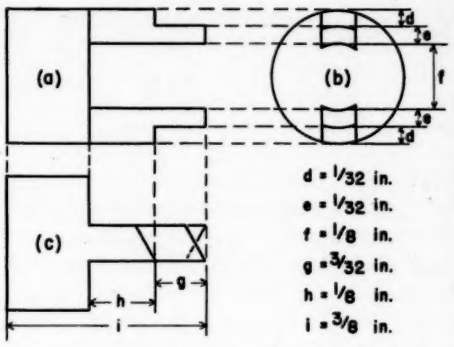

FIG. 3. Diagram of cutting piece. (*a*) Side view. (*b*) Front end view. (*c*) Top view.

The author wishes to acknowledge the cooperation of John R. Hoffman of the laboratory shop who constructed the cutting tool.

The Use of Columbia Resin No. 39 as an Optical Cement

HAROLD W. COLES, HARRY DEUBERRY, AND FRANCIS P. CURRY
Bausch and Lomb Optical Company, Rochester, New York
(Received April 25, 1944)

1. INTRODUCTION

THE high altitudes reached by present aircraft and resulting exposure of optical equipment to very low temperatures have made it imperative to improve the ability of the lens cements to withstand the shock of sudden large temperature changes. With the exception of a limited usage of synthetic resins, the cementing of lenses has largely been done with Canada balsam. Such cements do not absorb the differential contraction of large lenses when the temperature drops to −20°C or lower. The effects of shrinkage factors become apparent and the lenses do not "recover" when returned again to normal temperature.

Attention, therefore, was focused on Columbia Resin No. 39 (CR-39) and its analogs because of their shrinkage factors at low temperatures.[1]

A preliminary report of this work, largely with a cement prepared from CR-39, is desirable at this time because of the demand for a cement having the properties of this resin. Results have been obtained which indicate that CR-38 is likewise a suitable cement. Experimental data will be given in a later paper which will also include tests made with combinations of CR-39 with other resins.

2. PREPARATION OF THE RESIN FOR CEMENTING

The CR-39 monomer, after the addition of 3 percent catalyst, can be used directly for cementing, but it is found more convenient to gel the monomer partially before use to aid the truing operations.

The catalyst, benzoyl peroxide, is dissolved in the monomer with stirring. The thin liquid is then filtered through a Pyrex funnel with fritted glass bottom of medium porosity and having an asbestos layer carefully washed to remove fine fibers. A liquid results, having a clarity such that no particles are visible under 10-power magnification.

The filtrate is then transferred in a dust-free room to suitable containers for partial curing. Since the control of gelation is very sensitive to the size and shape of container, flat-bottomed specimen vials, 5 mm high and 17-mm outside diameter, were found to give a more uniform gel. For best results an electrically heated constant temperature water-bath is used and wire trays are employed to support the vials. With care, the gel may be prepared in glass syringes or tin tubes for easier application.

Since in going from the monomer to a solid state the refractive index (*D* line, 20°C) increases from 1.450 to 1.505, this property can be used to follow the gelation process. Repeated trials have shown that CR-39 gels, having consistencies such that bubbles can be easily worked out of the cement layer, will have refractive indices (white light at 27°C) from 1.4580 to 1.4585. Time studies (monomer heated in vial, and then removed to refractometer at 27°C for index determination) show that these indices are reached in approximately 105 minutes at 70°C, 80 minutes at 75°C, and 32 minutes at 85°C. This range of indices is a fortunate one, because it represents a stage in the polymerization where there is apparently very little change in the index for an appreciable period. However, the viscosity continues to change during this time. At 70°C, this time interval is about 15 minutes and, for this reason, this temperature is chosen for the curing. It might be mentioned here that CR-38 cures more slowly than CR-39. The vials of gel, as well as the monomer itself and monomer containing catalyst, are stored in a refrigerator (5°C). Slow polymerization will take place at room temperature, particularly in the presence of light.

3. CEMENTING OF LENSES AND PRISMS

In general, the actual cementing of lenses with CR-39 cement (called PKR-15) is more practical

[1] Bulletin No. 2 on "Properties of Columbia Resin CR-39," Pittsburgh Plate Glass Company, Grant Building, Pittsburgh, Pennsylvania. Anonymous, Modern Plastics **20**, 88–90, 120, 122 (1942). A. Pechukas, Plastics and Resin Ind. 1, 21 (1943). A. Pechukas, F. Strain, and W. R. Dial, Modern Plastics **20**, 101–2, 138 (1943).

than with a hot cement because of the ease of operation on lenses when cool. There is less chance of cracking of lenses and blisters can be worked out with more freedom.

Since this is a thermosetting cement, the lens must be trued perfectly before setting. It is, therefore, necessary to set the lens by the application of outside heat while the lens is trued in an optical truing machine, or held by mechanical fixtures.

The procedure for cementing with PKR-15 is as follows:

1. The lenses are cleaned using cotton swab and acetone.

2. As many vials of cement as are needed for the day's work are removed from the refrigerator and allowed to warm up to approximately room temperature. This is done as a precaution against condensation of moisture on the inside of the vial.

3. Lenses to be trued by optical means are given a preliminary heating by stove or oven before cementing in order to polymerize partially the cement for truing.

Prisms and lenses to be trued by mechanical means do not require this preheating.

4. Each lens is taken in order and the PKR-15 applied to the lens surface by means of platinum or gold wire loops, or a syringe of plunger or bulb type. The lenses are pressed together and the blisters are worked out in the usual manner. Excess gel on the edges is wiped off, the use of solvents being avoided.

5. After truing by optical means, the lenses are placed on a tray and covered by a pill box or cloth to allow for gradual cooling. This treatment does not, of course, apply to lenses or prisms trued mechanically.

6. The tray of lenses is then inspected in the usual manner.

7. After inspection, the lenses are placed in a "cold" oven and raised slowly to 80°C. This temperature is maintained for 8 hours and the oven is then allowed to cool to room temperature.

8. It is sometimes considered advisable to allow the lens to cool and then remove from oven before complete polymerization in order to check and test for surface quality, etc. In the event of rejection, the lenses can be readily taken apart with acetone if only partly polymerized, but require long soaking in acetone if completely hardened.

4. DISCUSSION OF RESULTS

After experience had been gained, it was possible to secure cemented pieces which did not show run-ins, distorted surfaces, and blisters when kept in an oven at 100°C and which did not reveal any evidence of separation when exposed to ice-box temperatures of −40°C to −50°C for 24 hours. It was not possible to separate the lenses with sharp blows at the low temperatures. Some lenses withstood 100°C for four weeks and others were not harmed by two weeks exposure at −40°C. Lenses cemented with PKR-15 showed no distortion of surfaces either immediately after cementing or after long standing (6 months). Apparently, the unequal coefficients of expansion of the two kinds of glasses are equalized by the resin layer. It is thus more elastic in its effect on lens surfaces than many hot cements such as Canada balsam.

Sample lenses likewise were successful in passing the following cycle. They were held at −54°C for two hours, then placed immediately in an oven at 38°C (saturated humidity) overnight and finally transferred at once to an oven at 71°C. This cycle was repeated five times.

Cementing and truing with PKR-15 have a time advantage over hot cements for use in large lenses as the time of heating and cooling of lenses is eliminated. This is an important factor when quantity production is considered.

Lenses cemented with PKR-15 can be separated by heating to a high temperature (250–275°C) until the cement film ruptures, by long immersion in acetone, or by soap, water, and ammonia under pressure in an autoclave.

5. OTHER PROPERTIES OF CR-39

Photo-transmission curves of lenses cemented with PKR-15 were determined using the Hardy-G.E. recording spectrophotometer. Cast sheets of CR-39 resin, one-quarter inch thick, show a transmission of 92.02 percent in the region of 480 mμ to 700 mμ, which rapidly drops off at 480 mμ, and is 82.5 percent at 400 mμ. In contrast, cover glasses cemented with PKR-15 revealed a transmission about 92 percent from 400 mμ to 700 mμ.

Lenses, cemented with PKR-15, show no fluorescence.

Cold flow determinations upon CR-39 films which will be described elsewhere revealed that it had very little cold flow and CR-38 films even less. Film thicknesses of 100 μ and a shearing load of 5 kg at a constant temperature of 23°C were employed. The CR-39 film gave an immediate shear of 4 μ which increased gradually, so that at the end of 45 hours it had reached 8 μ. There was no further change up to 90 hours at which time the load was removed. The film immediately recovered 50 percent of the total change, going back to a shearing distance of 4 μ. These results indicate the tenacity with which CR-39 acts as a cement and the difficulty of separating lenses so cemented by severe shocks.

6. CONCLUSIONS

At the end of about one year of intensive work on the use of CR-39 (PKR-15) as an optical cement, it can be stated that this resin appears to be a satisfactory cement for both small and large lenses and prisms. Lenses and prisms cemented with PKR-15 have successfully passed all the usual tests applied to such lenses and, in particular, do not shatter at very low temperatures. With the exception of prolonged weathering tests, which are incomplete, all the tests mentioned in this general preliminary report indicate that the substitution of CR-39 for balsam cement is an important contribution to the efforts being made to secure a cold-resistant cement.

7. ACKNOWLEDGMENT

The authors acknowledge the cooperation and advice of Dr. A. Pechukas, Research Director of the Columbia Chemical Division, Pittsburgh Plate Glass Company, and his associates. They are also indebted to members of the Bausch and Lomb Optical Company for help and advice in this work.

American Standard Dimensions for Industrial X-Ray Sheet Film (Inch Sizes)—Z38.1.25–1944*

1. FILM SIZE

Nominal	Minimum	Normal	Maximum
1⅞ × 16	$1\frac{53}{64} \times 15\frac{60}{64}$	$1\frac{54}{64} \times 15\frac{62}{64}$	$1\frac{55}{64} \times 16$
3½ × 10	$3\frac{29}{64} \times 9\frac{60}{64}$	$3\frac{30}{64} \times 9\frac{62}{64}$	$3\frac{31}{64} \times 10$
3½ × 17	$3\frac{29}{64} \times 16\frac{60}{64}$	$3\frac{30}{64} \times 16\frac{62}{64}$	$3\frac{31}{64} \times 17$
4 × 5	$3\frac{59}{64} \times 4\frac{58}{64}$	$3\frac{60}{64} \times 4\frac{60}{64}$	$3\frac{61}{64} \times 4\frac{62}{64}$
4 × 10	$3\frac{61}{64} \times 9\frac{60}{64}$	$3\frac{62}{64} \times 9\frac{62}{64}$	4 × 10
4½ × 10	$4\frac{28}{64} \times 9\frac{60}{64}$	$4\frac{30}{64} \times 9\frac{62}{64}$	$4\frac{32}{64} \times 10$
4½ × 15	$4\frac{29}{64} \times 14\frac{60}{64}$	$4\frac{30}{64} \times 14\frac{62}{64}$	$4\frac{31}{64} \times 15$
4½ × 17	$4\frac{29}{64} \times 16\frac{60}{64}$	$4\frac{30}{64} \times 16\frac{62}{64}$	$4\frac{31}{64} \times 17$
5 × 7	$4\frac{59}{64} \times 6\frac{58}{64}$	$4\frac{60}{64} \times 6\frac{60}{64}$	$4\frac{61}{64} \times 6\frac{62}{64}$
5 × 12	$4\frac{61}{64} \times 11\frac{60}{64}$	$4\frac{62}{64} \times 11\frac{62}{64}$	$4\frac{63}{64} \times 12$
6½ × 8½	$6\frac{27}{64} \times 8\frac{27}{64}$	$6\frac{29}{64} \times 8\frac{29}{64}$	$6\frac{31}{64} \times 8\frac{31}{64}$
7 × 17	$6\frac{58}{64} \times 16\frac{60}{64}$	$6\frac{60}{64} \times 16\frac{62}{64}$	$6\frac{62}{64} \times 17$
8 × 10	$7\frac{58}{64} \times 9\frac{59}{64}$	$7\frac{60}{64} \times 9\frac{61}{64}$	$7\frac{62}{64} \times 9\frac{63}{64}$
10 × 12	$9\frac{58}{64} \times 11\frac{58}{64}$	$9\frac{60}{64} \times 11\frac{60}{64}$	$9\frac{62}{64} \times 11\frac{62}{64}$
11 × 14	$10\frac{60}{64} \times 13\frac{60}{64}$	$10\frac{62}{64} \times 13\frac{62}{64}$	11 × 14
14 × 17	$13\frac{60}{64} \times 16\frac{60}{64}$	$13\frac{62}{64} \times 16\frac{62}{64}$	14 × 17

(All dimensions given in inches.)

* Approved January 20, 1944 by American Standards Association. Sponsor: Optical Society of America.

American Standard Dimensions for Graphic Arts Sheet Film (Inch Sizes)—Z38.1.26–1944*

1. FILM SIZES

Nominal	Minimum	Normal	Maximum
5 × 7	$4\frac{59}{64} \times 6\frac{58}{64}$	$4\frac{60}{64} \times 6\frac{60}{64}$	$4\frac{61}{64} \times 6\frac{62}{64}$
8 × 10	$7\frac{58}{64} \times 9\frac{59}{64}$	$7\frac{60}{64} \times 9\frac{61}{64}$	$7\frac{62}{64} \times 9\frac{63}{64}$
$8\frac{1}{2} \times 11$	$8\frac{28}{64} \times 10\frac{60}{64}$	$8\frac{30}{64} \times 10\frac{62}{64}$	$8\frac{32}{64} \times 11$
10 × 12	$9\frac{58}{64} \times 11\frac{58}{64}$	$9\frac{60}{64} \times 11\frac{60}{64}$	$9\frac{62}{64} \times 11\frac{62}{64}$
11 × 14	$10\frac{60}{64} \times 13\frac{60}{64}$	$10\frac{62}{64} \times 11\frac{62}{64}$	11 × 14
12 × 17	$11\frac{62}{64} \times 16\frac{62}{64}$	12 × 17	$12\frac{2}{64} \times 17\frac{2}{64}$
12 × 18	$11\frac{62}{64} \times 17\frac{62}{64}$	12 × 18	$12\frac{2}{64} \times 18\frac{2}{64}$
14 × 17	$13\frac{62}{64} \times 16\frac{62}{64}$	14 × 17	$14\frac{2}{64} \times 17\frac{2}{64}$
16 × 20	$15\frac{62}{64} \times 19\frac{62}{64}$	16 × 20	$16\frac{2}{64} \times 20\frac{2}{64}$
18 × 22	$17\frac{62}{64} \times 21\frac{62}{64}$	18 × 22	$18\frac{2}{64} \times 22\frac{2}{64}$
20 × 24	$19\frac{62}{64} \times 23\frac{62}{64}$	20 × 24	$20\frac{2}{64} \times 24\frac{2}{64}$

(All dimensions given in inches.)

* Approved January 20, 1944 by American Standards Association. Sponsor: Optical Society of America.

American Standard Dimensions for Medical X-Ray Sheet Film (Inch and Centimeter Sizes)—Z38.1.27–1944*

1. INCH SIZES

Nominal	Minimum	Normal	Maximum
4 × 5	$3\frac{59}{64} \times 4\frac{58}{64}$	$3\frac{60}{64} \times 4\frac{60}{64}$	$3\frac{61}{64} \times 4\frac{62}{64}$
5 × 7	$4\frac{59}{64} \times 6\frac{58}{64}$	$4\frac{60}{64} \times 6\frac{60}{64}$	$4\frac{61}{64} \times 6\frac{62}{64}$
$6\frac{1}{2} \times 8\frac{1}{2}$	$6\frac{27}{64} \times 8\frac{27}{64}$	$6\frac{29}{64} \times 8\frac{29}{64}$	$6\frac{31}{64} \times 8\frac{31}{64}$
8 × 10	$7\frac{58}{64} \times 9\frac{59}{64}$	$7\frac{60}{64} \times 9\frac{61}{64}$	$7\frac{62}{64} \times 9\frac{63}{64}$
10 × 12	$9\frac{58}{64} \times 11\frac{58}{64}$	$9\frac{60}{64} \times 11\frac{60}{64}$	$9\frac{62}{64} \times 11\frac{62}{64}$
11 × 14	$10\frac{60}{64} \times 13\frac{60}{64}$	$10\frac{62}{64} \times 13\frac{62}{64}$	11 × 14
14 × 17	$13\frac{60}{64} \times 16\frac{60}{64}$	$13\frac{62}{64} \times 16\frac{62}{64}$	14 × 17
7 × 17	$6\frac{58}{64} \times 16\frac{60}{64}$	$6\frac{60}{64} \times 16\frac{62}{64}$	$6\frac{62}{64} \times 17$
8 × 36	$7\frac{60}{64} \times 35\frac{60}{64}$	$7\frac{62}{64} \times 35\frac{62}{64}$	8 × 36
14 × 36	$13\frac{60}{64} \times 35\frac{60}{64}$	$13\frac{62}{64} \times 35\frac{62}{64}$	14 × 36

2. CENTIMETER SIZES

Nominal	Minimum	Normal	Maximum
13 × 18	12.7 × 17.7	12.8 × 17.8	12.9 × 17.9
18 × 24	17.7 × 23.7	17.8 × 23.8	17.9 × 23.9
24 × 30	23.7 × 29.7	23.8 × 29.8	23.9 × 29.9
30 × 40	29.7 × 39.7	29.8 × 39.8	29.9 × 39.9

* Approved January 20, 1944 by American Standards Association. Sponsor: Optical Society of America.

American Standard Dimensions for Professional Portrait and Commercial Sheet Film (Inch Sizes)—Z38.1.28–1944*

FOREWORD

IN the preparation of this standard, the subcommittee was aware of the opportunity afforded it to simplify the list of sheet film sizes regarded as standard and also to organize the dimensions themselves in some systematic relationship to the nominal sizes. The first of these aims has been accomplished: The finished standard lists the the sizes in wide commercial use in America and omits obsolete and seldom employed sizes. Film manufacturers may, however, be called upon to supply some of the odd sizes to users who require them.

In the matter of relating film dimension systematically to the nominal sizes, the committee encountered one significantly difficulty because of the historical background of sheet films. When they were first introduced as a replacement material for photographic glass plates, "sheaths" or "kits" were provided by the film manufacturers to permit the use of sheet films in plate holders. These holders normally accommodated glass plates of approximately full nominal size, but the "sheaths" or "kits" naturally encroached somewhat on this area in the plate holder because of the thickness of the material used for them, and thus required the films to be cut considerably below the nominal dimension. Moreover, no attempt seems to have been made to correlate the different sheath sizes, and so there is no uniformity in the deviation from the nominal in the films smaller than 11 × 14.

Eventually, sheet film holders which did not require a "sheath" or "kit" were introduced, but these quite naturally were designed to accommodate the film of the same size used in the sheaths. These dimensions, therefore, have become so firmly established in the trade, and so much equipment that requires film of these dimensions is used, that the committee found it necessary to compromise between the ideal and the practical conditions.

The sizes 11 × 14 and larger either are not used in holders or, if holders have been made, were not handicapped by a previous "sheath" or "kit" for a plate holder; therefore, they were designed to take a full nominal-sized film. Thus, on these sizes the committee was able to adopt the nominal dimensions as maximum and to place suitable uniform slitting tolerances below the maximum.

The committee suggests that if new sizes are introduced in the future, they follow the dimensional practice set up in the present standard for 11 × 14 inches and larger—that is, establish the nominal size as the maximum dimension and allow a suitable minus tolerance.

1. FILM DIMENSIONS

Nominal	Minimum	Normal	Maximum
2¼ × 3¼	2 13/64 × 3 13/64	2 14/64 × 3 14/64	2 15/64 × 3 15/64
2½ × 3½	2 27/64 × 3 29/64	2 28/64 × 3 31/64	2 29/64 × 3 33/64
3¼ × 4¼	3 11/64 × 4 13/64	3 12/64 × 4 13/64	3 13/64 × 4 15/64
3¼ × 5½	3 11/64 × 5 25/64	3 12/64 × 5 27/64	3 13/64 × 5 29/64
4 × 5	3 59/64 × 4 55/64	3 60/64 × 4 60/64	3 61/64 × 4 63/64
4¼ × 6½	4 13/64 × 6 25/64	4 14/64 × 6 28/64	4 15/64 × 6 30/64
4¾ × 6½	4 41/64 × 6 25/64	4 42/64 × 6 28/64	4 43/64 × 6 30/64
5 × 7	4 59/64 × 6 55/64	4 60/64 × 6 60/64	4 61/64 × 6 63/64
5 × 8	4 59/64 × 7 60/64	4 60/64 × 7 63/64	4 61/64 × 8
6½ × 8½	6 27/64 × 8 27/64	6 28/64 × 8 29/64	6 31/64 × 8 31/64
7 × 10	6 55/64 × 9 59/64	6 60/64 × 9 61/64	6 63/64 × 9 63/64
7 × 17	6 55/64 × 16 60/64	6 60/64 × 16 63/64	6 63/64 × 17
8 × 10	7 55/64 × 9 59/64	7 60/64 × 9 61/64	7 63/64 × 9 63/64
8 × 20	7 55/64 × 19 55/64	7 60/64 × 19 60/64	7 63/64 × 19 63/64
10 × 12	9 55/64 × 11 59/64	9 60/64 × 11 60/64	9 63/64 × 11 63/64
11 × 14	10 60/64 × 13 60/64	10 63/64 × 13 63/64	11 × 14
12 × 20	11 60/64 × 19 60/64	11 63/64 × 19 63/64	12 × 20
14 × 17	13 60/64 × 16 60/64	13 63/64 × 16 63/64	14 × 17
16 × 20	15 60/64 × 19 60/64	15 63/64 × 19 63/64	16 × 20
18 × 22	17 60/64 × 21 60/64	17 63/64 × 21 63/64	18 × 22
20 × 24	19 60/64 × 23 60/64	19 63/64 × 23 63/64	20 × 24
22 × 28	21 60/64 × 27 60/64	21 63/64 × 27 63/64	22 × 28
24 × 30	23 60/64 × 29 60/64	23 63/64 × 29 63/64	24 × 30
28 × 36	27 60/64 × 35 60/64	27 63/64 × 35 63/64	28 × 36
30 × 40	29 60/64 × 39 60/64	29 63/64 × 39 63/64	30 × 40

(All dimensions given in inches.)

* Approved January 20, 1944 by American Standards Association. Sponsor: Optical Society of America.

American Standard Dimensions for Professional Portrait and Commercial Sheet Film (Centimeter Sizes)—Z38.1.29–1944*

1. FILM DIMENSIONS

Nominal	Minimum	Normal	Maximum
4.5 × 6	4.3 × 5.8	4.35 × 5.85	4.4 × 5.9
6.5 × 9	6.3 × 8.8	6.35 × 8.85	6.4 × 8.9
9 × 12	8.8 × 11.8	8.85 × 11.85	8.9 × 11.9
10 × 15	9.8 × 14.8	9.85 × 14.85	9.9 × 14.9
12 × 16.5	11.8 × 16.3	11.85 × 16.35	11.9 × 16.4
13 × 18	12.7 × 17.7	12.8 × 17.8	12.9 × 17.9
18 × 24	17.7 × 23.7	17.8 × 23.8	17.9 × 23.9
24 × 30	23.7 × 29.7	23.8 × 29.8	23.9 × 29.9
30 × 40	29.7 × 39.7	29.8 × 39.8	29.9 × 39.9

(All dimensions given in inches.)

* Approved January 20, 1944 by American Standards Association. Sponsor: Optical Society of America.

American Standard Dimensions for Photographic Dry Plates (Inch Sizes)—Z38.1.30–1944*

1. CUTTING SIZE

Nominal size	Standard	Tolerance	Thickness	
			Minimum	Maximum
2 × 2	$1\frac{15}{16} \times 1\frac{15}{16}$	$\pm \frac{1}{64}$	0.038	0.043
2 × 10	$1\frac{63}{64} \times 9\frac{31}{32}$	$\pm \frac{1}{64}$	0.038	0.043
$2\frac{1}{4} \times 3\frac{1}{4}$	$2\frac{15}{64} \times 3\frac{15}{64}$	$\pm \frac{1}{64}$	0.048	0.053
$2\frac{1}{2} \times 2\frac{1}{2}$	$2\frac{31}{64} \times 2\frac{31}{64}$	$\pm \frac{1}{64}$	0.048	0.053
$3\frac{1}{4} \times 3\frac{1}{4}$	$3\frac{15}{64} \times 3\frac{15}{64}$	$\pm \frac{1}{64}$	0.048	0.053
$3\frac{1}{4} \times 4$	$3\frac{15}{64} \times 3\frac{63}{64}$	$\pm \frac{1}{64}$	0.048	0.053
$3\frac{1}{4} \times 4\frac{1}{4}$	$3\frac{15}{64} \times 4\frac{15}{64}$	$\pm \frac{1}{64}$	0.058	0.063
$3\frac{1}{4} \times 5\frac{1}{2}$	$3\frac{15}{64} \times 5\frac{15}{32}$	$\pm \frac{1}{64}$	0.058	0.063
4 × 5	$3\frac{63}{64} \times 4\frac{63}{64}$	$\pm \frac{1}{64}$	0.058	0.063
4 × 10	$3\frac{31}{32} \times 9\frac{31}{32}$	$\pm \frac{1}{64}$	0.038	0.043
$4\frac{1}{4} \times 6\frac{1}{2}$	$4\frac{15}{64} \times 6\frac{15}{32}$	$\pm \frac{1}{64}$	0.058	0.063
$4\frac{3}{4} \times 6\frac{1}{2}$	$4\frac{11}{16} \times 6\frac{15}{32}$	$\pm \frac{1}{64}$	0.058	0.063
5 × 7	$4\frac{63}{64} \times 6\frac{31}{32}$	$\pm \frac{1}{64}$	0.058	0.063
$6\frac{1}{2} \times 8\frac{1}{2}$	$6\frac{15}{32} \times 8\frac{15}{32}$	$\pm \frac{1}{64}$	0.058	0.063
8 × 10	$7\frac{31}{32} \times 9\frac{31}{32}$	$\pm \frac{1}{64}$	0.058	0.063
10 × 12	$9\frac{31}{32} \times 11\frac{31}{32}$	$\pm \frac{1}{64}$	0.070	0.080
11 × 14	$10\frac{31}{32} \times 13\frac{31}{32}$	$\pm \frac{1}{64}$	0.080	0.095
14 × 17	$13\frac{15}{16} \times 16\frac{15}{16}$	$\pm \frac{1}{32}$	0.080	0.095
16 × 20	16 × 20	$\pm \frac{1}{32}$	0.120	0.130
18 × 22	18 × 22	$\pm \frac{1}{32}$	0.120	0.130
20 × 24	20 × 24	$\pm \frac{1}{32}$	0.120	0.130
22 × 28	22 × 28	$\pm \frac{1}{32}$	0.190	0.200
24 × 31	24 × 31	$\pm \frac{1}{32}$	0.190	0.200
26 × 34	26 × 34	$\pm \frac{1}{32}$	0.190	0.200
28 × 32	28 × 32	$\pm \frac{1}{32}$	0.190	0.200
28 × 36	28 × 36	$\pm \frac{1}{32}$	0.190	0.200
30 × 40	30 × 40	$\pm \frac{1}{32}$	0.190	0.200

(All dimensions given in inches.)

2. SQUARENESS

The diagonal in either direction shall not exceed the diagonal of a square-cornered plate of maximum length and width.

* Approved January 20, 1944 by American Standards Association. Sponsor: Optical Society of America.

American Standard Dimensions for Photographic Dry Plates (Centimeter Sizes)—Z38.1.31–1944†

1. CUTTING SIZE

Nominal Size (Centimeters)	Standard (Millimeters)	Tolerance (Millimeters)	Thickness Minimum (Millimeters)	Thickness Maximum (Millimeters)
*4.5 × 6	44 × 59	± 0.5	1.0	1.3
*4.5 × 10.7	44 × 106	± 0.5	1.0	1.3
*6 × 9	59 × 89	± 0.5	1.0	1.3
*6 × 13	59 × 129	± 0.5	1.0	1.3
*6.5 × 9	64 × 89	± 0.5	1.0	1.3
9 × 12	89 × 119	± 0.5	1.2	1.5
10 × 15	99 × 149	± 0.5	1.2	1.5
12 × 16.5	119 × 164	± 0.5	1.5	1.8
13 × 18	129 × 179	± 0.5	1.5	1.8
18 × 24	179 × 239	± 0.5	1.5	1.8
24 × 30	238 × 298	± 1.0	1.7	2.0
30 × 40	298 × 398	± 1.0	2.0	2.4
40 × 50	398 × 498	± 1.0	3.0	3.3
50 × 60	498 × 598	± 1.0	3.0	3.3

* These sizes may also be supplied on extra-thin glass, in which case the thickness range is: Minimum 0.7 mm; Maximum 1.0 mm.

2. SQUARENESS

The diagonal in either direction shall not exceed the diagonal of a square-cornered plate of maximum length and width.

† Approved January 20, 1944 by American Standards Association. Sponsor: Optical Society of America.